Consolidated Competition Ballistics

A Comprehensive Mathematical Manual with Reloading Guide and Julia Implementations

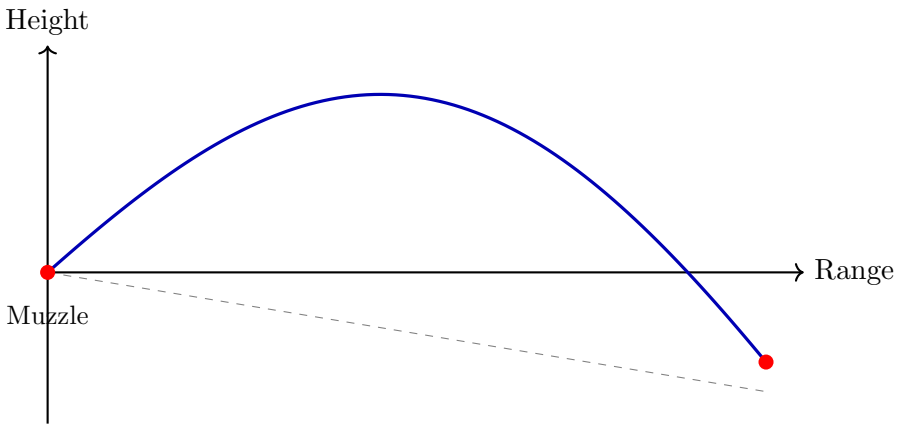

Trajectory with aerodynamic drag and gravity

Merging Core Theory, Advanced Effects, and Practical Shooting Tools
Drag Models (G1–G8), Coriolis & Eötvös Effects, Spin Drift,
Aerodynamic Jump, Wind Deflection, and Handloading Data

Version 3.8 — November 4, 2026

Abstract

This manual provides a rigorous mathematical treatment of competition rifle ballistics. Version 3.1 brought accuracy improvements to the 3-DOF engine (coordinate-system alignment) and outlined a roadmap for a 6-DOF expert mode. Version 3.2 (2026-08-22) replaced the G1 and G7 drag tables, whose supersonic branches had been fabricated, and removed the $4/\pi$ factor that had been masking them; every trajectory figure in this manual was recomputed.

Version 3.2 records that the 6-DOF is no longer a roadmap: it is implemented and validated against three published cases — McCoy's .308 in 168 gr textbook example, the 105 mm HE M1 shell, and the 5.56 mm NATO family measured at the Ballistic Research Laboratory. This edition adds the moment-of-inertia estimator that feeds it (Section 8.8), the measured coefficient sets it can be run on, and the reasons a set may not be trusted. It also corrects an inclined-fire example that had drifted 10 % from what both implementations return, and qualifies the recommendation of spline interpolation, which is right for the dense standard drag tables and wrong for sparse measured ones.

Version 3.3 (2026-08-25) corrects the G7 ballistic coefficient of the Sierra 175 gr MatchKing in the bullet data table (0.259 to 0.243, the value published by the sources that table cites) and the transonic ranges derived from it. It also adds Chapter 14: the dispersion statistics, hit-probability model and Bayesian muzzle-velocity truing behind the analysis tools of the online calculator.

Version 3.4 (2026-09-30) corrects two errors in that chapter. The extreme-spread factors of Table 14.1 were those of the range of a *one-dimensional* normal sample; a group's extreme spread is measured in the plane, and its factor is larger (3.066 instead of 2.326 at five shots), so the dispersion σ had been overstated by up to 42 %. The truing section used the shot-to-shot standard deviation of the chronograph as the uncertainty of the mean velocity; it now uses the standard error $s/\sqrt{n}$ combined with the device's accuracy, observes the centre of a group rather than a single impact, and tests whether the two estimates are compatible. Finally, the hit probability no longer assumes a circular dispersion: the wind uncertainty was composed into a single σ applied to both axes, which spread it vertically. Each source is now composed on its own axis, with the velocity spread added vertically, and the probability is integrated numerically. The worked example also used a wind sensitivity 2.6 times the solver's; it has been recomputed.

Version 3.5 (2026-10-20) replaces the "representative" load tables, whose charges had no source and, for the 6mm BR, exceeded the maxima published for the same bullet and powder (by up to 2.9 gr for the 107 gr MatchKing with Varget), with excerpts of published tables for the named bullet and powder (Section 10.4). The 6mm BR worked example (Section 10.5) no longer gives a charge: it uses the median of the published maximum velocities (2670 instead of 2920 fps) and the published bullet length, and has been recomputed; its chronograph string, which no measurement supported, gives way to the solver's velocity sensitivity. The library function `velocity_vertical_dispersion`, and two others built the same way, had never run; they are repaired.

Version 3.6 (2026-10-20) gives a source to the three tables of the reloading chapter that had none. The cartridge table now reports the maximum velocities published by nine load guides and the G7 coefficients published by Berger; it had the .284 Winchester at 2850–2950 fps with 180 gr bullets, above every published maximum (2743 fps), and listed the 6.5×47 Lapua as a "Palma variant", a match that admits only the .308 and the .223. The disciplines column gives way to the rules of ICFRA, the ISSF and the PRS. The temperature tables replace three unsourced classes of powders with the coefficients published by makers, independent

testers and military laboratories: the "standard" class at 1.5–2.0 fps/°F matches the military ammunition of the 1920s, not IMR 4064 (0.37 to 1.08 in three tests), and the same powder can differ by a factor of ten from one test to another. The barrel-life table now states the end point and source of each figure; the two wear laws in $N^{0.7}$ and $N^{0.5}$, for which no source was found and which the published tests contradict, are removed. Finally, the SAAMI pressure of the .338 Lapua Magnum was the C.I.P. maximum converted to psi (60,916); the SAAMI figure is 65,000 psi.

Version 3.7 (2026-10-20) adds to the 6-DOF chapter a worked comparison of the 6-DOF, a point mass and the 3-DOF G7 solver on the same shot (Table 8.1): with the same drag, the point mass stays within 1.7 % of the 6-DOF, while the choice of drag curve moves the result by 2.5 to 4.2 %. The binding constraint is the data, as the chapter says.

Version 3.8 (2026-10-22) corrects the length of the Berger 105 gr Hybrid Target in the 6mm BR worked example: 1.282 in, attributed to Berger, is the value of a collective length list; Berger publishes 1.256 in [Berger Bullets]. The muzzle S_g rises from 1.49 to 1.58, above the 1.5 threshold of full BC, and the spin drift at 1000 yards from 8.2 to 8.5 inches.

Contents

Notation and Conventions **ix**

1 Introduction to Competition Rifle Ballistics **1**
1.1 Motivation: Why Math Matters in Marksmanship . . . 1
1.2 Scope and Purpose . . . 1
1.3 Overview of Ballistic Phases . . . 1
1.4 Historical Context . . . 2

2 Atmospheric Model **3**
2.1 Motivation: Why Air Density is King . . . 3
2.2 ICAO Standard Atmosphere . . . 4
2.2.1 Temperature Lapse Rate . . . 4
2.2.2 Pressure–Altitude Relationship . . . 4
2.3 Air Density . . . 5
2.3.1 Humidity Correction . . . 5
2.4 Speed of Sound . . . 6
2.5 Density Altitude . . . 6
2.6 Julia Implementation: Atmospheric Model . . . 7

3 Interior Ballistics **9**
3.1 Motivation: The Engine of the Bullet . . . 9
3.2 The Thermodynamic Problem . . . 9
3.2.1 Noble–Abel Equation of State . . . 9
3.2.2 Energy Balance . . . 10
3.3 Simplified Closed-Bomb Model . . . 10
3.4 Burn Rate Law . . . 10
3.4.1 Geometric Form Function . . . 11
3.5 Le Duc Velocity Model . . . 11
3.6 Pressure–Travel Relationship . . . 11
3.6.1 Anchoring on Load Data . . . 12
3.6.2 Limits . . . 12
3.7 Muzzle Velocity Estimation for Handloaders . . . 12
3.7.1 Temperature Sensitivity of Muzzle Velocity . . . 13

4 Transitional Ballistics **15**
4.1 Motivation: The Chaos of the Muzzle . . . 15
4.2 Muzzle Gas Dynamics . . . 15
4.3 Muzzle Tip-Off and Initial Yaw . . . 16
4.4 Base Drag Transition . . . 16
4.5 Crown Effects . . . 16

5 Exterior Ballistics: Core Theory **17**
5.1 Motivation: The Math of Free Flight . . . 17

5.2 Vacuum Trajectory (The Baseline) . . . 17
5.3 Aerodynamic Drag . . . 18
5.3.1 The Drag Equation . . . 18
5.3.2 Drag Coefficient and Mach Number . . . 18
5.3.3 Analytical Solution for 1D Drag . . . 18
5.4 Ballistic Coefficient . . . 19
5.4.1 Standard Conditions for BC . . . 19
5.5 Standard Drag Models (G1 through G8) . . . 20
5.5.1 G7 Drag Function . . . 21
5.5.2 Drag Functions vs. Siacci Tables: a Common Confusion . . . 21
5.6 Doppler Radar Drag Measurement . . . 21
5.6.1 Measurement Principle . . . 22
5.6.2 Extracting $C_D(Ma)$ from Radar Data . . . 22
5.6.3 Advantages over Classical Methods . . . 22
5.6.4 Interpolation of Tabular Drag Data . . . 22
5.7 Equations of Motion: 3-DOF Point-Mass Model . . . 23
5.7.1 Coordinate System . . . 23
5.7.2 Vector Equation of Motion . . . 24
5.7.3 Scalar Component Equations . . . 24
5.7.4 Using the Ballistic Coefficient . . . 24
5.8 Numerical Integration . . . 24
5.8.1 Euler Method . . . 24
5.8.2 Runge–Kutta (RK4) & Area Scaling . . . 25

6 Exterior Ballistics: Advanced Effects **27**
6.1 Motivation: Beyond Gravity . . . 27
6.2 Wind Deflection . . . 27
6.2.1 Wind Components (Vectors) . . . 27
6.2.2 Simple Approximation . . . 28
6.2.3 The Lag Rule (The Didion Approximation) . . . 28
6.3 Spin Drift . . . 28
6.3.1 Gyroscopic Stability Factor . . . 29
6.4 Coriolis and Eötvös Effects . . . 29
6.4.1 Coriolis Acceleration . . . 29
6.4.2 Horizontal Deflection . . . 29
6.4.3 Vertical Deflection (Eötvös Effect) . . . 30
6.4.4 Implementation . . . 30
6.5 Aerodynamic Jump . . . 30
6.6 Magnus Effect . . . 30

7 Complete 3-DOF Ballistic Solver **31**
7.1 Motivation: From Paper to Code . . . 31

8 Six-Degree-of-Freedom (6-DOF) Model **33**
8.1 Motivation: Unlocking the Gyroscope . . . 33
8.2 State Vector and Reference Frames . . . 34
8.2.1 Coordinate Systems (Inertial vs Body) . . . 34
8.2.2 Euler Angles and Orientation . . . 35
8.2.3 The 12-Component State Vector . . . 35
8.3 Translational Equations of Motion . . . 35
8.3.1 Total Angle of Attack . . . 35
8.3.2 Aerodynamic Force Components . . . 36

8.4 Rotational Equations of Motion . . . 36
8.4.1 Aerodynamic Moments . . . 36
8.4.2 Summary of Moment Components . . . 37
8.5 Kinematic Equations . . . 37
8.6 Quaternion Formulation (Singularity-Free) . . . 37
8.7 Aerodynamic Coefficient Database . . . 38
8.7.1 Typical Values for Match Bullets . . . 38
8.7.2 Measured Sets: What Actually Exists . . . 38
8.7.3 Deriving C_{D_0} from the Ballistic Coefficient . . . 39
8.8 Moments of Inertia . . . 39
8.8.1 Why the Solid-Cylinder Form Is Not Good Enough . . . 40
8.8.2 Integration over the Actual Contour . . . 40
8.8.3 Default Contour, and What It Costs . . . 40
8.8.4 Constructions the Model Does Not Cover . . . 41
8.9 Spin Rate and Initial Conditions . . . 41
8.10 Stability Revisited from 6-DOF Theory . . . 41
8.10.1 Gyroscopic Stability . . . 41
8.10.2 Dynamic Stability . . . 42
8.11 Comparison: 3-DOF vs. 6-DOF . . . 42
8.12 Julia Implementation: 6-DOF Solver . . . 42

9 Angular Measurement and Sighting Systems 45
9.1 Motivation: Speaking the Language of the Scope . . . 45
9.2 Minute of Angle (MOA) . . . 45
9.3 Milliradian (Mil, MRAD) . . . 45

10 Reloading Guide for Competition Shooters 47
10.1 Motivation: Controlling the Variables . . . 47
10.2 Cartridge Selection for Competition . . . 47
10.3 Propellant Selection . . . 48
10.4 Published Load Data (Excerpts) . . . 49
10.5 Complete Worked Example: 6mm BR at 1000 Yards . . . 51
10.5.1 Step 1: Component Data . . . 51
10.5.2 Step 2: Stability Check . . . 51
10.5.3 Step 3: Atmospheric Conditions . . . 51
10.5.4 Step 4: Solver Setup and Trajectory . . . 52
10.5.5 Step 5: Analysis of Results . . . 53
10.5.6 Step 6: What the Chronograph SD Means at 1000 Yards . . . 53
10.5.7 Step 7: DOPE Card Summary . . . 54
10.6 Interpreting Chronograph Data . . . 54
10.6.1 Velocity SD Impact on Vertical Dispersion . . . 55

11 Ballistic Reference Tables 57
11.1 Bullet Data for Common Competition Bullets . . . 57
11.2 Sample Trajectory Table . . . 57

12 Special Topics 59
12.1 Motivation: The Edges of the Envelope . . . 59
12.2 Transonic Stability . . . 59
12.3 Inclined Fire (Rifleman's Rule) . . . 59
12.4 Barrel Harmonics and Optimal Charge Weight . . . 60

13 Error Budget and Sensitivity Analysis **61**
13.1 Motivation: Knowing Your Weakest Link . . . 61
13.2 Sensitivity Coefficients . . . 61

14 Dispersion, Hit Probability and Velocity Truing **63**
14.1 Motivation: From Groups to Decisions . . . 63
14.2 The Rayleigh Model of a Centered Group . . . 63
14.3 From Group Size to Sigma . . . 64
14.4 Composing Independent Variance Sources, Axis by Axis . . . 64
14.5 Hit Probability on a Circular Target . . . 65
14.6 Bayesian Truing of the Muzzle Velocity . . . 66
14.7 Implementation . . . 67

15 Ballistic Implications for Reloading **69**
15.1 Motivation: Crafting the Perfect Formula . . . 69
15.2 The Reloader's Equation: What You Control . . . 69
15.3 Muzzle Velocity: The Central Reloading Output . . . 69
15.3.1 Charge Weight and Velocity . . . 69
15.3.2 Velocity Consistency and Vertical Dispersion . . . 69
15.3.3 Achieving Low SD: Quantitative Checklist . . . 70
15.4 BC Sensitivity and Bullet Selection . . . 70
15.5 Temperature Effects: Propellant and Atmosphere . . . 70
15.5.1 Combined Temperature Effect . . . 70
15.6 Seating Depth and Internal Ballistic Coupling . . . 71
15.7 Pressure Estimation and Safety Margins . . . 72
15.8 Barrel Life . . . 72
15.9 Load Development Workflow . . . 73

A Detailed Mathematical Derivations **75**
A.1 Motivation: Showing the Work . . . 75
A.2 Derivation of the Point-Mass Equations of Motion . . . 75
A.3 Derivation of the Coriolis Terms . . . 75
A.4 Derivation of Spin Drift via Yaw of Repose . . . 75

B Companion Julia Package **77**

C Greenhill's Formula and Twist Rate Selection **79**
C.1 Motivation: Keeping the Bullet Pointy-End Forward . . . 79

Glossary **87**

List of Tables

3.1 Measured muzzle velocity vs. barrel length, .308 Win / Lapua 155 gr Scenar . 13

5.1 BRL Standard Drag Models [McCoy, 2012, Ingalls, 1886] 20
5.2 Selected G7 drag coefficient values [McCoy, 2012] 21

8.1 Same shot, five models: vertical shift at 1000 yards for an 11 °C drop in ammunition temperature, launch angle held constant 34
8.2 Typical aerodynamic coefficients for a 6.5 mm 140 gr VLD match bullet . . . 38
8.3 Measured aerodynamic sets carried by the implementation 38
8.4 Comparison of 3-DOF and 6-DOF models 42

10.1 Competition cartridges: published maximum velocities and published G7 ballistic coefficients 48
10.2 Temperature claims of the makers and published measurements of σ_T 49
10.3 6.5 Creedmoor: published loads [Hodgdon Powder Company, 2024, Vihtavuori, 2026] 50
10.4 .308 Winchester: published loads [Hodgdon Powder Company, 2024, Vihtavuori, 2026] 50
10.5 6mm Creedmoor: published loads [Hodgdon Powder Company, 2024, Vihtavuori, 2026] 50
10.6 6mm BR Norma: published loads [Vihtavuori, 2026, Reload Swiss, 2025, Sierra Bullets, 2020b, Western Powders, 2020] 50
10.7 Computed trajectory: 6mm BR, 105 gr Berger Hybrid, $v_0 = 2670$ fps, 27.8 °C (82°F), 29.75 in Hg, 55% RH. 8 mph wind at 60°. 100 yd zero. 1:7.5 RH twist, 45.4°N, firing West. 53
10.8 DOPE card: 6mm BR, 105 Berger Hybrid, 2670 fps assumed (replace with the chronographed velocity). Ottawa, 27.8 °C (82°F), 29.75 inHg. Wind hold is per 1 mph full crosswind. 54
10.9 Typical velocity consistency: factory ammunition vs. optimized handloads . . 54

11.1 Ballistic data for popular competition bullets [Litz, 2015b] 57
11.2 Trajectory: 6.5 CM, 140 gr Berger Hybrid, $BC_{G7} = 0.311$, $v_0 = 2700$ fps, 100 yd zero, sea level standard atmosphere 57

12.1 Transonic transition ranges for common competition cartridges at sea-level standard conditions, *computed with the solver of Chapter 7* rather than quoted. The transonic zone is defined as $0.9 \le Ma \le 1.1$ ($\approx$ 310–380 $\frac{\text{m}}{\text{s}}$). Ballistic coefficients from Table 11.1 where listed, otherwise from Litz [2015b]. 59

13.1 Error budget: 6.5 Creedmoor, 140 gr, $BC_{G7} = 0.311$, 2700 fps at 1000 yd . . 61

14.1 Expected extreme spread of an n-shot group, in units of the per-axis σ (simulation of 2×10^6 and 4×10^6 groups per n, standard error 0.0004, cross-checked against the lookup table of the `shotGroups` package, Wollschläger, 2025, and Table 6 of Grubbs, 1991) 64

15.1 Velocity sensitivity: vertical shift per 1 fps change, 6.5 CM 140 gr 70
15.2 Estimated velocity SD contributions by reloading variable 70
15.3 Published velocity coefficients σ_T of rifle ammunition 71
15.4 SAAMI maximum average pressure (transducer) for competition cartridges [Sporting Arms and Ammunition Manufacturers' Institute, 2025] 72
15.5 Published barrel lives and the end point each one counts to 73

List of Figures

2.1 The aerodynamic drag force opposes the bullet's velocity. Notice that the force scales linearly with air density ρ. 3
2.2 ICAO Standard Atmosphere profiles (troposphere, 0–11 km). Temperature decreases linearly at $L = 6.5$ K/km, while pressure and density follow power laws with exponents $n = 5.256$ and $n - 1 = 4.256$ respectively. The dashed vertical line marks 1500 m, a typical mountain shooting altitude where density is already reduced by $\approx 14\,\%$. 5
2.3 Relative change in air density for common deviations from ICAO standard conditions (15 °C, sea level, 1013 hPa, dry air). Negative values indicate reduced density and less aerodynamic drag. Altitude and temperature are the dominant factors; humidity is negligible ($< 2\,\%$). 6
2.4 Schematic trajectory comparison for a 6.5 mm 140 gr VLD bullet ($B_C = 0.311$ G7, $v_0 = 2700$ fps) under different atmospheric conditions. The spread between extreme conditions exceeds 1 m at 1000 m (> 3 MOA), demonstrating the necessity of atmospheric corrections for long-range shooting. Curves are polynomial approximations scaled by density ratio. 7

3.1 The thermodynamic system of a rifle cartridge. Expanding gases from burning propellant create immense pressure P that forces the bullet down the bore. . 9

4.1 Transitional ballistics: The bullet exiting the muzzle gets overtaken by rapidly expanding, supersonic propellant gases. A symmetrical gas release here is paramount to precision (a tight group). 15

5.1 Schematic drag coefficient vs. Mach number for G1 and G7 reference projectiles. 18
5.2 Schematic silhouettes of three reference projectiles (nose to the right). The blunt, flat-based G1 differs markedly from a modern match bullet, whereas the long boat-tailed G7 closely matches it; G8 shares the G7 nose but keeps a flat base. 20
5.3 Drag coefficient of the G1 and G7 reference shapes versus Mach number (G7 values from Table 5.2; G1 representative BRL data). Both rise sharply through the transonic region, but the slender G7 has a markedly lower, flatter peak—the physical reason its B_C stays nearly constant across the supersonic range. 20

6.1 Decomposition of the total wind vector into range (w_x) and lateral (w_z) components. Only the w_z component causes side-to-side deflection. 27

8.1 The Earth-fixed inertial frame versus the bullet's Body-fixed frame. As the bullet pitches and yaws, the body frame rotates independently of the earth frame. 35

Notation and Conventions

Throughout this manual, the following conventions are used:

Symbol	Meaning	Typical Units
m	Projectile mass	gr or kg
d	Projectile caliber (diameter)	in or m
v, $\boldsymbol{v}$	Velocity (scalar, vector)	ft/s or $\frac{\text{m}}{\text{s}}$
v_0	Muzzle velocity	ft/s or $\frac{\text{m}}{\text{s}}$
C_D	Drag coefficient (dimensionless)	—
B_C	Ballistic coefficient	$\frac{\text{lbf}}{\text{in}^2}$
SD	Sectional density $= m/d^2$	$\frac{\text{lbf}}{\text{in}^2}$
i or FF	Form factor (dimensionless)	—
ρ	Air density	$\frac{\text{kg}}{\text{m}^3}$
A	Cross-sectional area $= \pi d^2/4$	m^2
g	Gravitational acceleration	$\frac{\text{m}}{\text{s}^2}$
Ma	Mach number $= v/a$	—
a	Local speed of sound	$\frac{\text{m}}{\text{s}}$
T	Temperature	K, °C, or °F
P	Barometric pressure	hPa or in Hg
H	Relative humidity	%
θ	Launch (elevation) angle	° or mil
ϕ	Latitude	°
ψ	Azimuth (heading)	°
ω_E	Earth's angular velocity	$7.2921 \times 10^{-5}\ \frac{\text{rad}}{\text{s}}$
S_g	Gyroscopic stability factor	—
τ	Twist rate	in. per turn
r	Range	yd or m
Δy	Vertical drop	in or m
E_k	Kinetic energy	J or ft·lbf

Default values. Parameters shown in [default: blue brackets] indicate default values used when the specific value is unknown. These are based on ICAO standard atmosphere and common competition shooting conditions.

Unit systems. All derivations use SI units internally. Conversion factors to Imperial units (grains, feet per second, inches, etc.) are provided throughout.

Chapter 1

Introduction to Competition Rifle Ballistics

1.1 Motivation: Why Math Matters in Marksmanship

When firing a rifle at a target 100 yards away, marksmanship is almost entirely about human mechanics: trigger control, breathing, and steady hold. However, as the range stretches to 1,000 yards and beyond, marksmanship transforms into applied physics. A perfectly executed trigger pull is mathematically guaranteed to miss if the shooter has not correctly accounted for the temperature of the air, the spin of the earth, or the aerodynamic decay of their bullet.

This manual is written for the shooter who wants to stop guessing and start calculating.

1.2 Scope and Purpose

This manual provides a rigorous mathematical treatment of the ballistic phenomena relevant to precision rifle competition, including but not limited to: F-Class, Palma, Benchrest, PRS (Precision Rifle Series), NRL (National Rifle League), High-Power, and long-range target shooting. The goal is to equip the competitive shooter with both the theoretical foundations and the practical computational tools needed to predict bullet trajectories to the highest possible accuracy.

Competition shooting demands sub-MOA accuracy at distances often exceeding 1000 yd. At these ranges, small errors in modeling atmospheric drag, spin drift, Coriolis deflection, or wind become dominant factors in the miss distance. This manual addresses each of these systematically.

1.3 Overview of Ballistic Phases

The flight of a bullet from ignition to impact is conventionally divided into four phases [McCoy, 2012]:

1. **Interior Ballistics** — The physics of the bullet inside the barrel, from primer ignition through propellant combustion to muzzle exit. Key outputs: muzzle velocity, chamber pressure, barrel time.
2. **Transitional (Intermediate) Ballistics** — The brief phase as the bullet exits the muzzle and the propellant gases dissipate. Muzzle blast interaction, base drag changes, and initial yaw (tip-off) are determined here.
3. **Exterior Ballistics** — The free-flight trajectory from muzzle to target. This is the dominant focus of competition ballistics: aerodynamic drag, gravity drop, wind deflection, spin drift, Coriolis and Eötvös effects, Magnus force, and aerodynamic jump.

4. **Terminal Ballistics** — Bullet behavior at impact. While less critical for paper-target competition, terminal effects matter for steel-target energy requirements and for hunting-oriented competitions.

1.4 Historical Context

The mathematical study of projectile motion dates to Galileo and Newton, but modern exterior ballistics began with the work of Bashforth, who conducted some of the earliest systematic drag measurements [Bashforth, 1873]. The Siacci method (1880s) introduced the concept of the ballistic coefficient and drag functions that remain in use today [Siacci, 1888]. In the 20th century, the US Army Ballistic Research Laboratory (BRL) at Aberdeen Proving Ground produced the definitive drag function tables—G1 through G8—that form the backbone of modern ballistic computation [McCoy, 2012, Ingalls, 1886].

Modern computational ballistics, exemplified by solvers such as those described by Litz [2015a] and implemented in software like Bryan Litz's Applied Ballistics suite, use 3-DOF and 6-DOF point-mass models with empirically measured drag data and atmospheric corrections.

Chapter 2

Atmospheric Model

The atmosphere is the invisible medium through which the bullet travels. In a vacuum, a bullet would follow a perfect parabola. In reality, the air acts as a viscous fluid that constantly robs the bullet of its kinetic energy, slowing it down and exposing it to wind. Accurate modeling of air density, speed of sound, and viscosity is the absolute prerequisite to all exterior ballistic calculations.

2.1 Motivation: Why Air Density is King

A shooter might carefully measure their muzzle velocity and bullet weight, but fail to account for the environment. The primary motivation for using a precise atmospheric model is that the environment dynamically changes the aerodynamic drag fighting the bullet.

To understand this, consider the fundamental aerodynamic drag force equation. Before we present it, let's clearly define the physical quantities involved:

- F_{drag}: The drag force opposing the bullet's motion (measured in Newtons, N).
- ρ (rho): The mass density of the air the bullet is currently flying through (measured in $\frac{\text{kg}}{\text{m}^3}$).
- C_d: The drag coefficient, a dimensionless number characterizing how "slippery" the bullet is.
- A: The frontal cross-sectional area of the bullet (measured in m^2).
- v: The velocity of the bullet relative to the surrounding air mass (measured in $\frac{\text{m}}{\text{s}}$).

With these defined, the drag force is expressed as:

$$F_{\text{drag}} = \frac{1}{2}\rho\, C_d\, A\, v^2 \tag{2.1}$$

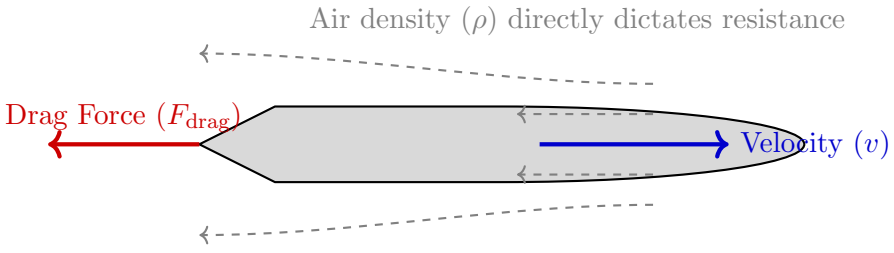

Figure 2.1: The aerodynamic drag force opposes the bullet's velocity. Notice that the force scales linearly with air density ρ.

As seen in Eq. (2.1), the drag force is *directly proportional* to the air density ρ. Consequently, a 10% error in calculating the air density results in exactly a 10% error in the computed drag. This will directly and non-linearly affect vertical drop and wind drift.

At long ranges, these effects are substantial. For example, at 1,000 meters, the difference between typical summer (hot, thin air) and winter (cold, dense air) conditions can exceed one full meter (over 3 MOA) of vertical drop for a standard competition cartridge. By understanding and actively calculating these variables, a shooter stops relying on empirical "dope cards" and can mathematically guarantee first-round hits across varying climates.

2.2 ICAO Standard Atmosphere

To have a baseline for comparison, aerodynamicists and ballisticians use the International Civil Aviation Organization (ICAO) standard atmosphere. This defines standard "sea level" conditions [International Civil Aviation Organization, 1993, U.S. Committee on Extension to the Standard Atmosphere, 1976]. Let's define the benchmark variables:

$$
\begin{aligned}
T_0 &= 288.15\,\mathrm{K} \quad (15\,^\circ\mathrm{C}, 59\,^\circ\mathrm{F}) \quad \text{(Standard Temperature)} \\
P_0 &= 101\,325\,\mathrm{Pa} \quad (29.92\ \text{in Hg}) \quad \text{(Standard Pressure)} \\
\rho_0 &= 1.2250\,\frac{\mathrm{kg}}{\mathrm{m}^3} \quad \text{(Standard Density)} \\
a_0 &= 340.294\,\frac{\mathrm{m}}{\mathrm{s}} \quad (1116.45\,\mathrm{ft/s}) \quad \text{(Speed of Sound)} \\
H_0 &= 0\% \quad \text{(Relative Humidity: completely dry air)}
\end{aligned}
$$

Default values: $T_0 = 288.15$ K (15 °C), $P_0 = 101325$ Pa, $\rho_0 = 1.225$ kg/m^3, $H_0 = 0\%$.

2.2.1 Temperature Lapse Rate

Below 11 000 m (troposphere), the standard lapse rate is:

$$
T(h) = T_0 - L \cdot h, \qquad L = 0.0065\,\frac{\mathrm{K}}{\mathrm{m}}
$$

where h is the altitude above sea level in meters.

2.2.2 Pressure–Altitude Relationship

Using the barometric formula for the troposphere:

$$
P(h) = P_0 \left(\frac{T(h)}{T_0} \right)^{g_0/(L\,R_{\mathrm{air}})} = P_0 \left(1 - \frac{L\,h}{T_0} \right)^{5.2559}
$$

where $g_0 = 9.806\,65\ \frac{\mathrm{m}}{\mathrm{s}^2}$ and $R_{\mathrm{air}} = 287.0528\ \frac{\mathrm{J}}{\mathrm{kg \cdot K}}$.

Figure 2.2 shows how temperature, pressure, and density vary with altitude across the troposphere.

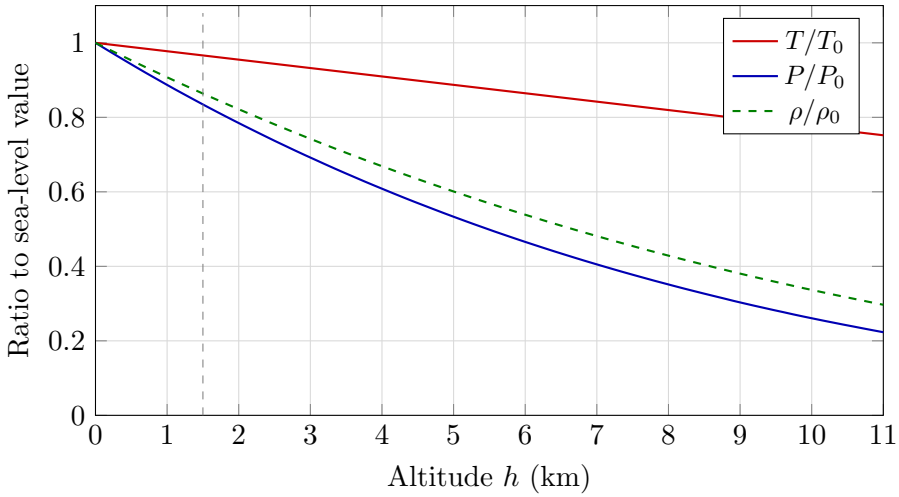

Figure 2.2: ICAO Standard Atmosphere profiles (troposphere, 0–11 km). Temperature decreases linearly at $L = 6.5$ K/km, while pressure and density follow power laws with exponents $n = 5.256$ and $n - 1 = 4.256$ respectively. The dashed vertical line marks 1500 m, a typical mountain shooting altitude where density is already reduced by $\approx 14\,\%$.

2.3 Air Density

The ideal gas law gives the dry-air density:

$$\rho_{\text{dry}} = \frac{P}{R_{\text{air}}\, T}$$

2.3.1 Humidity Correction

Humid air is *less dense* than dry air because water vapor ($M_w = 18.015\ \frac{\text{g}}{\text{mol}}$) is lighter than diatomic nitrogen ($M_{N_2} = 28.014\ \frac{\text{g}}{\text{mol}}$) and oxygen ($M_{O_2} = 31.998\ \frac{\text{g}}{\text{mol}}$).

The saturation vapor pressure (August–Roche–Magnus formula):

$$e_s(T) = 6.1078 \times 10^{\frac{7.5\,(T-273.15)}{T-35.85}} \quad \text{[hPa]}$$

The partial pressure of water vapor:

$$e = \frac{H}{100}\, e_s(T)$$

Corrected density accounting for humidity (virtual temperature method):

$$\rho = \frac{P - 0.3780\, e}{R_{\text{air}}\, T} \tag{2.2}$$

where P is the total barometric pressure, e is the partial pressure of water vapor, T is the absolute temperature, and R_{air} is the specific gas constant for dry air.

The factor 0.3780 arises from $(1 - M_w/M_{\text{air}}) = 1 - 18.015/28.964 \approx 0.3780$.

Figure 2.3 compares the relative importance of temperature, pressure, and humidity on air density under typical field conditions.

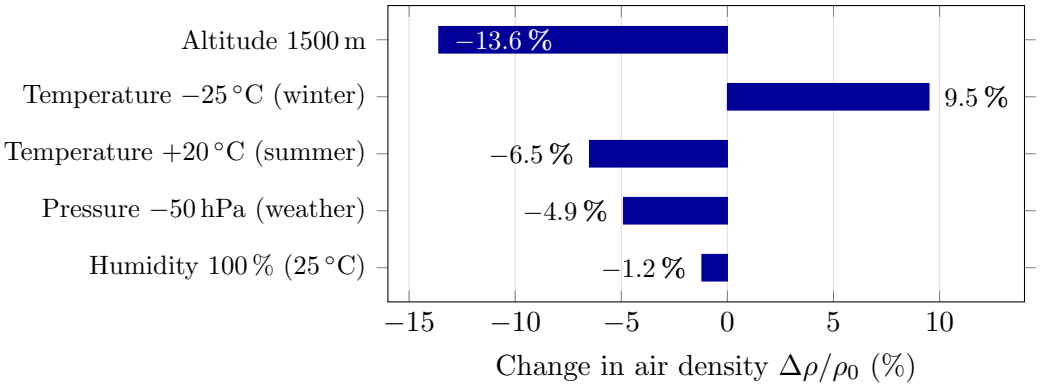

Figure 2.3: Relative change in air density for common deviations from ICAO standard conditions (15 °C, sea level, 1013 hPa, dry air). Negative values indicate reduced density and less aerodynamic drag. Altitude and temperature are the dominant factors; humidity is negligible ($< 2\,\%$).

2.4 Speed of Sound

The speed of sound in air depends primarily on temperature:

$$a = \sqrt{\gamma\, R_{\text{air}}\, T} = 20.0468\,\sqrt{T}$$

where $\gamma = 1.4$ is the ratio of specific heats for air.

At the ICAO standard temperature (15 °C): $a_0 = 20.0468\sqrt{288.15} = 340.29\ \frac{\text{m}}{\text{s}}$.

2.5 Density Altitude

Shooters often use density altitude (DA) as a single parameter that encapsulates the combined effects of temperature, pressure, and humidity on air density. DA is the altitude in the standard atmosphere that has the same density ρ as the actual conditions:

$$\text{DA} = \frac{T_0}{L}\left[1 - \left(\frac{\rho}{\rho_0}\right)^{1/(n-1)}\right] \tag{2.3}$$

where T_0 is the standard sea-level temperature, ρ_0 is the standard sea-level density, L is the temperature lapse rate, and $n = g_0/(L\,R_{\text{air}}) = 5.2559$.

With the ICAO values ($T_0/L = 44\,330.77\,\text{m} = 145\,442.16\,\text{ft}$, $1/(n-1) = 0.234969$), Eq. (2.3) gives the form used by shooters' calculators:

$$\text{DA} \approx 145442.16\left(1 - \left(\frac{\rho}{\rho_0}\right)^{0.234969}\right) \quad \text{[feet]}$$

Figure 2.4 illustrates the practical impact of atmospheric conditions on trajectory for a typical competition cartridge.

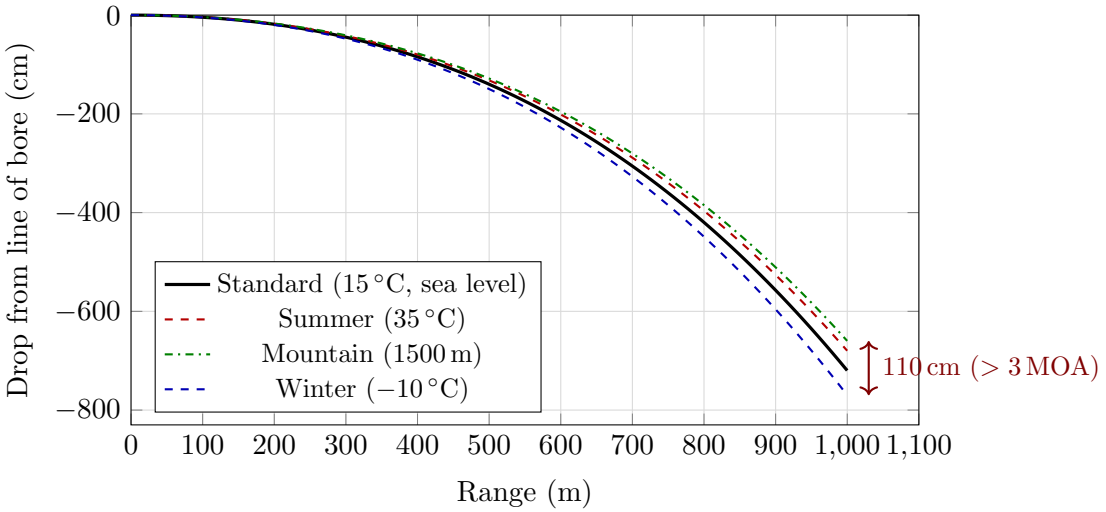

Figure 2.4: Schematic trajectory comparison for a 6.5 mm 140 gr VLD bullet ($B_C = 0.311$ G7, $v_0 = 2700$ fps) under different atmospheric conditions. The spread between extreme conditions exceeds 1 m at 1000 m (> 3 MOA), demonstrating the necessity of atmospheric corrections for long-range shooting. Curves are polynomial approximations scaled by density ratio.

2.6 Julia Implementation: Atmospheric Model

```julia
# See CompetitionBallistics.jl, module Atmosphere
# Key functions:
#   std_temperature(h)            -> T [K]
#   std_pressure(h)               -> P [Pa]
#   air_density(; P, T, H)        -> rho [kg/m^3]
#   speed_of_sound(T)             -> a [m/s]
#   density_altitude(rho)         -> DA [m]
#   saturation_vapor_pressure(T)  -> e_s [Pa]
```

Listing 2.1: Atmospheric model in Julia

Chapter 3

Interior Ballistics

3.1 Motivation: The Engine of the Bullet

Before a bullet can fight the wind or drop over a thousand yards, it must be launched. Interior ballistics is the study of what happens inside the rifle's chamber and barrel from the moment the firing pin strikes the primer until the bullet exits the muzzle. It governs the brutal and violent conversion of chemical energy stored in the gunpowder (propellant) into the kinetic energy of the projectile.

For the competition shooter, interior ballistics dictates the two most important initial conditions of any shot:

1. **Muzzle Velocity (v_0)**: The speed at which the bullet leaves the barrel.
2. **Consistency (SD and ES)**: The Standard Deviation and Extreme Spread of that velocity across multiple shots. A high extreme spread guarantees vertical stringing (missing high or low) at extended ranges, rendering all exterior ballistic math mathematically pointless.

To understand how a cartridge achieves a specific muzzle velocity, we must treat the rifle chamber as a high-pressure thermodynamic engine.

Online implementation (note). A web implementation of the 0D model below (a Gordon's Reloading Tool–style solver) is available on Tireur.org. It is intended strictly as an *educational* tool: validation against published manufacturer data shows that it currently *under-predicts* both peak pressure and muzzle velocity, so it should be used to study trends—not for absolute load development [Channel, 2021]. Always verify any charge against official manufacturer data.

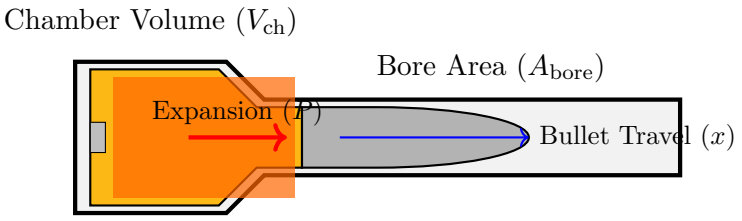

Figure 3.1: The thermodynamic system of a rifle cartridge. Expanding gases from burning propellant create immense pressure P that forces the bullet down the bore.

3.2 The Thermodynamic Problem

3.2.1 Noble–Abel Equation of State

When gunpowder burns, it creates gas. At the extreme pressures found in a rifle chamber (often exceeding 60,000 PSI or 400 MPa), these gases are packed so tightly that they deviate

significantly from the "ideal gas" behavior taught in high school physics ($PV = nRT$). The gas molecules themselves take up physical space!

To account for this, we use the Noble–Abel equation [Corner, 1950, Carlucci and Jacobson, 2008], which introduces an "excluded volume" or co-volume:

$$P\,(V - \eta) = n\,R_u\,T_g$$

Let's define these variables:

- P: The chamber pressure of the expanding gas.
- V: The total volume available for the gas to occupy (chamber volume plus barrel volume behind the bullet).
- η (eta): The total co-volume, representing the physical space the gas molecules occupy ($\eta = n \cdot b$).
- n: The number of moles of gas produced.
- R_u: The universal gas constant ($8.3145\,\frac{\mathrm{J}}{\mathrm{mol \cdot K}}$).
- T_g: The absolute temperature of the propellant gas.

By subtracting the co-volume η from the total volume V, the Noble-Abel equation prevents the gas pressure from inaccurately dropping to zero.

3.2.2 Energy Balance

The first law of thermodynamics applied to the propellant–projectile system:

$$Q_{\text{prop}} = E_k + E_{\text{heat}} + E_{\text{friction}} + E_{\text{gas KE}} + E_{\text{residual}}$$

The total chemical energy released by the propellant charge:

$$Q_{\text{prop}} = C \cdot f \cdot z$$

where C is the charge mass, f is the impetus (force constant, energy per unit mass), and z is the fraction of charge burned ($0 \le z \le 1$).

3.3 Simplified Closed-Bomb Model

In a closed bomb (no projectile motion), the pressure is:

$$P = \frac{C\,f\,z}{V_{\text{ch}} - C\,(1 - z)/\rho_p - C\,z\,\eta_{\text{sp}}}$$

where V_{ch} is the chamber volume, ρ_p is the solid propellant density, and η_{sp} is the specific co-volume.

3.4 Burn Rate Law

The rate of gas generation follows a geometric burn rate law. For a single-perforated cylindrical grain:

$$\frac{\mathrm{d}z}{\mathrm{d}t} = \frac{S(z)}{V_g(z)}\,\beta\,P^n$$

For small arms propellants, the empirical Vieille law [Corner, 1950] is commonly used:

$$r_b = \beta\,P^n$$

where r_b is the linear regression rate ($\frac{\mathrm{m}}{\mathrm{s}}$), and typical values are $n \approx 0.6$–0.9.

3.4.1 Geometric Form Function

For common grain geometries, the fraction burned z relates to the linear fraction burned $\xi = e/e_0$ through a form function:

$$z(\xi) = \xi\,(1 + \theta\,\xi)$$

where θ is the form factor: $\theta = 0$ for a slab, $\theta > 0$ for progressive, and $\theta < 0$ for degressive grains.

Note on software models. Production tools such as GRT and QuickLOAD extend this classical framework with proprietary, calibrated sub-models—notably a multi-stage form function (three stages in GRT versus two in QuickLOAD) and detailed energy-loss and effective-mass (Lagrange/Sebert) terms—fitted to closed-bomb and ballistic measurements [Corner, 1950, Kneubühl, 2018, Channel, 2021, Anderson and Fickie, 1987]. These calibrated internals are not fully published; the equations above are the open, literature-based formulation.

3.5 Le Duc Velocity Model

Le Duc's hyperbola approximates the velocity of the projectile as a function of its travel. It was taught at the French artillery school of Fontainebleau [Challéat, 1904] and used by the U.S. Navy after Alger [1911]:

$$v(x) = \frac{a\,x}{b + x} \tag{3.1}$$

where x is the projectile travel from its seated position and a, b are constants. As $x \to \infty$, $v \to a$: a is the velocity in a barrel of infinite length, and $v(b) = a/2$.

3.6 Pressure–Travel Relationship

Differentiating Eq. (3.1) gives the acceleration $\mathrm{d}v/\mathrm{d}t = v\,\mathrm{d}v/\mathrm{d}x = a^2 b\,x/(b + x)^3$. The pressure this acceleration requires depends on where it is taken along the gas column, since the gas behind the projectile must be accelerated too. Under the Lagrange approximation, where the gas velocity varies linearly from zero at the breech face to v at the projectile base, the breech pressure p_B and the space-mean pressure $\bar{p}$ are related to the base pressure p_S by [Carlucci and Jacobson, 2008, p. 71, eqs. 3.54 and 3.59]

$$p_B = p_S\left(1 + \frac{C}{2m}\right), \qquad \bar{p} = p_S\left(1 + \frac{C}{3m}\right)$$

where m is the projectile mass and C the charge mass. Writing m_p for $m + C/2$ (breech), $m + C/3$ (space-mean) or m (base), the pressure along the travel is

$$P(x) = \frac{m_p}{A_{\mathrm{bore}}}\,v\,\frac{\mathrm{d}v}{\mathrm{d}x} = \frac{m_p\,a^2\,b\,x}{A_{\mathrm{bore}}\,(b + x)^3}$$

with $A_{\mathrm{bore}} = \pi d^2/4$. The peak occurs at $x_{\max} = b/2$, where $v = a/3$:

$$P_{\max} = \frac{4\,m_p\,a^2}{27\,A_{\mathrm{bore}}\,b} \tag{3.2}$$

Load data and C.I.P. or SAAMI limits give the chamber pressure, so the companion libraries default to the breech, $m_p = m + C/2$ (`at = :breech` in Julia, `at: 'breech'` in JavaScript).

For a .308 Winchester with 47.5 gr under a 130 gr bullet, $1 + C/2m = 1.18$. Written with the projectile mass alone, Alger's formulas give the pressure on the base; he put the chamber pressure, where gauges read it, 15 to 20 % higher, and Patterson [1912] 12 %, both on naval guns. The effective mass $m + C/3$ often used for the kinetic energy of projectile and gas belongs to the space-mean pressure, not to the chamber pressure.

3.6.1 Anchoring on Load Data

The constants are not known in advance. The site's estimators take them from a muzzle velocity v_0 at travel L and a peak pressure $P_{\max}$. The condition $v(L) = v_0$ gives $a = v_0(b + L)/L$, and Eq. (3.2) becomes the quadratic

$$K b^2 + (2KL - 1)\, b + KL^2 = 0, \qquad K = \frac{4\, m_p\, v_0^2}{27\, A_{\text{bore}}\, P_{\max}\, L^2}$$

Its two roots have the product L^2. The smaller one puts the peak in the first half of the travel and is the one retained (`leduc_anchor`). Real roots exist only if $P_{\max} \geq (16/27)\, m_p v_0^2/(A_{\text{bore}} L)$.

Example, from the Reload Swiss 2025 guide [Reload Swiss, 2025]: .308 Winchester, Fox Bullets 130 gr (the guide names no model), 47.5 gr of RS52, 928 $\frac{\text{m}}{\text{s}}$ and 3548 bar from a 600 mm barrel, hence 548.8 mm of travel behind a 51.2 mm case. Then $a = 1108\ \frac{\text{m}}{\text{s}}$ and $b = 106.3$ mm: the chamber pressure peaks at 53 mm of travel and falls to 528 bar at the muzzle. On the base, the peak is 3000 bar.

3.6.2 Limits

- Two constants fix only a shape. On an instrumented 5.56×45 test barrel, with the curve anchored in the same way on the measured muzzle velocity and peak case-mouth pressure, the measured pressure peaked near 3 cm of travel against 4.4 cm for the curve. After the peak the curve fell below the measurement: about 520 bar at the muzzle against 900 [Yoon et al., 2010]. This rests on a single shot. A muzzle pressure should not be read off the curve.
- Anchored on the C.I.P. pressure and used to transfer a velocity to a shorter barrel, the curve was tested on 27 cut-down series, 25 of them by Marr [Marr, 2013–2018]. Its median error, 35 and 31 ft/s on the reference and validation sets, against 41 and 42 ft/s for the fixed exponent of Eq. (3.3), is not a significant difference cartridge by cartridge. Powley's expansion ratio does better in the median; Le Duc's hyperbola does better where velocity flattens out beyond 24 inches (6 mm and 6.5 Creedmoor).

3.7 Muzzle Velocity Estimation for Handloaders

An empirical power law relates muzzle velocity to barrel length:

$$v_0 \approx v_{\text{ref}} \left(\frac{L_{\text{barrel}}}{L_{\text{ref}}} \right)^k \tag{3.3}$$

Measured cut-down tests put k near 0.18–0.20 for the .308 Winchester. Marr [2014] cut one barrel from 28 to 16.5 inches with four loads (147 to 180 gr): from the published end velocities, $k = 0.176$ to 0.196, or 20.9 ft/s to 24.6 ft/s per inch. Other cartridges spread much wider. Over 19 published cut-down series on eight cartridges, between 31 and 16 inches [Marr, 2013–2018], least-squares fits give k from 0.11 to 0.31, median 0.17: low for the 7.62×39, 6.5 Creedmoor and 6 mm Creedmoor (0.11–0.16), 0.15–0.18 for the .224 Valkyrie,

near 0.18 for the .223 Remington and .308 Winchester, high for the .300 Winchester Magnum (0.26) and the .243 Winchester (0.26–0.31, end points only). Two loads in the same rifle can differ by 0.05 (.243 Winchester), four loads in one 7 mm Rem. Mag. barrel by 0.09, and some series flatten out beyond 24 inches. A default exponent therefore gives an order of magnitude; a second measured point on the actual rifle gives k. The companion libraries (Julia and JavaScript) default to this median, $k = 0.17$. The site's estimators apply instead, to rifle cartridges, Powley's expansion-ratio rule, $v_0 \propto \sqrt{1 - R^{-1/4}}$ with $R = 1 + Ax/U$ (x bullet travel, U usable case capacity), in the form of the kwk.us calculator [kwk.us]. Tested on 45 cut-down series, it predicted the shorter barrels better than a fixed exponent on 17 of 20 rifles, including all seven barrels of three experimenters other than Marr [Hodgdon Powder Company, 2026, Eagleman Long Range, 2023, AccurateShooter.com, 2011]; the gain is small near the .308's expansion ratio and large on magnums. Handgun cartridges keep the power law, with $k = 0.15$ on bullet travel. The companion libraries provide this rule as `powley_barrel_correction` (Julia) and `powleyBarrelCorrection` (JavaScript).

As a practical validation of Eq. (3.3), consider measured data for the .308 Winchester with Lapua 155 gr Scenar ammunition:

Table 3.1: Measured muzzle velocity vs. barrel length, .308 Win / Lapua 155 gr Scenar

Barrel length (in)	v_0 **(m/s)**	v_0 **(fps)**
20	820	2690
24	845	2772
26	860	2822

This yields about 6.7 $\frac{\text{m}}{\text{s}}$ (22 ft/s) per inch between 20 and 26 inches, and an exponent $k = 0.18$, in line with the cut-down tests above; the former default, $k = 0.27$, would predict 2887 ft/s at 26 inches instead of the 2822 ft/s in the table. The origin of these three values is not recorded. Note that the gain per inch diminishes with longer barrels, as the propellant gas expansion cools and pressure drops.

3.7.1 Temperature Sensitivity of Muzzle Velocity

Propellant burn rate is temperature-dependent. The temperature coefficient:

$$\Delta v_0 = \sigma_T \, \Delta T \tag{3.4}$$

where σ_T is the temperature sensitivity coefficient, which depends on the propellant. One published test [Zant and Middlebrook, 2016] heated and cooled 6.5×47 Lapua ammunition between 25 °F and 140 °F (a 115 °F swing): Hodgdon H4350 changed by 25 ft/s ($\sigma_T \approx$ 0.22 fps/°F), Hodgdon Varget by 46 ft/s (0.40), IMR 4166 by 47 ft/s (0.41) and IMR 4451 by 68 ft/s (0.59 fps/°F). Powders not designed for temperature stability are not part of that test.

[default: $\sigma_T = 1.0$ velocity unit per degree — a placeholder, above every value measured in the test above]

Chapter 4

Transitional Ballistics

4.1 Motivation: The Chaos of the Muzzle

Transitional (or intermediate) ballistics covers the violent and chaotic fraction of a millisecond between interior ballistics (the barrel) and exterior ballistics (free flight). It represents the exact moment the bullet exits the protective confinement of the muzzle and punches into the atmosphere.

Why does a shooter care about this microsecond? Because this is where the bullet is most vulnerable. A perfectly loaded cartridge and a perfectly aimed rifle can be completely ruined by a bad muzzle crown or inconsistent gas release, which will instantly destabilize the bullet before its flight even begins.

4.2 Muzzle Gas Dynamics

When the bullet finally unplugs the barrel, the high-pressure propellant gases (still trapped behind the bullet at pressures of 10–70 MPa) suddenly vent into the atmosphere. Because these gases are incredibly hot and highly pressurized, they expand outward at velocities *faster* than the bullet itself. The bullet is essentially blasted from behind by its own exhaust.

This creates a complex and turbulent shock-wave structure just inches in front of the muzzle [Carlucci and Jacobson, 2008]:

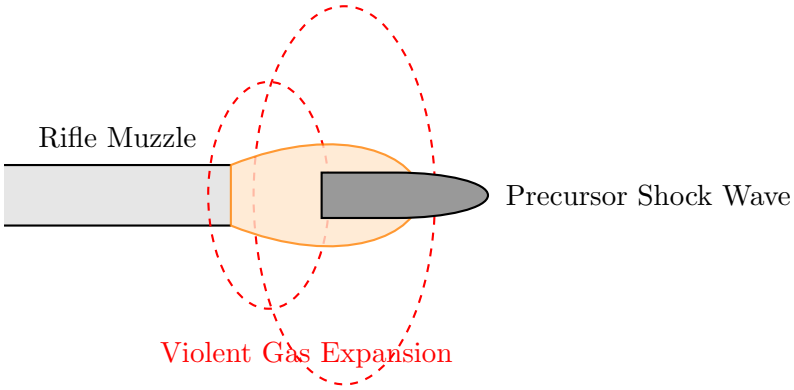

Figure 4.1: Transitional ballistics: The bullet exiting the muzzle gets overtaken by rapidly expanding, supersonic propellant gases. A symmetrical gas release here is paramount to precision (a tight group).

The structure consists of:

1. **Muzzle blast wave**: A spherical shock radiating outward (the "bang" you hear).
2. **Precursor blast**: Produced from the column of air that was compressed ahead of the bullet inside the barrel.

3. **Bottle shock**: The characteristic diamond-pattern Mach disk structure formed by the underexpanded supersonic gas jet accelerating past the bullet.

4.3 Muzzle Tip-Off and Initial Yaw

The concept of "tip-off" is critical. If the muzzle crown is damaged, or if the bullet's base is not perfectly square, the escaping gases will vent asymmetrically.

Let's define the variables for this instability:

- ω (omega): The angular velocity or "tip-off rate" imparted to the bullet ($\frac{\text{rad}}{\text{s}}$).
- α_0 (alpha zero): The initial yaw angle of the bullet as it exits the muzzle (degrees).

Asymmetric gas forces impart a small angular velocity (ω). The resulting initial yaw angle α_0 is typically small (0.5°–3°) for match-grade ammunition. However, any yaw at the muzzle drastically increases early aerodynamic drag and causes the bullet to precess (wobble) in flight, opening up group sizes.

4.4 Base Drag Transition

Inside the barrel, the base of the bullet is pushed forward by thousands of PSI of pressure. The moment it exits, this high pressure rapidly drops to the ambient atmospheric pressure, creating a sudden vacuum effect behind the bullet. This causes *base drag* to increase significantly, transitioning from a suppressed value to its full free-flight aerodynamic penalty over a distance of approximately 5–20 calibers from the muzzle [McCoy, 2012].

4.5 Crown Effects

Because of this violent gas transition, the muzzle crown (the final machined edge at the barrel's exit) is one of the most critical parts of the rifle. It must be perfectly concentric and perpendicular to the bore axis to ensure gases release symmetrically around the entire circumference of the bullet base at the exact same microsecond.

Chapter 5

Exterior Ballistics: Core Theory

5.1 Motivation: The Math of Free Flight

Once the bullet escapes the muzzle, all active propulsion ceases. The projectile enters "free flight." From this point until it strikes the target, the bullet's path is entirely at the mercy of classical physics. Exterior ballistics is the mathematical prediction of this flight path. For a competitive shooter, this is the core of their craft: translating the laws of physics into correct scope dial adjustments.

To predict where a bullet will land, we must solve equations of motion that account for two primary forces:

1. **Gravity**: Continually accelerating the bullet toward the earth, determining "drop."
2. **Aerodynamic Drag**: The immense friction of the air, rapidly bleeding off the bullet's velocity and magnifying the time gravity has to act.

5.2 Vacuum Trajectory (The Baseline)

Before conquering air resistance, we must understand the baseline system. In a perfect vacuum (ignoring air resistance), the trajectory is a simple parabola. While this model is *useless for real-world rifle ballistics* (because supersonic drag dominates behavior), it serves as a mathematical foundation.

Let's define the fundamental launch parameters:

- t: Time elapsed since the bullet left the muzzle (seconds, s).
- v_0: Initial muzzle velocity (e.g., $\frac{\text{m}}{\text{s}}$ or ft/s).
- θ (theta): The launch elevation angle, or "look-up" angle of the barrel relative to the horizontal.
- g: Standard gravitational acceleration ($9.806\,65\,\frac{\text{m}}{\text{s}^2}$).
- $x(t)$: The horizontal distance traveled at time t.
- $y(t)$: The vertical height of the bullet at time t.

Using basic Newtonian mechanics, the parametric equations of motion in a vacuum are:

$$x(t) = v_0 \cos\theta \cdot t \tag{5.1}$$

$$y(t) = v_0 \sin\theta \cdot t - \frac{1}{2} g\, t^2 \tag{5.2}$$

Eliminating time t from Eq. (5.1) and substituting it into Eq. (5.2) yields the single continuous trajectory equation in terms of horizontal distance x:

$$\boxed{y(x) = x \tan\theta - \frac{g x^2}{2 v_0^2 \cos^2\theta}}$$

The range in vacuum:

$$R_{\text{vac}} = \frac{v_0^2 \sin 2\theta}{g}$$

5.3 Aerodynamic Drag

5.3.1 The Drag Equation

The aerodynamic drag force opposes the bullet's motion through the air:

$$\boxed{F_D = \frac{1}{2}\,\rho\, v^2\, C_{\text{D}}(Ma)\, A}$$

The drag deceleration:

$$a_D = \frac{F_D}{m} = \frac{\rho\, v^2\, C_{\text{D}}\, A}{2\, m}$$

5.3.2 Drag Coefficient and Mach Number

The drag coefficient C_{D} is fundamentally a function of Mach number $Ma = v/a$, Reynolds number Re, and projectile geometry. For small-arms bullets, Re effects are secondary, and C_{D} is treated as a function of Ma alone [McCoy, 2012].

The C_{D}–Ma curve has characteristic regimes: subsonic ($Ma \lesssim 0.9$) with low, nearly constant C_{D}; transonic ($0.9 \lesssim Ma \lesssim 1.2$), where the flow around the bullet is partly subsonic and partly supersonic, with a sharp rise; and supersonic ($Ma \gtrsim 1.2$) with gradually decreasing C_{D}. The bounds depend on the projectile shape: for the caliber .50 M33 ball bullet, spark shadowgraphs show the first locally supersonic flow at Mach 0.89, the low end of the transonic region, and an everywhere-supersonic flow, except near the nose tip, at Mach 1.24 [McCoy, 2012, p. 58].

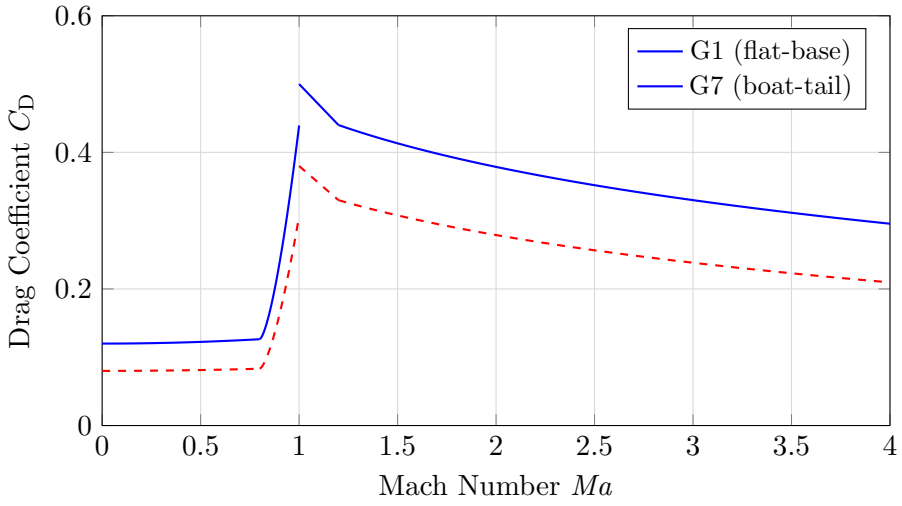

Figure 5.1: Schematic drag coefficient vs. Mach number for G1 and G7 reference projectiles.

5.3.3 Analytical Solution for 1D Drag

While modern ballistics requires numerical integration (see Section 5.8), a simplified 1D model where C_{D} is assumed constant provides useful insights into the scaling of range and velocity with respect to the ballistic coefficient.

Consider purely horizontal motion with drag as the only force:

$$\frac{\mathrm{d}v}{\mathrm{d}t} = -k\,v^2, \quad \text{where } k = \frac{\rho\,C_\mathrm{D}\,A}{2\,m}$$

Separating variables and integrating:

$$\int_{v_0}^{v} \frac{\mathrm{d}v'}{(v')^2} = -k \int_0^t \mathrm{d}t' \implies -\left[\frac{1}{v'}\right]_{v_0}^{v} = -k\,t$$

The velocity as a function of time is:

$$\boxed{v(t) = \frac{v_0}{1 + k\,v_0\,t}} \tag{5.3}$$

Integrating once more to find the distance $x(t)$:

$$x(t) = \int_0^t \frac{v_0}{1 + k\,v_0\,t'}\mathrm{d}t' = \frac{1}{k}\ln(1 + k\,v_0\,t)$$

Solving for t in terms of x:

$$t = \frac{e^{kx} - 1}{k\,v_0}$$

Substituting this into Eq. (5.3) yields the velocity as a function of distance:

$$\boxed{v(x) = v_0 e^{-kx}}$$

This exponential decay demonstrates how the "Physics BC" (contained within k) determines the velocity retention of the projectile.

5.4 Ballistic Coefficient

The ballistic coefficient B_C is defined as:

$$\boxed{B_\mathrm{C} = \frac{\mathrm{SD}}{i} = \frac{m}{i\,d^2}}$$

where $\mathrm{SD} = m/d^2$ is the sectional density and i is the form factor:

$$i(Ma) = \frac{C_\mathrm{D}^{\mathrm{bullet}}(Ma)}{C_\mathrm{D}^{\mathrm{std}}(Ma)}$$

B_C is only meaningful when referenced to a specific drag model (G1, G7, etc.).

5.4.1 Standard Conditions for BC

By convention, B_C values are quoted at standard atmosphere conditions. To use B_C at non-standard conditions:

$$B_{C\,\mathrm{actual}} = B_{C\,\mathrm{std}} \cdot \frac{\rho_0}{\rho_\mathrm{actual}}$$

5.5 Standard Drag Models (G1 through G8)

Table 5.1: BRL Standard Drag Models [McCoy, 2012, Ingalls, 1886]

Model	Reference Projectile Shape	Primary Use
G1	Flat-base with 2-caliber ogive nose	Traditional default; hunting bullets
G7	Long, secant-ogive, boat-tail	**Best for modern VLD match bullets**
G8	Similar to G7 with flat base	Flat-base match bullets
GL	Blunt-nose lead bullet	Cast lead bullets

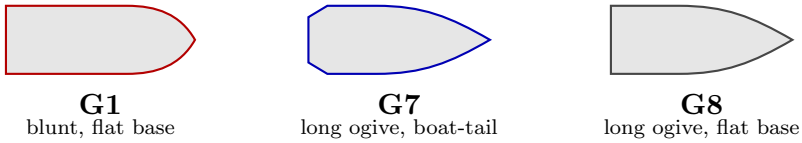

Figure 5.2: Schematic silhouettes of three reference projectiles (nose to the right). The blunt, flat-based G1 differs markedly from a modern match bullet, whereas the long boat-tailed G7 closely matches it; G8 shares the G7 nose but keeps a flat base.

For competition rifle shooting, G7 is strongly preferred over G1 for modern VLD boat-tail bullets because the G7 reference shape more closely matches these bullets, resulting in a form factor i closer to 1.0 and a more constant B_C across the velocity range [Litz, 2015a, p. 23].

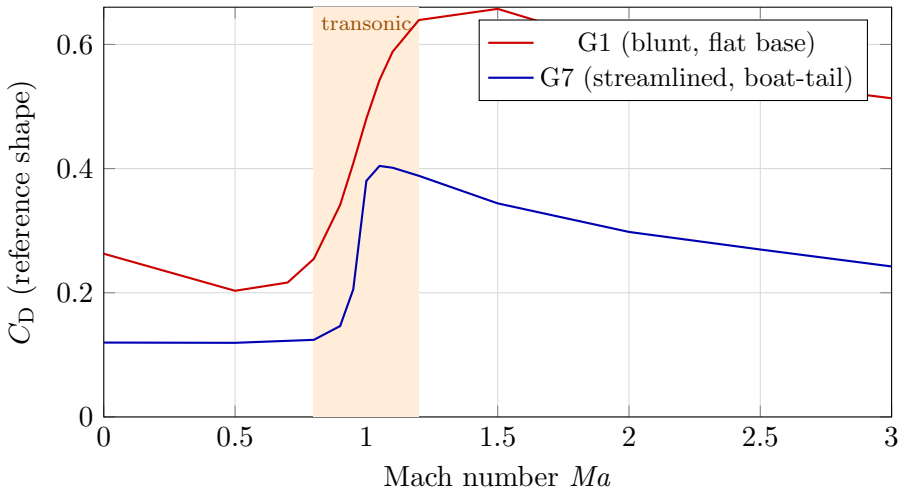

Figure 5.3: Drag coefficient of the G1 and G7 reference shapes versus Mach number (G7 values from Table 5.2; G1 representative BRL data). Both rise sharply through the transonic region, but the slender G7 has a markedly lower, flatter peak—the physical reason its B_C stays nearly constant across the supersonic range.

5.5.1 G7 Drag Function

Table 5.2: Selected G7 drag coefficient values [McCoy, 2012]

Ma	$C_{\mathrm{D}}^{\mathrm{G7}}$	Ma	$C_{\mathrm{D}}^{\mathrm{G7}}$	Ma	$C_{\mathrm{D}}^{\mathrm{G7}}$
0.00	0.1198	1.00	0.3803	2.00	0.2980
0.50	0.1194	1.05	0.4043	2.50	0.2697
0.80	0.1242	1.10	0.4014	3.00	0.2424
0.90	0.1464	1.20	0.3884	3.50	0.2154
0.95	0.2054	1.50	0.3440	4.00	0.1935

The values above are reproduced verbatim from the table embedded in the solver (`G7_RAW` in `CompetitionBallistics.js`); the solver interpolates this same data at run time, so the documentation and the implementation are guaranteed to agree.

5.5.2 Drag Functions vs. Siacci Tables: a Common Confusion

The $C_{\mathrm{D}}(Ma)$ tables (G1, G7, ...) are *aerodynamic* data: C_{D} is dimensionless and depends only on the projectile geometry and the Mach number, *not* on the atmosphere. They are therefore identical whether one takes them from McCoy [McCoy, 2012] or from an equivalent published tabulation. The atmosphere only enters our solver through the *actual* air density ρ and speed of sound $a(T)$, both recomputed from the ICAO model (§2.2) at every step via $D = \frac{1}{2}\rho\, C_{\mathrm{D}}(Ma)\, A\, i/m$, with $i = \mathrm{SD}/B_{\mathrm{C}}$ the form factor.

What *does* depend on the standard atmosphere are the integrated *Siacci tables* $S(V), A(V), I(V), T(V)$, because their integration involves the standard density and speed of sound. This is the well-known caveat that Siacci tables computed under the ICAO atmosphere differ from those in McCoy's book. **Our solver uses no Siacci table**—it integrates the 3-DOF equations numerically—so this caveat does not apply here.

The single genuine consistency requirement is that the user-supplied B_{C} be referenced to the same standard atmosphere as the code, namely ICAO ($\rho_0 = 1.225\,\frac{\mathrm{kg}}{\mathrm{m}^3}$, 15 °C, dry). Modern G7 values (Berger, Hornady, Litz/Applied Ballistics) are all ICAO-referenced. Older *Army Standard Metro* (ASM) B_{C} values (29.53 inHg, 78 % RH) carry a ≈ 0.4–0.5 % density offset.

Warning on Legacy Calculators: Many legacy ballistic calculators — JBM Ballistics among them, until it withdrew its online calculators in 2026 — enable the Army Standard Metro atmosphere by default. If a modern ICAO-referenced G7 BC is input into an ASM-default calculator without explicitly disabling the Metro setting, the solver will silently apply a density offset. Because ASM air is lighter than ICAO air, this introduces an artificial trajectory error that grows significantly at extended ranges. The `CompetitionBallistics` engine exclusively uses the modern ICAO standard, ensuring native 1:1 compatibility with all contemporary manufacturer BCs without requiring any error-prone conversions.

5.6 Doppler Radar Drag Measurement

The drag coefficient tables (G1, G7, etc.) originate from experimental measurements. The modern gold standard is *Doppler radar tracking*, which has largely superseded earlier spark-range and yaw-card methods [McCoy, 2012, Braun, 1958].

5.6.1 Measurement Principle

A continuous-wave (CW) Doppler radar illuminates the bullet in flight and measures the frequency shift of the reflected signal:

$$f_D = \frac{2\,v\,\cos\theta_r}{\lambda}$$

where f_D is the Doppler shift frequency, v is the bullet velocity, θ_r is the angle between the velocity vector and the radar beam, and λ is the radar wavelength. The velocity is sampled at rates of 1–10 kHz, yielding a near-continuous $v(t)$ record over the entire flight.

5.6.2 Extracting $C_{\mathrm{D}}(Ma)$ from Radar Data

From the measured velocity–time history, the drag coefficient is extracted by inverting the equation of motion. For a near-horizontal trajectory:

$$C_{\mathrm{D}}(Ma) = -\frac{2\,m}{\rho\,A\,v^2}\,\frac{\mathrm{d}v}{\mathrm{d}t}$$

The derivative $\mathrm{d}v/\mathrm{d}t$ is computed numerically from the sampled $v(t)$ data. Since numerical differentiation amplifies noise, the raw data is first smoothed using a Savitzky–Golay filter or a cubic smoothing spline before differentiation.

The Mach number at each time step is:

$$Ma(t) = \frac{v(t)}{a\big(T(h(t))\big)}$$

where a is the local speed of sound, corrected for the altitude $h(t)$ along the trajectory.

5.6.3 Advantages over Classical Methods

Doppler radar provides the complete $C_{\mathrm{D}}(Ma)$ curve from a *single firing*, whereas spark-range methods require many shots at different velocities. This is the method used by:

- The BRL/ARL at Aberdeen Proving Ground to produce the definitive G1–G8 tables.
- Bryan Litz (Applied Ballistics) to measure custom drag curves for individual bullet models, published as "CDM" (Custom Drag Model) data [Litz, 2015b].
- Military proving grounds worldwide for projectile development.

The custom drag model approach bypasses the form-factor approximation entirely: instead of $C_{\mathrm{D}} = i \cdot C_{\mathrm{D}}^{\mathrm{std}}$, the actual measured $C_{\mathrm{D}}(Ma)$ curve for the specific bullet is used directly. This eliminates the error from form-factor variation with Mach number and is the most accurate approach available.

5.6.4 Interpolation of Tabular Drag Data

Whether using the standard G1/G7 tables or a custom Doppler-derived curve, the drag coefficient must be evaluated at arbitrary Mach numbers during trajectory integration. Two interpolation methods are common:

Linear interpolation (used in many legacy solvers): Given tabular data $\{(Ma_i, C_{D,i})\}$, find the bracketing interval $[Ma_k, Ma_{k+1}]$ and compute:

$$C_{\mathrm{D}}(Ma) = C_{D,k} + \frac{C_{D,k+1} - C_{D,k}}{Ma_{k+1} - Ma_k}\,(Ma - Ma_k)$$

Linear interpolation introduces slope discontinuities at each table point. In the transonic region where C_D changes rapidly, these discontinuities can produce small but systematic trajectory errors.

Cubic spline interpolation (recommended): A natural cubic spline $S(Ma)$ is fitted through all n data points, producing a C^2-continuous curve (continuous through the second derivative). The spline on each interval $[Ma_k, Ma_{k+1}]$ is:

$$S(Ma) = a_k + b_k\,(Ma - Ma_k) + c_k\,(Ma - Ma_k)^2 + d_k\,(Ma - Ma_k)^3$$

where the coefficients $\{a_k, b_k, c_k, d_k\}$ are determined by enforcing continuity of S, S', and S'' at interior knots, plus natural boundary conditions ($S'' = 0$ at endpoints). This requires solving a tridiagonal linear system of size n, which is $O(n)$ and needs to be done only once during initialization.

Cubic spline interpolation is particularly important in the transonic region ($0.9 < Ma < 1.2$) where the C_D curve has its steepest gradient. The smooth derivative ensures that the drag force varies smoothly as the bullet decelerates through the sound barrier, eliminating artificial trajectory perturbations.

The spline is better only where the table is dense

This recommendation holds for the *standard* tables and must not be carried over to sparse measured ones. A decimation test — remove every second node, rebuild both interpolants on what remains, and score them on the removed values, whose truth is known — reverses the verdict according to the sampling:

Table	Nodes	Linear	Spline
G7 standard	65	0.099 %	**0.049 %**
G1 standard	53	0.424 %	**0.069 %**
McCoy .308 C_{D_0}	15	**0.68 %**	8.89 %
McCoy 105 mm C_{D_0}	12	**2.86 %**	6.93 %

The criterion is not "spline versus linear" but *sampling density relative to curvature*. McCoy's range-reduced tables are sparse and deliberately clustered on the transonic knee — his points sit at $Ma = 0.90, 0.95, 1.00, 1.05, 1.10, 1.20$ — so the steep rise imposes derivatives that the spline propagates as oscillation into the neighbouring intervals, where it becomes up to thirteen times worse than a straight line. The 6-DOF coefficient sets therefore read their tables *linearly*, on purpose.

The companion Julia implementation (Appendix B) provides both linear and cubic spline interpolation via the `DragModels` module. Since 2026-08-14 `drag_coefficient` defaults to the spline, matching the JavaScript port and this section; it previously defaulted to linear, in contradiction with both.

5.7 Equations of Motion: 3-DOF Point-Mass Model

5.7.1 Coordinate System

We use a ground-fixed, flat-Earth coordinate system: x (downrange), y (vertical, upward positive), z (cross-range, positive right).

5.7.2 Vector Equation of Motion

$$\boxed{m\,\frac{\mathrm{d}\boldsymbol{v}}{\mathrm{d}t} = -\frac{1}{2}\,\rho\,\|\boldsymbol{v}_{\mathrm{rel}}\|\,\boldsymbol{v}_{\mathrm{rel}}\,C_{\mathrm{D}}(Ma)\,A + m\,\boldsymbol{g}} \tag{5.4}$$

where $\boldsymbol{v}_{\mathrm{rel}} = \boldsymbol{v} - \boldsymbol{v}_{\mathrm{wind}}$ and $\boldsymbol{g} = (0, -g, 0)^T$.

5.7.3 Scalar Component Equations

$$\frac{\mathrm{d}v_x}{\mathrm{d}t} = -\frac{\rho\,C_{\mathrm{D}}\,A}{2\,m}\,v_{\mathrm{rel}}\,(v_x - w_x) \tag{5.5}$$

$$\frac{\mathrm{d}v_y}{\mathrm{d}t} = -\frac{\rho\,C_{\mathrm{D}}\,A}{2\,m}\,v_{\mathrm{rel}}\,(v_y - w_y) - g$$

$$\frac{\mathrm{d}v_z}{\mathrm{d}t} = -\frac{\rho\,C_{\mathrm{D}}\,A}{2\,m}\,v_{\mathrm{rel}}\,(v_z - w_z) \tag{5.6}$$

where $v_{\mathrm{rel}} = \sqrt{(v_x - w_x)^2 + (v_y - w_y)^2 + (v_z - w_z)^2}$.

5.7.4 Using the Ballistic Coefficient

Substituting the form factor relationship $C_{\mathrm{D}} = i \cdot C_{\mathrm{D}}^{\mathrm{std}}$ and the ballistic coefficient definition $B_{\mathrm{C}} = m/(i\,d^2)$:

$$\frac{\rho\,C_{\mathrm{D}}\,A}{2\,m} = \frac{\rho\,C_{\mathrm{D}}^{\mathrm{std}}\,\pi}{8\,B_{\mathrm{C}}}$$

where i is the projectile's form factor, $C_{\mathrm{D}}^{\mathrm{std}}$ is the drag coefficient of the standard projectile (G1 or G7), and d is the caliber.

5.8 Numerical Integration

Since the system of equations (5.5)–(5.6) has no closed-form solution due to the non-linear dependence of C_{D} on velocity, it must be solved numerically.

5.8.1 Euler Method

The simplest numerical approach is the first-order Euler method, which updates the state vector using the derivative at the beginning of each time step Δt:

$$\begin{aligned}
v_x^{n+1} &= v_x^n + \Delta t\left(-\frac{\rho\,C_{\mathrm{D}}\,A}{2\,m}\,v^n\,(v_x^n - w_x)\right)\\
v_y^{n+1} &= v_y^n + \Delta t\left(-\frac{\rho\,C_{\mathrm{D}}\,A}{2\,m}\,v^n\,(v_y^n - w_y) - g\right)\\
x^{n+1} &= x^n + v_x^n\,\Delta t\\
y^{n+1} &= y^n + v_y^n\,\Delta t
\end{aligned}$$

where $v^n = \sqrt{(v_x^n - w_x)^2 + (v_y^n - w_y)^2 + (v_z^n - w_z)^2}$. While intuitive and easy to implement, the Euler method requires very small time steps to maintain stability and accuracy.

5.8.2 Runge–Kutta (RK4) & Area Scaling

Modern ballistic solvers use higher-order methods, typically the 4th-order Runge–Kutta (RK4) method, which provides a much better balance of speed and accuracy by sampling the derivative at multiple points within the time step [Kutta, 1901, p. 443]:

$$\begin{aligned}
\boldsymbol{k}_1 &= h\,\boldsymbol{f}(t_n, \boldsymbol{y}_n) \\
\boldsymbol{k}_2 &= h\,\boldsymbol{f}(t_n + h/2, \boldsymbol{y}_n + \boldsymbol{k}_1/2) \\
\boldsymbol{k}_3 &= h\,\boldsymbol{f}(t_n + h/2, \boldsymbol{y}_n + \boldsymbol{k}_2/2) \\
\boldsymbol{k}_4 &= h\,\boldsymbol{f}(t_n + h, \boldsymbol{y}_n + \boldsymbol{k}_3) \\
\boldsymbol{y}_{n+1} &= \boldsymbol{y}_n + \tfrac{1}{6}(\boldsymbol{k}_1 + 2\boldsymbol{k}_2 + 2\boldsymbol{k}_3 + \boldsymbol{k}_4)
\end{aligned}$$

where h is the time step, $\boldsymbol{y}_n$ is the full state vector (x, y, z, v_x, v_y, v_z) at time t_n, and $\boldsymbol{f}$ is the vector of derivatives (velocities and accelerations).

Version 3.1 Mathematical Corrections: It is critical to apply the RK4 integration to the *full state vector* rather than decoupling position and velocity (a common error that degrades long-range accuracy). The drag term itself carries no free parameter: with $A = \pi d^2/4$ the physical frontal area and $i = \mathrm{SD}/B_\mathrm{C}$ the form factor, both d^2 and m cancel out of $a = \rho\, C_\mathrm{D}\, i\, A\, v^2/(2m)$, leaving the ballistic coefficient alone in control of the trajectory—exactly as it should be.

A correction factor that should never have been there. Until 2026-08-22 this section justified multiplying the deceleration by $4/\pi$, on the grounds that the shooting definition of sectional density (referred to d^2) had to be bridged to the BRL tables (referred to $\pi d^2/4$). The derivation above does not produce that factor. What it actually did was compensate for supersonic drag-table values that were wrong (see the warning in `G7_RAW`), tuned so that one particular .308 load arrived at 1000 yards near a plausible velocity. A global factor calibrated on a single operating point is right at that point and wrong everywhere else. Both the factor and the bad table data have been removed.

A typical time step of $h = 0.0005\,\mathrm{s}$ to $0.001\,\mathrm{s}$ is sufficient.

Chapter 6

Exterior Ballistics: Advanced Effects

6.1 Motivation: Beyond Gravity

While gravity is a merciless absolute, it is highly predictable. A shooter simply needs a precise laser rangefinder to account for drop. The true separator of amateur and expert long-range shooters is the mastery of *advanced exterior ballistics*, primarily wind deflection and gyroscopic drift.

Why is wind reading considered a dark art? Because wind is invisible, highly volatile, and acts on a bullet in a deeply counter-intuitive way. The most crucial concept in long-range shooting is realizing that wind does *not* blow a bullet straight sideways like a piece of paper. Instead, wind deflection is entirely governed by how much *drag* the bullet experiences.

6.2 Wind Deflection

Wind is the single largest variable in long-range competition shooting.

6.2.1 Wind Components (Vectors)

Before calculating deflection, we must break the total wind vector into its forward/backward and left/right components relative to the shooter's line of sight.

Let's clearly define our variables:

- W: The absolute wind velocity ($\frac{\text{m}}{\text{s}}$ or mph).
- α_w (alpha w): The angle of the wind vector relative to the line of fire (e.g., 90° is a full crosswind).
- w_x: The headwind (negative) or tailwind (positive) velocity vector.
- w_z: The lateral crosswind velocity vector.

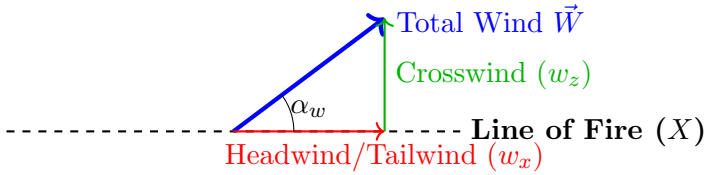

Figure 6.1: Decomposition of the total wind vector into range (w_x) and lateral (w_z) components. Only the w_z component causes side-to-side deflection.

Given wind speed W at angle α_w relative to the line of fire:

$$w_x = -W \cos \alpha_w \quad \text{(headwind/tailwind)}$$
$$w_z = W \sin \alpha_w \quad \text{(crosswind)}$$

6.2.2 Simple Approximation

A crude but sometimes useful first-order approximation for lateral drift (crosswind drift) is:

$$\Delta z_{\text{wind}} \approx \frac{W \sin \alpha_w}{v_{\text{avg}}} \cdot R$$

where v_{avg} is the average bullet velocity over the range distance R. This formula assumes the bullet instantly acquires the transverse velocity of the wind, taking a straight angle path. This is physically unrealistic for high-velocity projectiles, but works for air rifles at short distance.

6.2.3 The Lag Rule (The Didion Approximation)

To understand wind deflection accurately, we use the Didion approximation, often known mathematically as the "Lag Rule" [McCoy, 2012]; Litz calls the same quantity *lag time* [Litz, 2015a, p. 63].

- Δz_{wind}: Total lateral deflection of the bullet at the target.
- t_{actual}: The actual time of flight of the bullet in the real atmosphere.
- R: the range to the target.
- $v_0 \cos\theta$: The horizontal component of the muzzle velocity.
- $\left(t_{\text{actual}} - \frac{R}{v_0 \cos\theta}\right)$: This bracket is the "Lag Time". It represents the extra time the bullet takes to reach the target *compared to if it had traveled in a perfect vacuum.*

$$\Delta z_{\text{wind}} \approx W \sin \alpha_w \cdot \left(t_{\text{actual}} - \frac{R}{v_0 \cos\theta}\right)$$

This equation is remarkably accurate (typically within 5% of a complex 6-DOF solver) and provides an intuitive physical breakthrough: **wind deflection is entirely caused by aerodynamic drag**. If a bullet had zero drag (a vacuum time of flight), the bracket equals zero, and wind drift is zero! The more slippery a bullet is, the smaller the gap between t_{actual} and vacuum time, resulting in less wind deflection.

6.3 Spin Drift

A spin-stabilized bullet develops a slow lateral drift in the direction of its spin. The empirical formula widely used for spin drift is Litz's [Litz, 2015a, eq. 6.1, p. 97], $\Delta z = 1.25\,(S_g{+}1.2)\,t^{1.83}$, fitted to Doppler radar measurements of match-grade projectiles. This manual and its solver use it with the S_g dependence corrected:

$$\boxed{\Delta z_{\text{spin}} = 1.25 \cdot 2.95 \sqrt{S_g/1.75} \cdot t^{1.83}}$$

where Δz_{spin} is the horizontal deflection in inches, S_g is the gyroscopic stability factor, and t is the time of flight in seconds.

Why $\sqrt{S_g}$. For a given bullet fired from barrels of different twist, the lateral acceleration from the yaw of repose is proportional to the spin rate p, the rate of spin decay does not depend on p, and $S_g \propto p^2$: drift is therefore exactly proportional to $\sqrt{S_g}$, an identity rather than a fit, confirmed to 0.00 % by integrating the modified point-mass drift with measured coefficients for two bullets. Litz's linear form departs from it as the bullet becomes overstabilized: relative to the integration, -1 % at $S_g = 1.2$, $+5$ % at 2.4, $+15$ % at 3.7 and

+24 % at 4.9. The corrected form replaces Litz's term $(S_g + 1.2)$ by $2.95\sqrt{S_g/1.75}$, which equals it at $S_g = 1.75$, where he fitted the formula $(1.75 + 1.2 = 2.95)$, and changes match bullets at S_g 1.5–2.2 by less than 3 %; it matters for light bullets in fast twists (a 55 gr .223 in a 1:7 barrel, $S_g \approx 3.8$, drifts 14 % less than Litz's form predicts).

Two limits remain. Between different bullets at the same S_g, drift also scales with I_y/I_x and $C_{L\alpha}/C_{M\alpha}$, which neither form captures (tracer rounds drift up to 42 % more than predicted). And the time exponent 1.83 is low for typical ranges: the integration gives 2.00 out to about 1000 yd, which makes the formula read some 10 % high at 600 yd when calibrated at 1000 yd.

6.3.1 Gyroscopic Stability Factor

The Miller stability formula [Miller, 2005]:

$$\boxed{S_g \approx \frac{30\,m}{T_w^2\,d^3\,l\,(1+l^2)} \cdot \left(\frac{v_0}{2800}\right)^{1/3} \cdot \frac{T}{T_0} \cdot \frac{P_0}{P}} \tag{6.1}$$

where m is bullet mass in grains, T_w is twist rate in calibers per turn, d is caliber in inches, l is bullet length in calibers, v_0 is muzzle velocity in fps, T is ambient temperature, P ambient pressure, and $T_0 = 518.67$ R (15 °C, 59 °F), $P_0 = 29.92$ in Hg are the standard reference conditions.

Two points are easy to get wrong. The velocity correction is a *cube root*, not a direct ratio: the discrepancy stays under 2.5% between 2700 and 2900 fps but reaches 27% at 4000 fps. And the atmospheric correction goes as T/T_0, not its inverse — the overturning moment scales with air density $\rho \propto P/T$, so $S_g \propto 1/\rho$: hot or thin air *raises* S_g. A bullet marginally stable at sea level gains stability at altitude.

For adequate stability, $S_g > 1.0$; values of 1.3–2.0 are typical for match bullets. Below $S_g \approx 1.5$ the bullet flies with residual pitching and yawing that costs measurable BC — Litz reports a 9% BC loss for a .30 calibre 185 gr LRBT fired at 2800 ft/s from a 1:13-inch twist ($S_g = 1.2$) [Litz, 2014]; his book shows a 6 mm 95 gr VLD losing 12% of its G7 BC at $S_g = 1.07$ compared with $S_g = 1.67$ (0.218 against 0.249) [Litz, 2015a, fig. 10.3, p. 163].

6.4 Coriolis and Eötvös Effects

6.4.1 Coriolis Acceleration

In an Earth-fixed reference frame:

$$\boldsymbol{a}_{\text{Cor}} = -2\,\boldsymbol{\omega}_E \times \boldsymbol{v} \tag{6.2}$$

where $\boldsymbol{a}_{\text{Cor}}$ is the Coriolis acceleration, $\boldsymbol{\omega}_E$ is the Earth's angular velocity vector, and $\boldsymbol{v}$ is the projectile's velocity vector. The scalar magnitude of the Earth's rotation is $\omega_E = 7.2921 \times 10^{-5}\ \frac{\text{rad}}{\text{s}}$.

6.4.2 Horizontal Deflection

$$\boxed{\Delta z_{\text{Cor}} \approx \omega_E \sin\phi \cdot R \cdot t} \tag{6.3}$$

where Δz_{Cor} is the horizontal deflection, ϕ is the shooter's latitude, R is the range, and t is the time of flight.

Always to the right in the Northern Hemisphere, left in the Southern. At 45 N, 1000 yd, $t \approx 1.5$ s: $\Delta z \approx 2.8$ inches (≈ 0.27 MOA).

6.4.3 Vertical Deflection (Eötvös Effect)

$$\boxed{\Delta y_{\text{Eot}} \approx \omega_E \cos\phi \sin\psi \cdot R \cdot t} \tag{6.4}$$

where Δy_{Eot} is the vertical deflection (Eötvös effect) and ψ is the firing azimuth (heading).

Firing East ($\psi = 90°$) results in a positive vertical deflection (the bullet shoots higher due to the increased centrifugal force), while firing West ($\psi = 270°$) results in a negative deflection. At 45°N, 1000 yd, the effect is approximately ±3 to 4 inches.

6.4.4 Implementation

The closed-form expressions (6.3) and (6.4) are *approximations*; the solver does not use them directly. Instead it applies the exact acceleration (6.2) at every RK4 step, decomposing $\boldsymbol{\omega}_E$ into the shot frame (x downrange, y up, z right) as a function of *both* latitude ϕ and firing azimuth ψ:

$$\boldsymbol{\omega}_E = \omega_E\big(\cos\phi\cos\psi,\ \sin\phi,\ -\cos\phi\sin\psi\big).$$

Equations (6.3) and (6.4) are then recovered as the leading-order integrals of $-2\,\boldsymbol{\omega}_E \times \boldsymbol{v}$. Numerically, firing East at 45°N raises the 1000 yd impact by ≈ 2.4 inches and West lowers it by the same amount, while the horizontal drift stays ≈ 2.4 inches right regardless of azimuth—consistent with the azimuth-independent form of Eq. (6.3).

6.5 Aerodynamic Jump

For a spin-stabilized bullet with initial yaw α_0 [McCoy, 2012]:

$$\theta_{\text{jump}} = \frac{C_{L_\alpha}}{2\,k_t^2}\,\frac{\alpha_{\text{trim}}}{p_s - r_s}$$

where θ_{jump} is the jump angle, C_{L_α} is the lift force derivative, k_t is the transverse radius of gyration, α_{trim} is the equilibrium yaw angle, p_s is the dimensionless spin rate, and r_s is the dimensionless stability derivative.

In practice, aerodynamic jump is absorbed into zero-offset and has a random component that contributes to group size rather than a systematic bias.

6.6 Magnus Effect

$$F_{\text{Magnus}} = \frac{1}{2}\rho\, v^2\, A\, C_{N_{p\alpha}}\,\frac{p\,d}{2\,v}\,\alpha$$

where F_{Magnus} is the Magnus force, $C_{N_{p\alpha}}$ is the Magnus force coefficient, p is the axial spin rate, d is the caliber, and α is the yaw angle.

For typical small yaw angles ($\alpha < 1$ deg), the Magnus contribution is sub-0.1 MOA at 1000 yd and is usually neglected.

Chapter 7

Complete 3-DOF Ballistic Solver

7.1 Motivation: From Paper to Code

We have spent several chapters deriving the physical forces acting on a bullet. However, writing these equations on a chalkboard does not help a shooter hit a steel plate at 1,000 yards. The forces of drag and gravity are dynamic—they change continuously every fraction of a second as the bullet slows down and changes angle.

To actually predict the trajectory, we cannot just plug numbers into a single algebra equation. We must build a *numerical solver* that simulates the flight step-by-step. A 3-Degrees-of-Freedom (3-DOF) solver tracks the bullet's x, y, z position through space treating it as a simple "point mass" while applying empirical corrections for rotation. This is the industry standard for commercial ballistic apps.

The complete 3-DOF ballistic solver is implemented in the companion file `CompetitionBallistics.jl` (see Appendix B). The solver includes: G1/G7 drag model interpolation from BRL tables, full Runge-Kutta 4th order (RK4) integration of the 3-DOF equations of motion, automatic zero-angle finding (sighting-in), Coriolis and Eötvös corrections, post-hoc spin drift calculations, and wind deflection.

To ensure the physical integrity of our implementation, every trajectory in this manual is checked nightly against an independent third-party point-mass solver (`py-ballisticcalc`), on a frozen grid of fourteen cases covering three drag models, three atmospheres, wind, spin drift and Coriolis. The comparison is a second opinion, not an oracle: when it disagrees, the arbiter is published data (McCoy, Litz) or measured DOPE.

Earlier editions of this section claimed cross-validation against JBM Ballistics. That claim did not survive scrutiny — the first genuine third-party comparison, on 2026-08-22, showed velocity errors of 6 to 9 % at 1000 yards — and JBM withdrew its online calculators in 2026 in any case. A validation claim that nothing re-checks is worth exactly nothing; that is why the check is now automated and runs every night.

The `ShotParameters` struct accepts all physical inputs (bullet mass, Ballistic Coefficient, muzzle velocity, atmospheric conditions, wind, latitude, twist rate, etc.) and the `solve_trajectory()` function returns a vector of `TrajectoryPoint` records containing time, position, velocity, Mach number, and kinetic energy at each integration step.

```
include("CompetitionBallistics.jl")
using .CompetitionBallistics.ExteriorBallistics

params = ShotParameters(
    mass_grains=140.0, caliber_in=0.264,
    bc=0.311, drag_model=:G7,
    muzzle_vel_fps=2700.0, zero_range_yd=100.0,
    wind_speed_mph=10.0, wind_angle_deg=90.0,
    target_range_yd=1000.0,
```

```
    twist_in=8.0, bullet_length_in=1.34,
)
trajectory_table(params, step_yd=100)
```

Listing 7.1: Example: running the 3-DOF solver in Julia

Chapter 8

Six-Degree-of-Freedom (6-DOF) Model

8.1 Motivation: Unlocking the Gyroscope

The 3-DOF point-mass model discussed previously is excellent for most conventional shooting scenarios. However, it completely ignores the fact that a bullet is a rapidly spinning chunk of metal (spinning up to 300,000 RPM). A 3-DOF model uses "empirical patches" (fudge factors like the Didion lag rule or empirical spin drift formulas) to estimate the effects of this spin.

When shooting at extreme long range, or when using modern high-BC bullets that border on being aerodynamically unstable, these patches lose their footing, and a Six-Degree-of-Freedom (6-DOF) model becomes the appropriate tool.

Note: when 6-DOF is actually required. It is worth stating plainly, before developing the equations, that this chapter is not a correction the 3-DOF trajectory is waiting for. McCoy [2012] is explicit: 6-DOF trajectories *are not required for routine work in exterior ballistics*. If the total angle of attack is small everywhere along the flight path, a point-mass trajectory is "often sufficiently accurate for all practical purposes", and where a drift solution is also wanted, the modified point-mass method is accurate for all but the highest quadrant elevation angles. The criterion is the *yaw level*, not the range: six-degrees-of-freedom methods are required whenever a projectile experiences large-yaw flight — an artillery or mortar shell at high quadrant elevation, or a projectile launched sidewise into a several-hundred-mile-per-hour crosswind. McCoy's own worked example, a .308", 168 gr Sierra International match bullet fired flat to 1000 yards, never exceeds five degrees of pitch and yaw, and he notes that its flight dynamic analysis "can actually be done by simpler methods". Sport shooting, including at long range, sits entirely on the small-yaw side of that line; the 6-DOF model earns its keep in stability and flight-dynamic analysis.

Note: the binding constraint is data, not algorithm. A 6-DOF solution "gives the most accurate solution possible . . . provided that all the aerodynamic forces and moments, and the initial conditions, are known to a high degree of accuracy" [McCoy, 2012]. That proviso is the whole difficulty. The full coefficient set — normal force, overturning moment, pitch and roll damping, Magnus force and moment — is measured in a spark range or a wind tunnel and is published for almost no commercial bullet; the semi-empirical codes shooters know by name supply only fragments of it (MCDRAG returns the zero-yaw drag coefficient alone). Practitioners of the method have a motto for what follows: *GI-GO*, garbage in, garbage out. No computed trajectory or flight dynamic analysis can be any better than the quality of its input data, and a 6-DOF run fed with placeholder coefficients is worth less than a 3-DOF run fed with a measured ballistic coefficient.

A worked comparison. The temperature example of Section 15.5 puts a figure on both notes. McCoy's .308 in, 168 gr bullet — the 6-DOF validation case, 2600 fps, with its measured aerodynamic coefficients — is launched at the angle that zeros it at 1000 yards (14.465 mrad)

and kept at that angle while the muzzle velocity drops by $T_c \times 11\,^{\circ}\mathrm{C}$, for a powder at $T_c = 0.15$ and one at 0.40 m/s/°C. Table 8.1 gives the vertical shift of the point of impact at 1000 yards in five runs.

Table 8.1: Same shot, five models: vertical shift at 1000 yards for an 11 °C drop in ammunition temperature, launch angle held constant

Model	**Drag**	$T_c = 0.15$	$T_c = 0.40$
6-DOF, McCoy's initial yaw rate (25 rad/s)	measured	6.51 cm	17.54 cm
6-DOF, no initial yaw rate	measured	6.45 cm	17.32 cm
Point mass	measured, zero-yaw C_{D0}	6.43 cm	17.24 cm
3-DOF, G7 BC 0.209	G7, BC fitted to the 6-DOF remaining velocity	6.79 cm	18.19 cm
3-DOF, G7 BC 0.212	G7, BC fitted to the 6-DOF time of flight	6.71 cm	17.98 cm

With the same drag, the point mass stays within 1.2 to 1.7 % of the full 6-DOF, and most of that gap is the yaw-induced drag of McCoy's initial yaw rate: without it, the 6-DOF falls to 6.45 and 17.32 cm. The G7 runs are 2.5 to 4.2 % higher, about twice as far off, and the cause is the drag curve, not the degrees of freedom: the G7 form factor of this bullet falls from 1.19 at Mach 2.3 to 1.11 at Mach 1.1, which no single ballistic coefficient can follow. The ratio between the two powders is 2.7 in every model. The yaw-induced drag is the one effect that shows in absolute terms: with the same zero-yaw drag, the 6-DOF arrives at 1000 yards at 306.8 m/s instead of 313.3 m/s, and 25 cm lower. It depends on an initial yaw rate that no shooter knows for a given rifle; a 3-DOF run whose ballistic coefficient is fitted to an observed trajectory absorbs it, as the BC 0.209 row does for the remaining velocity.

A 6-DOF model treats the bullet as a spinning rigid body. It tracks three translational coordinates (forward, up, sideways) and three rotational coordinates (yaw, pitch, roll). By doing this, a 6-DOF solver predicts yaw, precession, nutation, spin decay, and all complex gyroscopic phenomena from absolute first principles. This chapter develops the full 6-DOF equations of motion.

8.2 State Vector and Reference Frames

To track rotation, we can no longer just look at the bullet against the earth; we must look at the earth from the perspective of the bullet.

8.2.1 Coordinate Systems (Inertial vs Body)

We require two rigidly defined reference frames:

- **Earth-fixed (inertial) frame** $\{O; \boldsymbol{e}_x, \boldsymbol{e}_y, \boldsymbol{e}_z\}$: The stationary world the shooter sits in.
  - x: Downrange towards target.
  - y: Vertically upward.
  - z: Horizontal to the right.
- **Body-fixed frame** $\{G; \boldsymbol{b}_1, \boldsymbol{b}_2, \boldsymbol{b}_3\}$: An internal frame locked inside the bullet, with its origin at the bullet's center of mass G.
  - $\boldsymbol{b}_1$: Pointing directly out the nose along the symmetry axis.
  - $\boldsymbol{b}_2, \boldsymbol{b}_3$: Pointing out the sides (transverse plane).

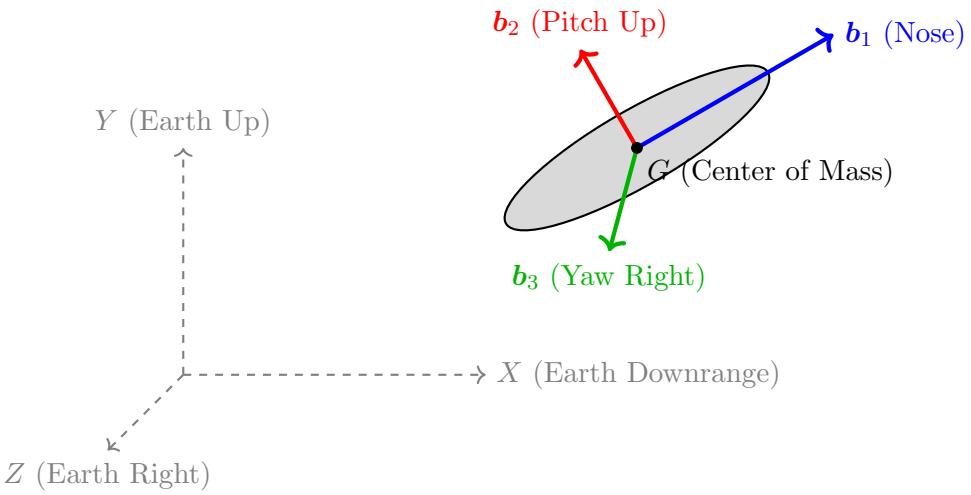

Figure 8.1: The Earth-fixed inertial frame versus the bullet's Body-fixed frame. As the bullet pitches and yaws, the body frame rotates independently of the earth frame.

8.2.2 Euler Angles and Orientation

The instantaneous orientation of the bullet's body frame relative to the stationary inertial frame is described by three Euler angles in the aerospace (yaw-pitch-roll) convention:

- ψ: yaw angle (rotation about $\boldsymbol{e}_y$)
- ϑ: pitch angle (rotation about intermediate axis)
- φ: roll (spin) angle (rotation about $\boldsymbol{b}_1$)

The rotation matrix from inertial to body frame is:

$$\boldsymbol{R} = \boldsymbol{R}_1(\varphi)\,\boldsymbol{R}_2(\vartheta)\,\boldsymbol{R}_3(\psi)$$

8.2.3 The 12-Component State Vector

The full state vector is:

$$\boldsymbol{Y} = \big(x,\ y,\ z,\ u,\ v,\ w,\ \varphi,\ \vartheta,\ \psi,\ p,\ q,\ r\big)^T$$

where (x, y, z) is position, (u, v, w) is velocity in the inertial frame, $(\varphi, \vartheta, \psi)$ are Euler angles, and (p, q, r) are angular velocity components in the body frame: p is the spin rate about $\boldsymbol{b}_1$, and q, r are pitch and yaw rates.

8.3 Translational Equations of Motion

Newton's second law in the inertial frame:

$$\boxed{m\,\frac{\mathrm{d}\boldsymbol{v}}{\mathrm{d}t} = \boldsymbol{F}_{\text{grav}} + \boldsymbol{F}_{\text{drag}} + \boldsymbol{F}_{\text{lift}} + \boldsymbol{F}_{\text{Magnus}} + \boldsymbol{F}_{\text{pitch damp}}}$$

8.3.1 Total Angle of Attack

The total angle of attack α_t is the angle between the velocity vector $\boldsymbol{v}$ and the body symmetry axis $\boldsymbol{b}_1$:

$$\alpha_t = \arccos\left(\frac{\boldsymbol{v}\cdot\boldsymbol{b}_1}{\|\boldsymbol{v}\|}\right)$$

For small angles, this decomposes into:

$$\alpha \approx \vartheta - \gamma \quad \text{(pitch-plane angle of attack)}$$
$$\beta \approx \psi_b - \psi_v \quad \text{(yaw-plane angle of attack)}$$

where γ is the flight path angle.

8.3.2 Aerodynamic Force Components

All forces are expressed in terms of dimensionless coefficients, reference area $A = \pi d^2/4$, and dynamic pressure $\bar{q} = \frac{1}{2}\rho v^2$:

Axial drag force (opposing velocity along the symmetry axis):

$$F_{\text{drag}} = -\bar{q}\, A\, C_{D_0}(Ma) - \bar{q}\, A\, C_{D_{\alpha^2}}(Ma)\, \alpha_t^2$$

where C_{D_0} is the zero-yaw drag coefficient and $C_{D_{\alpha^2}}$ is the yaw-drag coefficient.

Normal (lift) force (perpendicular to the symmetry axis, in the yaw plane):

$$F_N = \bar{q}\, A\, C_{N_\alpha}(Ma)\, \alpha_t$$

where C_{N_α} is the normal force derivative (lift-curve slope).

Magnus force (perpendicular to both the spin axis and the velocity–axis plane):

$$F_{\text{Magnus}} = \bar{q}\, A\, C_{N_{p\alpha}}(Ma)\, \frac{p\, d}{2\, v}\, \alpha_t$$

8.4 Rotational Equations of Motion

The general rotational equation for a rigid body in compact tensor form is:

$$\boxed{\dot{\boldsymbol{\omega}} = \boldsymbol{I}^{-1}(\boldsymbol{M} - \boldsymbol{\omega} \times \boldsymbol{I}\,\boldsymbol{\omega})} \tag{8.1}$$

where $\boldsymbol{I}$ is the inertia tensor, $\boldsymbol{\omega} = (p, q, r)^T$ is the angular velocity in the body frame, and $\boldsymbol{M}$ is the total external moment. The cross-product term $\boldsymbol{\omega} \times \boldsymbol{I}\,\boldsymbol{\omega}$ represents the gyroscopic coupling.

For an axially symmetric projectile (body of revolution) with I_x (axial) and $I_y = I_z$ (transverse), the inertia tensor is diagonal and Eq. (8.1) expands to the scalar Euler equations:

$$\begin{aligned} I_x\, \dot{p} &= M_x \\ I_y\, \dot{q} + (I_x - I_y)\, p\, r &= M_q \\ I_y\, \dot{r} - (I_x - I_y)\, p\, q &= M_r \end{aligned}$$

8.4.1 Aerodynamic Moments

Overturning (pitching) moment — the moment that tends to increase the angle of attack:

$$M_{\text{pitch}} = \bar{q}\, A\, d\, C_{M_\alpha}(Ma)\, \alpha_t$$

where C_{M_α} is the pitching moment coefficient derivative. For statically stable configurations, $C_{M_\alpha} < 0$ (restoring moment). For bullets, $C_{M_\alpha} > 0$ (statically unstable; stability comes from spin).

Spin-damping moment — the torque that decelerates spin:

$$M_{\text{spin}} = \bar{q}\, A\, d^2\, C_{l_p}(Ma)\, \frac{p\, d}{2\, v}$$

where $C_{l_p} < 0$ is the spin-damping coefficient.

Pitch-damping moment — opposes pitch/yaw rate:

$$M_{\text{damp}} = \bar{q}\, A\, d^2\, \left(C_{M_q} + C_{M_{\dot{\alpha}}}\right)\, \frac{d}{2\, v}\, (q \text{ or } r)$$

Magnus moment:

$$M_{\text{Magnus}} = \bar{q}\, A\, d^2\, C_{M_{p\alpha}}(Ma)\, \frac{p\, d}{2\, v}\, \alpha_t$$

8.4.2 Summary of Moment Components

The total moments about each body axis:

$$\begin{aligned}
M_x &= \bar{q}\, A\, d^2\, C_{l_p}\, \frac{p\, d}{2v} \\
M_q &= \bar{q}\, A\, d \left[C_{M_\alpha}\, \alpha - C_{M_{p\alpha}}\, \frac{pd}{2v}\, \beta + \left(C_{M_q} + C_{M_{\dot{\alpha}}}\right) \frac{qd}{2v} \right] \\
M_r &= \bar{q}\, A\, d \left[C_{M_\alpha}\, \beta + C_{M_{p\alpha}}\, \frac{pd}{2v}\, \alpha + \left(C_{M_q} + C_{M_{\dot{\alpha}}}\right) \frac{rd}{2v} \right]
\end{aligned}$$

8.5 Kinematic Equations

The Euler angle rates relate to the body-frame angular velocities:

$$\begin{aligned}
\dot{\varphi} &= p + (q \sin\varphi + r \cos\varphi) \tan\vartheta \\
\dot{\vartheta} &= q \cos\varphi - r \sin\varphi \\
\dot{\psi} &= (q \sin\varphi + r \cos\varphi) \sec\vartheta
\end{aligned}$$

For small angles of attack ($\alpha_t < 10°$), typical of rifle bullets, these simplify considerably.

8.6 Quaternion Formulation (Singularity-Free)

The Euler-angle formulation has a singularity at $\vartheta = \pm 90°$ (gimbal lock). For robust numerical integration, the unit quaternion $\boldsymbol{q} = (q_0, q_1, q_2, q_3)^T$ is preferred:

$$\frac{\mathrm{d}}{\mathrm{d}t} \begin{pmatrix} q_0 \\ q_1 \\ q_2 \\ q_3 \end{pmatrix} = \frac{1}{2} \begin{pmatrix} 0 & -p & -q & -r \\ p & 0 & r & -q \\ q & -r & 0 & p \\ r & q & -p & 0 \end{pmatrix} \begin{pmatrix} q_0 \\ q_1 \\ q_2 \\ q_3 \end{pmatrix}$$

The rotation matrix from the quaternion:

$$\boldsymbol{R} = \begin{pmatrix} 1 - 2(q_2^2 + q_3^2) & 2(q_1 q_2 - q_0 q_3) & 2(q_1 q_3 + q_0 q_2) \\ 2(q_1 q_2 + q_0 q_3) & 1 - 2(q_1^2 + q_3^2) & 2(q_2 q_3 - q_0 q_1) \\ 2(q_1 q_3 - q_0 q_2) & 2(q_2 q_3 + q_0 q_1) & 1 - 2(q_1^2 + q_2^2) \end{pmatrix}$$

After each integration step, renormalize: $\boldsymbol{q} \leftarrow \boldsymbol{q} / \|\boldsymbol{q}\|$.

8.7 Aerodynamic Coefficient Database

8.7.1 Typical Values for Match Bullets

The aerodynamic coefficients are functions of Mach number. Typical values for a 6.5 mm, 140 gr VLD match bullet at $Ma \approx 2.4$ (muzzle) [McCoy, 2012, Carlucci and Jacobson, 2008]:

Table 8.2: Typical aerodynamic coefficients for a 6.5 mm 140 gr VLD match bullet

Coefficient	Symbol	Typical Value	Description
Zero-yaw drag	C_{D_0}	0.15–0.30	From G7 table via BC
Yaw drag	$C_{D_{\alpha^2}}$	2.0–5.0	Drag increase with yaw
Lift-curve slope	C_{N_α}	2.0–3.5	Normal force per rad
Overturning moment	C_{M_α}	2.0–4.0	Destabilizing (positive)
Spin damping	C_{l_p}	-0.005 to -0.02	Retards spin
Pitch damping	$C_{M_q} + C_{M_{\dot\alpha}}$	-5 to -15	Damps yaw oscillation
Magnus force	$C_{N_{p\alpha}}$	-0.5 to $+0.5$	Cross-spin force
Magnus moment	$C_{M_{p\alpha}}$	-0.5 to $+0.5$	Cross-spin moment

[default: Values in the Julia implementation when not user-specified.]

8.7.2 Measured Sets: What Actually Exists

The table above is a range of plausible magnitudes, not a coefficient set. A 6-DOF run needs actual numbers, and the constraint is severe: the full set is measured in a spark photography range and published for almost no commercial bullet. The implementation therefore marks every set with a `provenance` field and warns once per session when a solver runs on placeholder values — a right solver fed invented coefficients returns results that are *credible and wrong*, which is a worse failure than a wrong solver returning visible nonsense.

Seven projectiles are presently carried with a measured set, all from BRL spark-range reports by R. L. McCoy and all in the public domain:

Table 8.3: Measured aerodynamic sets carried by the implementation

Projectile	Source	Mach range	Note
.308 in 168 gr Sierra Intl.	McCoy [2012], App. A	0.0–2.5	Textbook case 9.1
105 mm HE M1	McCoy [2012], App. B	0.0–2.5	Artillery, case 9.2
5.56 mm SS-109	BRL-MR-3476 (1985)	0.74–2.63	Ball
5.56 mm M855	BRL-MR-3476 (1985)	0.67–2.73	Ball
5.56 mm L110	BRL-MR-3476 (1985)	1.89–2.54	Tracer, thin
5.56 mm M856	BRL-MR-3476 (1985)	1.12–2.57	Tracer

The 5.56 mm sets are the first *small-arms* Magnus and pitch-damping data the library carries, and they cover the whole useful flight band of the cartridge. Their tables are transcribed round by round, exactly as printed, and every curve the library uses is derived from those rows at load time — there is no second, hand-copied copy that can drift out of step.

Three limits are recorded with them, and each is a trap for the unwary.

The tabulated C_D is measured at the round's own yaw, not at zero yaw. It is reduced with $C_{D_0} = C_D - C_{D_{\alpha^2}} \sin^2 \alpha_t$, taking $C_{D_{\alpha^2}} = 3.5$; that coefficient is not measured by the report,

but pairs of rounds fired at the same Mach and different yaw bracket it between 3.4 and 5. Keeping only the near-zero-yaw rounds instead leaves *two* points for the M855, both supersonic, and the curve then clamps a supersonic value straight across the transonic peak.

These sets cannot produce a limit cycle. Each $C_{M_{p\alpha}}$ value is a single round at a single angle of attack, so the curve is a function of Mach only and the yaw dependence is unresolved — and it is precisely the sign change of the Magnus moment with yaw that fixes limit-cycle amplitude. The scatter hints at the behaviour (the M855 runs from +0.10 at 1.90° to −0.59 at 2.87°) but three points cannot separate a Mach effect from a yaw effect, and pretending otherwise would be invention.

Sparse tables extrapolate silently. A table lookup clamps at its ends, which for nine rounds means answering confidently at a Mach nobody fired: the L110 tracer has three Magnus points, all above $Ma1.89$. The implementation returns the clamped value *and warns once* outside the band actually fired, with 2 % of slack so that an edge case does not train the reader to ignore the warning.

Physical characteristics — mass, centre of gravity and both moments of inertia — are additionally carried for the four 5.56 mm projectiles, the M118 Match, the 190 gr Sierra MatchKing and the 168 gr Sierra International (BRL-MR-3733, 1988), and for four .22 LR match bullets (BRL-MR-3877, 1990). The last of these covers a regime none of the others do: entirely subsonic flight, $Ma0.77$ to 1.03.

Validation. Feeding the measured coefficients of BRL-MR-3476 into the linearised theory of Section 8.10 reproduces the gyroscopic stability factors that the same report publishes from the same firings, to 3.5 % for the SS-109 and 5.3 % for the M855 (median 1.3 % and 0.5 %). The test barrel's twist is not published; the published S_g implies 7.01″ and 7.18″, which is the 1:7″ of the M16A2 and M249 that the report discusses in its dispersion section — an independent check that the set and the theory are mutually consistent.

8.7.3 Deriving C_{D_0} from the Ballistic Coefficient

The zero-yaw drag coefficient relates directly to the standard drag model and the ballistic coefficient:

$$C_{D_0}(Ma) = i \cdot C_D^{\mathrm{std}}(Ma) = \frac{\mathrm{SD}}{B_{\mathrm{C}}}\, C_D^{\mathrm{std}}(Ma)$$

This allows the 6-DOF model to use the same BC input as the 3-DOF model for the dominant drag term.

8.8 Moments of Inertia

For a rotationally symmetric bullet of mass m, length L, and diameter d:

$$I_x \approx \frac{1}{2}\, m\, r_g^2 \quad \text{(axial, about symmetry axis)} \tag{8.2}$$

$$I_y = I_z \approx m\left(\frac{L^2}{12} + \frac{r_g^2}{4}\right) \quad \text{(transverse)} \tag{8.3}$$

where $r_g = d/2$ is the radius of gyration. For a typical match bullet, $I_y/I_x \approx 5$–10.

8.8.1 Why the Solid-Cylinder Form Is Not Good Enough

Equations (8.2) and (8.3) treat the bullet as a solid cylinder of uniform density. Against the measured inertias of the .308 in 168 gr Sierra International (McCoy's Table 9.2) that approximation returns I_x high by 15.2 %, I_y high by 71.2 % and the ratio I_y/I_x high by 48.7 %. Since $S_g \propto I_x^2/I_y$, the error propagates to a gyroscopic stability factor of 1.32 where the published value is 1.70 — a shortfall of 22 %, which is the difference between declaring a load stable and declaring it marginal.

The cylinder is wrong for two independent reasons. It ignores the *shape* — a real bullet is an ogive over a cylinder over a boat tail, not a cylinder — and it ignores the *internal layout*, a gilding-metal jacket of nearly constant radial thickness around a lead core that does not fill it.

8.8.2 Integration over the Actual Contour

The companion implementation (`bullet_inertia`) integrates the solid of revolution directly. The external contour is described in calibers by four numbers: the ogive length as a fraction of total length, the meplat diameter, the boat-tail length and the boat-tail half-angle. The ogive is taken *tangent*, so its radius follows from the tangency condition

$$R = \frac{L_n^2 + a^2}{2a}, \qquad a = \frac{d - d_{\text{meplat}}}{2}$$

with L_n the ogive length. For the jacketed-lead construction the body is a shell of constant radial thickness with an open base, a lead core rising from that base, and a cavity above it; the core height is solved by bisection so that the integrated mass matches the bullet's actual weight. If no core height reproduces the weight — the bullet being denser than a solid-lead fill or lighter than the bare jacket — the routine falls back to a uniform density and says so.

Scored against the same reference bullet, given its published contour, this returns I_x to -0.2 %, I_y to $+2.4$ %, the ratio to $+2.6$ % and the centre of gravity to -0.5 %; S_g comes out at 1.693 against the published 1.70. On a 20 mm steel cone-cylinder of exactly known geometry (McCoy's Example 12.1) the integrator itself is good to -0.5 % on I_x and -4.0 % on I_y, which bounds the numerical error and shows that what remained wrong in the cylinder approximation was the *shape*, not the arithmetic.

8.8.3 Default Contour, and What It Costs

When no contour is supplied the defaults describe a modern boat-tailed match bullet: ogive fraction 0.541, boat tail 0.782 calibers at 7.5°, meplat 0.22 calibers. The first three are medians of measured populations — the ogive fraction and boat-tail length over 94 boat-tailed match bullets from a published manufacturer's dimension table, the boat-tail half-angle over 83 cones recorded by handloaders as two diameters and a height, from which the angle follows as $\arctan\big((d_{\text{maj}} - d_{\text{min}})/2h\big)$.

Flat-base bullets are a separate family, not a boat tail with zero length: they are shorter (L/d median 3.34 against 4.87) and carry proportionally longer ogives (0.638 against 0.541). Applying the boat-tail defaults to a flat base biases S_g by -9.7 %, always in the same direction.

Two cautions follow from the calibration and are worth stating plainly.

First, a default calibrated on one reference case is calibrated on its idiosyncrasy. An earlier default boat-tail length of 0.50 calibers matched the Sierra International almost exactly — and that bullet sits at the 2nd percentile of the modern match population, whose median is 0.782. It therefore scored well on the single case with published inertias while being wrong

for the bullets the library is actually used on. The present defaults deliberately score *worse* on that case ($-4.9\,\%$ on S_g instead of $-0.5\,\%$) and better on the population.

Second, the residual spread is irreducible by a better constant. Against each bullet's own measured contour the defaults leave a median absolute error of $3.8\,\%$ on S_g for boat tails and $4.1\,\%$ for flat bases, with a third of the population outside $\pm 5\,\%$. A linear rule in L/d was fitted and rejected: it bought 0.4 points of median error while widening the tails. What the spread wants is the dimension of the individual bullet, not a cleverer average.

Of the four contour parameters only the meplat remains uncalibrated, no public source publishing it. Sweeping it over its plausible range now moves I_x by $1.9\,\%$, I_y by $3.2\,\%$ and S_g by $0.9\,\%$ — against 6.3 / 4.2 / 9.7 % when the boat-tail angle was a guess as well.

8.8.4 Constructions the Model Does Not Cover

Two measured cases fall outside the jacketed-lead assumption and are useful as declared limits rather than as failures.

The 5.56 mm SS-109 and M855 carry a *steel penetrator* ahead of a lead rear core, so their mass is laid out in two materials. Given the published contour and true weight, the estimator lands 4–5 % low on I_x, 6–9 % low on I_y and 5–7 % low on the centre of gravity. That is the composite core showing.

The .22 LR match bullets are unjacketed lead, *heeled* — a rear section of reduced diameter — with a round nose ending in a spherical cap rather than a meplat. Neither the heel nor the round nose is expressible in the four contour parameters, so no contour is offered for them; only their measured inertias are tabulated.

In both cases the defaults happen to score better than the true contour. That is compensation between two errors, not accuracy, and it must not be read as a reason to prefer the defaults.

8.9 Spin Rate and Initial Conditions

The initial spin rate from the barrel twist rate τ (inches/turn):

$$p_0 = \frac{2\pi\, v_0}{\tau}$$

For a 1:8 twist barrel at 2700 fps: $p_0 = 2\pi \times 2700/(8/12) = 2\pi \times 4050 \approx 25{,}447$ rad/s ($\approx 243{,}000$ RPM).

8.10 Stability Revisited from 6-DOF Theory

8.10.1 Gyroscopic Stability

From the linearized 6-DOF equations, the gyroscopic stability factor is rigorously:

$$S_g = \frac{I_x^2\, p^2}{2\,\rho\, A\, d\, I_y\, v^2\, C_{M_\alpha}}$$

This is the exact form from which the Miller approximation (6.1) is derived.

8.10.2 Dynamic Stability

The dynamic stability factor from the 6-DOF linearization:

$$S_d = \frac{2\,C_{N_\alpha}}{C_{M_\alpha}} \cdot \frac{1}{S_g(S_g - 1)} \cdot \left(\frac{C_{N_\alpha} + \frac{2m}{\rho A d}\, k_t^2}{C_{M_q} + C_{M_{\dot{\alpha}}}} \right)^2$$

Full stability requires $S_g > 1$ and $0 < S_d < 2$.

8.11 Comparison: 3-DOF vs. 6-DOF

Table 8.4: Comparison of 3-DOF and 6-DOF models

Feature	**3-DOF**	**6-DOF**
State variables	6 (position + velocity)	13 (+ quaternion + angular velocity)
Spin drift	Empirical (Litz formula)	Predicted from first principles
Yaw/precession	Not modeled	Fully resolved
Magnus force	Neglected or lumped	Computed from $C_{N_{p\alpha}}$
Transonic behavior	No yaw prediction	Predicts instability onset
Aerodynamic data	BC only	BC + 7 additional coefficients
Computation speed	∼0.01 s	∼0.1–0.5 s
Prediction accuracy	Limited by the measured BC and its Mach dependence	Limited by the aerodynamic coefficients, published for almost no commercial bullet (Chapter 8)

For most competition shooting, the 3-DOF model with empirical spin drift and Coriolis corrections is sufficient. The 6-DOF model is valuable for: bullet design evaluation, predicting transonic stability limits, understanding anomalous dispersion, and academic study.

8.12 Julia Implementation: 6-DOF Solver

The 6-DOF solver is implemented in the `SixDOF` module within `CompetitionBallistics.jl` (Appendix B). Key structures:

```
using .CompetitionBallistics.SixDOF

aero = AeroCoefficients6DOF(
    Cd0_func   = (Ma) -> cd_g7(Ma) * 1.02,  # from BC
    Cda2       = 3.5,        # yaw drag
    CNa        = 2.8,        # lift-curve slope
    CMa        = 3.2,        # overturning moment
    Clp        = -0.010,     # spin damping
    CMq_CMad   = -8.0,       # pitch damping sum
    CNpa       = 0.1,        # Magnus force
    CMpa       = -0.2,       # Magnus moment
)

params6 = ShotParameters6DOF(
    mass_grains=140.0, caliber_in=0.264,
    bullet_length_in=1.34,
```

```
    muzzle_vel_fps=2700.0, twist_in=8.0,
    initial_yaw_deg=0.5,  # typical muzzle yaw
    aero=aero,
)

traj = solve_6dof(params6)
```

Listing 8.1: 6-DOF solver usage example

Chapter 9

Angular Measurement and Sighting Systems

9.1 Motivation: Speaking the Language of the Scope

All the ballistic math in the world is useless if you cannot translate it into a physical adjustment on the rifle scope. A ballistic solver calculates the drop of a bullet in linear units (like inches or centimeters). However, rifle scopes do not adjust in linear units; they adjust by changing angles.

When you turn the elevation dial on a scope, you are physically tilting the optic downward relative to the barrel so that you are forced to aim the barrel upward to compensate for drop. To hit the target, we must convert linear distance at the target (Δy) into an angular measurement at the scope. The two dominant angular languages in shooting are Minute of Angle (MOA) and Milliradian (Mil).

9.2 Minute of Angle (MOA)

A circle has 360 degrees. A Minute of Angle is exactly $1/60^{\text{th}}$ of one degree.

First, let's verify what this small angle actually means in radians:

$$1 \text{ MOA} = \frac{1^\circ}{60} \times \frac{\pi}{180^\circ} = 2.9089 \times 10^{-4} \text{ rad}$$

Because tangent of a very small angle is approximately equal to the angle in radians ($\tan(\theta) \approx \theta$), we can calculate exactly how much physical distance 1 MOA covers at 100 yards ($R = 3600$ inches):

$$\Delta y = R \cdot \theta_{\text{rad}} = 3600 \cdot 2.9089 \times 10^{-4} \approx 1.047 \text{ inches}$$

This is where the common (but slightly inaccurate) shooter's approximation comes from: 1 MOA $\approx$ 1 inch at 100 yd.

To convert your calculated bullet drop (Δy) at range R (ensuring both are in the same linear units, e.g., inches) into a scope dial adjustment in MOA, use this exact formula:

$$\boxed{\text{MOA Dial Adjustment} = \frac{\Delta y}{R} \cdot \frac{180 \times 60}{\pi} \approx \frac{\Delta y}{R} \cdot 3437.75}$$

9.3 Milliradian (Mil, MRAD)

While MOA is mathematically tied to the 360-degree circle (popular in the US), the Milliradian system operates on pure base-10 metric logic (popular internationally and in military

applications). A radian is the angle subtended when the arc length equals the radius. A milliradian is $1/1000^{\text{th}}$ of a radian.

$$1 \text{ mil} = 0.001 \text{ rad}$$

Because 1 mil = 0.001 rad, the math is incredibly elegant: 1 mil is exactly 1 meter at 1,000 meters, 10 centimeters at 100 meters, or 3.6 inches at 100 yards.

For mixed scope usage, the hard conversion is: 1 mil = 3.438 MOA.

To calculate the necessary dial adjustment on a Mil-based scope, using drop Δy and range R (again, matching linear units):

$$\boxed{\text{Mil Dial Adjustment} = \frac{\Delta y}{R} \times 1000}$$

Chapter 10

Reloading Guide for Competition Shooters

10.1 Motivation: Controlling the Variables

No amount of ballistic solver software can make up for inconsistent ammunition. Factory ammunition, even "match grade," is mass-produced and subject to tolerance stacking. To guarantee extreme precision (Standard Deviations in velocity below 10 FPS), competition shooters handload their own ammunition. Reloading is fundamentally about controlling variables—neck tension, seating depth, powder charge, and concentricity—so that every single round possesses the exact same interior ballistics.

Safety Warning: Handloading deals with immense explosive pressures near your face. Always cross-reference with current published load data from powder manufacturers. Start 10% below listed maximum charges and work up carefully while watching for pressure signs on the brass primer.

10.2 Cartridge Selection for Competition

Table 10.1 summarises, for the bullet weights a competitor would consider, the *maximum* loads published by nine load guides [Vihtavuori, 2026, Hodgdon Powder Company, 2024, Western Powders, 2020, Reload Swiss, 2025, ADI (Thales Australia), 2026, Norma Precision, 2023, Explosia a.s., 2019, Lyman Products Corporation, 2002, Sierra Bullets, 2020b,a]: the median of the maximum velocities, the range from the 10th to the 90th percentile over every bullet, powder and guide, and the test barrels the data were taken in. Reduced and subsonic loads (below 2000 fps) and barrels shorter than 20 in. are left out. These are maximum charges in test barrels: a competition load sits below them, and a longer barrel adds velocity (Table 3.1). The G7 ballistic coefficients are those Berger publishes for its match and hunting bullets of the same weights [Berger Bullets]; Berger publishes no 147 gr 6.5 mm bullet, and its 6.5 mm range stops at 144 gr.

Table 10.1: Competition cartridges: published maximum velocities and published G7 ballistic coefficients

Cartridge	**Bullet (gr)**	**Max v_0 (fps)** median [P10–P90]	**Loads** (guides)	**Test barrels** (in)	**G7 BC** (Berger)
6mm BR Norma	105–108	2669 [2550–2745]	34 (4)	23.6–26	.268–.287
6mm Creedmoor	105–115	2959 [2812–3042]	123 (4)	24–26	.268–.292
6mm Dasher	105–115	2917 [2836–2950]	9 (2)	30	.268–.292
6.5 Creedmoor	130–147	2687 [2549–2809]	319 (6)	23.6–25.6	.287–.336
6.5×47 Lapua	130–147	2698 [2529–2790]	134 (6)	23.6–30	.287–.336
.284 Win	175–185	2651 [2552–2712]	14 (2)	24	.336–.356
.308 Win	155–185	2644 [2467–2785]	873 (8)	23.6–24	.238–.295
.223 Rem	69–80	2813 [2664–2955]	265 (7)	23.6–24.4	.178–.216
.300 Win Mag	190–230	2825 [2627–2955]	190 (6)	24–25.6	.290–.368
.338 Lapua Mag	250–300	2742 [2588–2959]	157 (7)	23.6–28	.349–.421

Which match admits which cartridge is set by the rules. ICFRA F-Class Open admits any calibre up to and including 8 mm, F/TR only the .223 Remington and the .308 Winchester (rules F2.2 and F2.3) [International Confederation of Fullbore Rifle Associations, 2024a]; ICFRA Target Rifle, the discipline of the Palma match, the same two cartridges, with .308 bullets of 156 gr at most (rules T2.1 and T2.19.2.1) [International Confederation of Fullbore Rifle Associations, 2024b]; the ISSF 300 m events any calibre up to 8 mm (rule 7.4.6) [International Shooting Sport Federation, 2026]. In every division of the Precision Rifle Series, bullet diameter may not exceed .308 in. and muzzle velocity 3200 fps [American Rifleman, 2018]. The .338 Lapua Magnum is above both the F-Class Open and the PRS limits.

10.3 Propellant Selection

Selecting the proper propellant is a balance between achieving the desired muzzle velocity (v_0), maintaining a low velocity spread (σ_v), and staying safe across the temperatures the ammunition will see. Propellants are broadly categorized into single-base (nitrocellulose only) and double-base (nitrocellulose and nitroglycerine), but the base does not by itself decide the temperature sensitivity. Reload Swiss publishes coefficients of 0.20 to 0.90 m/s per kelvin across its range, each measured in one cartridge from several production lots; its nitroglycerine-impregnated RS60 is credited with 0.25 and its RS62 with 0.90 [Reload Swiss, 2019].

Makers describe their powders as “temperature stable” or “insensitive” without saying how much; Table 10.2 sets these claims beside the published measurements of the velocity coefficient σ_T (Section 15.5). The same powder measured by different testers can differ by a factor of ten, because the coefficient depends on the cartridge, the load, the temperature range and how the ammunition was conditioned.

Table 10.2: Temperature claims of the makers and published measurements of σ_T

Propellant	**Maker's claim**	**Measured σ_T (fps/°F), cartridge, source**
Hodgdon Varget	"insensitivity to hot/cold temperatures" [Hodgdon Powder Company, 2024]	0.06 (.308) [Hodgdon Powder Company, 2012]; 0.14 (6mm Dasher) [Zant, 2025]; 0.24 (.308) [Gear, 2022]; 0.40 (6.5×47) [Zant and Middlebrook, 2016]; 0.48 (.22-250) and 0.88 (6mm CM) [Haviland, 2022]; 0.63 (.308) and 0.85 (6mm BR) [Castleman, 2022a,b]
Hodgdon H4350	"insensitive to hot/cold temperatures" [Hodgdon Powder Company, 2024]	0.03 (.30-06) [Hodgdon Powder Company, 2012]; 0.14 (6mm CM) [Zant, 2025]; 0.22 (6.5×47) [Zant and Middlebrook, 2016]; faster when cold in one .243 load [Barsness, 2017]
Hodgdon H4895	"Extreme Extruded" line [Hodgdon Powder Company, 2024]	0.16 (.22-250) [Hodgdon Powder Company, 2012]; 0.77 (6mm BR) and 0.92 (.308) [Castleman, 2022b,a]
IMR 4451	Enduron: "insensitivity to temperature changes" [Hodgdon Powder Company, 2024]	0.59 (6.5×47) [Zant and Middlebrook, 2016]; faster when cold in one .257 Roberts load [Barsness, 2017]
IMR 4064	no claim in Hodgdon Powder Company [2024]	0.37 (.308) [Hodgdon Powder Company, 2012]; 0.79 (.308) [Castleman, 2022a]; 1.08 (.22-250) [Haviland, 2022]
Vihtavuori N140	"exceptional stability" [Vihtavuori, 2026]	0.40 (.308) and 0.65 (.22-250) [Hodgdon Powder Company, 2012]; 1.22 (.308) [Castleman, 2022a]
Vihtavuori N150	"enhanced temperature stability" [Vihtavuori, 2026]	0.41 (.308) [Castleman, 2022a]
Vihtavuori N555	"the most temperature stable powder in its class" [Vihtavuori, 2026]	none found
Alliant RL-16	"resists the natural tendency to generate more pressure at higher temperatures and less pressure at lower temperatures" [Alliant Powder]	none found
Alliant RL-15	not read	0.40 (.308) [Hodgdon Powder Company, 2012]; 1.47 (6mm BR) and 1.89 (.308) [Castleman, 2022b,a]
Reload Swiss RS52	"flat temperature behaviour" [Reload Swiss, 2025]	1.00 (.308), maker's coefficient [Reload Swiss, 2019]
Reload Swiss RS60	"excellent temperature behaviour" [Reload Swiss, 2025]	0.46 (8×68 S), maker's coefficient [Reload Swiss, 2019]

Hodgdon's own comparison, run by a maker against its competitors with the number of shots and the barrel unpublished, gives the lowest figures; the independent tests of Castleman (five shots per temperature, 1 to 36 °C) give two to ten times more for the same powders. In the .308, both put Varget among the least sensitive powders; Castleman also finds N150 and AR-Comp low, and Reloder 15, SO62, CFE 223 and N140 high. No measurement of RL-16, N555, N565 or Vectan's Tubal powders was found.

10.4 Published Load Data (Excerpts)

Each row below is copied from a powder or bullet maker's table *for the named bullet and powder*: starting and maximum charge, and the velocities the maker measured with them

in its test barrel. Velocities published in m/s (Vihtavuori, Reload Swiss) are converted to fps; C marks a compressed charge. A charge published for one bullet does not transfer to another bullet of the same weight: in the .308 Winchester with N150, Vihtavuori stops the 155 gr Berger Hybrid Target at 43.8 gr and the 155 gr Sierra HPBT at 46.5 gr [Vihtavuori, 2026]. Start at the published starting charge, work up while watching for pressure signs, and use the current edition of the manual: tables are revised.

Table 10.3: 6.5 Creedmoor: published loads [Hodgdon Powder Company, 2024, Vihtavuori, 2026]

Bullet	Powder	Charge (gr)	v_0 (fps)	Barrel	Source
140 Hornady ELD-M	H4350	36.0–40.0 C	2464–2660	24 in.	Hodgdon
147 Hornady ELD-M	H4350	36.7–41.8	2389–2680	24 in.	Hodgdon
140 Berger Hybrid Target	N565	42.7–47.1	2516–2733	650 mm	Vihtavuori
147 Hornady ELD Match	N565	41.7–46.0	2405–2654	650 mm	Vihtavuori

Table 10.4: .308 Winchester: published loads [Hodgdon Powder Company, 2024, Vihtavuori, 2026]

Bullet	Powder	Charge (gr)	v_0 (fps)	Barrel	Source
155 Sierra HPBT	Varget	44.0–47.0 C	2759–2909	24 in.	Hodgdon
168 Sierra HPBT	Varget	42.0–46.0 C	2520–2731	24 in.	Hodgdon
175 Sierra HPBT	Varget	42.0–45.0 C	2583–2690	24 in.	Hodgdon
155 Berger Hybrid Target	N150	40.3–43.8	2497–2720	610 mm	Vihtavuori
168 Sierra HPBT	N150	40.1–43.5	2441–2635	610 mm	Vihtavuori

Table 10.5: 6mm Creedmoor: published loads [Hodgdon Powder Company, 2024, Vihtavuori, 2026]

Bullet	Powder	Charge (gr)	v_0 (fps)	Barrel	Source
108 Hornady ELD-M	H4350	37.8–41.6	2802–3006	24 in.	Hodgdon
115 Berger VLD	H4350	36.8–40.5	2718–2895	24 in.	Hodgdon
105 Lapua Scenar	N565	42.1–46.3	2779–3028	660 mm	Vihtavuori

Table 10.6: 6mm BR Norma: published loads [Vihtavuori, 2026, Reload Swiss, 2025, Sierra Bullets, 2020b, Western Powders, 2020]

Bullet	Powder	Charge (gr)	v_0 (fps)	Barrel	Source
105 Lapua Scenar	N140	25.8–28.9	2448–2694	650 mm	Vihtavuori
105 Lapua Scenar	RS52	27.0–28.5	2556–2667	600 mm	Reload Swiss
107 Sierra MatchKing	Varget	23.5–27.1	2250–2550	24 in.	Sierra
107 Sierra HPBT MatchKing	Accurate 4064	26.2–29.1	2485–2704	26 in.	Western

Over the five manuals read for the 6mm BR Norma (the four above and Shooters World), the 42 maximum loads published for 105–108 gr bullets range from 2548 to 2800 fps, median 2668 fps. Norma rates its own 105 gr match load at 2789 fps from a 26-inch barrel [Norma Precision, 2026].

10.5 Complete Worked Example: 6mm BR at 1000 Yards

This section walks through a complete ballistic simulation for a 6mm BR Norma benchrest/F-Class load, from component data through atmospheric correction to a full trajectory table with all secondary effects. This serves as a template for any cartridge.

10.5.1 Step 1: Component Data

The bullet and rifle:

- **Bullet:** Berger 105 gr Hybrid Target, 6mm (.243 cal)
- **BC (G7):** 0.275 (Table 11.1)
- **Bullet length:** 1.256 in. [Berger Bullets]
- **Barrel twist:** 1:7.5 right-hand
- **Brass:** Lapua 6mm BR Norma; **primer:** CCI BR-4 small rifle benchrest
- **Muzzle velocity:** 2670 fps, assumed (see below)

None of the five manuals read for Table 10.6 lists this bullet in the 6mm BR Norma, so no powder or charge is given here: take both from a manual that lists the Berger 105 gr Hybrid, work up from its starting charge, and chronograph the result. The example assumes 2670 fps, the median of the 42 maximum loads those manuals publish for 105–108 gr bullets in this chambering (test barrels of 600 to 660 mm). Everything below is to be recomputed with the chronographed velocity.

10.5.2 Step 2: Stability Check

Using the Miller formula (6.1), at standard conditions:

$$d = 0.243 \text{ in.}, \quad l = 1.256/0.243 = 5.169 \text{ cal}, \quad T_w = 7.5/0.243 = 30.86 \text{ cal/turn}$$

$$\begin{aligned} S_g &= \frac{30 \times 105}{30.86^2 \times 0.243^3 \times 5.169 \times (1 + 5.169^2)} \times \left(\frac{2670}{2800}\right)^{1/3} \times \frac{518.67}{518.67} \\ &= \frac{3150}{30.86^2 \times 0.01435 \times 5.169 \times 27.72} \times 0.984 \\ &\approx 1.58 \end{aligned}$$

$S_g = 1.58$: above 1.5, the threshold above which the bullet realises its full BC, with little margin. At the match-day temperature and pressure of Step 3, the Miller correction raises it to 1.66. S_g grows along the trajectory, since the bullet loses velocity much faster than spin: the muzzle value is the minimum.

10.5.3 Step 3: Atmospheric Conditions

Match day conditions (summer F-Class match in Ottawa, Canada):

$$\begin{aligned} T &= 27.8\,^\circ\text{C} = 82\,^\circ\text{F} = 300.9 \text{ K} \\ P &= 29.75 \text{ in Hg} = 100\,750 \text{ Pa} \\ H &= 55\%, \quad \text{Altitude} = 250 \text{ ft} \end{aligned}$$

Air density from Eq. (2.2):

$$\begin{aligned} e_s &= 610.78 \times 10^{7.5 \times 27.7/(27.7+237.3)} = 3695 \text{ Pa} \\ e &= 0.55 \times 3695 = 2032 \text{ Pa} \\ \rho &= \frac{100\,750 - 0.3783 \times 2032}{287.058 \times 300.9} = \frac{99\,981}{86\,380} = 1.1575 \text{ kg/m}^3 \end{aligned}$$

Density ratio: $\rho/\rho_0 = 1.1575/1.2250 = 0.9449$. The air is 5.5% less dense than standard, so the bullet will retain velocity longer and shoot approximately 0.8 MOA flatter at 1000 yards compared to standard conditions.

Speed of sound (at 27.8 °C): $a = 20.047\sqrt{300.9} = 347.7$ m/s.

Muzzle Mach number: $Ma_0 = 813.8/347.7 = 2.34$ (well into the supersonic regime).

10.5.4 Step 4: Solver Setup and Trajectory

The complete Julia solver call for this scenario:

```
params_6br = ShotParameters(
    # Bullet: Berger 105 Hybrid Target
    mass_grains     = 105.0,
    caliber_in      = 0.243,
    bc              = 0.275,        # G7
    drag_model      = :G7,

    # Launch: median of published maximum loads, 105-108 gr
    muzzle_vel_fps  = 2670.0,
    sight_height_in = 1.5,
    zero_range_yd   = 100.0,

    # Atmosphere: Ottawa, summer match
    temp_F          = 82.0,         # 27.8 C
    pressure_inhg   = 29.75,
    humidity_pct    = 55.0,
    altitude_ft     = 250.0,

    # Wind: 8 mph from 2 o'clock (60 deg off nose)
    wind_speed_mph  = 8.0,
    wind_angle_deg  = 60.0,

    # Target
    target_range_yd = 1000.0,

    # Spin: 1:7.5 RH twist
    twist_in        = 7.5,
    twist_direction = 1,
    bullet_length_in = 1.256,       # Berger Bullet Reference Charts

    # Location: Ottawa, ON
    latitude_deg    = 45.4,
    azimuth_deg     = 270.0,       # firing West
    enable_coriolis = true,
    enable_spin_drift = true,
)

trajectory_table(params_6br, step_yd=100)
```

Listing 10.1: 6mm BR complete trajectory example

The solver output for this configuration (wind column: wind alone; spin column: spin drift alone):

Table 10.7: Computed trajectory: 6mm BR, 105 gr Berger Hybrid, $v_0 = 2670$ fps, 27.8 °C (82°F), 29.75 in Hg, 55% RH. 8 mph wind at 60°. 100 yd zero. 1:7.5 RH twist, 45.4°N, firing West.

Range (yd)	Drop (in)	Elev (MOA)	Vel (fps)	Mach	Energy (ft-lb)	ToF (s)	Wind (in)	Spin (in)
100	0.0	0.0	2512	2.20	1471	0.116	0.4	0.1
200	−4.1	2.0	2360	2.07	1298	0.239	1.7	0.3
300	−14.5	4.6	2213	1.94	1142	0.370	4.0	0.6
400	−32.0	7.6	2072	1.82	1000	0.510	7.4	1.1
500	−57.7	11.0	1935	1.70	873	0.660	12.0	1.7
600	−92.8	14.8	1803	1.58	758	0.821	17.9	2.5
700	−138.6	18.9	1675	1.47	654	0.994	25.2	3.6
800	−197.0	23.5	1551	1.36	561	1.180	34.2	4.9
900	−269.9	28.6	1431	1.25	478	1.381	45.0	6.5
1000	−360.0	34.4	1316	1.15	404	1.600	57.9	8.5

10.5.5 Step 5: Analysis of Results

Velocity retention. The bullet arrives at 1000 yards at 1316 fps (Mach 1.15), about 60 fps above the transonic band ($Ma \leq 1.1$, about 1255 fps at this temperature). Under standard conditions it arrives at 1269 fps (Mach 1.14). At a published-maximum velocity, the 6mm BR stays supersonic to 1000 yards with little margin; a slower load or a colder day takes it into the transonic band.

Total elevation. From the 100-yard zero, the shooter dials 34.4 MOA of elevation (about 10.0 mils). Under standard conditions this load needs 35.1 MOA, against 31.6 MOA for the 6.5 Creedmoor 140 gr at 2700 fps (Table 11.2): at published velocities, the 6mm BR is the slower of the two.

Wind deflection. The 8 mph wind at 60° produces a crosswind component $W_{\text{cross}} = 8 \sin 60° = 6.93$ mph and a headwind component $W_{\text{head}} = 8 \cos 60° = 4.0$ mph. The wind deflection at 1000 yards is 57.9 inches (5.5 MOA). A full-value 10 mph crosswind gives 83.3 inches under the match conditions; under standard conditions, 89.0 inches against 73.5 inches for the 6.5 Creedmoor (Table 11.2), about 21% more.

Spin drift. The 1:7.5 RH twist produces 8.5 inches of rightward drift at 1000 yards (0.81 MOA). This is a systematic bias that should be dialed into the scope or included in the wind hold.

Coriolis and Eötvös. Firing West at 45.4°N latitude:

- Horizontal Coriolis: ≈ 2.6 inches right (0.25 MOA), same direction as spin drift.
- Eötvös (firing West): ≈ 2.6 inches *down* (the bullet loses the "boost" of the Earth's rotation), adding about 0.25 MOA to the required elevation.

Total horizontal correction: Wind 57.9 in. + spin drift 8.5 in. + Coriolis 2.6 in. = 69.0 inches total rightward deflection (6.6 MOA).

10.5.6 Step 6: What the Chronograph SD Means at 1000 Yards

Chronograph the load and enter its mean velocity in the solver. Its standard deviation sets the vertical dispersion it causes downrange, which the library computes by differentiating the trajectory with respect to the muzzle velocity:

```
velocity_vertical_dispersion(params_6br, 1.0; range_yd = 1000)    # 0.32 in per fps
```

Under the match conditions, each fps of velocity SD costs 0.32 inch of vertical SD at 1000 yards: an SD of 5 fps gives 1.6 inches (0.15 MOA), an SD of 10 fps 3.2 inches (0.31 MOA), before any other source of dispersion.

10.5.7 Step 7: DOPE Card Summary

Table 10.8: DOPE card: 6mm BR, 105 Berger Hybrid, 2670 fps assumed (replace with the chronographed velocity). Ottawa, 27.8 °C (82°F), 29.75 inHg. Wind hold is per 1 mph full crosswind.

Range (yd)	Elevation (MOA)	Wind/1 mph (MOA)	Spin+Cor (MOA)
200	2.0	0.12	0.17
300	4.6	0.19	0.25
400	7.6	0.26	0.34
500	11.0	0.33	0.43
600	14.7	0.41	0.54
700	18.9	0.49	0.65
800	23.5	0.59	0.77
900	28.6	0.69	0.91
1000	34.3	0.80	1.06

This DOPE card gives the shooter all the information needed: dial the elevation, hold or dial the wind column multiplied by the estimated crosswind speed, and add the spin+Coriolis correction. The total process—from the mathematical models of Chapters 2–6 through the Julia solver of Chapter 7 to this practical output—represents the complete ballistic pipeline that this manual describes.

10.6 Interpreting Chronograph Data

$$\bar{v} = \frac{1}{N}\sum_{i=1}^{N} v_i, \qquad \text{ES} = v_{\max} - v_{\min}, \qquad \text{SD} = \sqrt{\frac{1}{N-1}\sum_{i=1}^{N}(v_i - \bar{v})^2}$$

Target values: ES $<$ 20 fps (excellent: $<$ 10), SD $<$ 8 fps (excellent: $<$ 4).

As a practical benchmark, the following table shows typical velocity consistency for factory versus hand-loaded ammunition:

Table 10.9: Typical velocity consistency: factory ammunition vs. optimized handloads

Ammunition type	ES (m/s)	ES (fps)
Standard factory match	9–10	30–33
Premium factory match	5–7	16–23
Optimized handloads	2–3	7–10
Benchrest-grade handloads	<2	<7

The gap between factory and hand-loaded ammunition is the primary motivation for reloading in competition shooting: reducing velocity spread by a factor of 3–5 translates directly into tighter vertical dispersion at long range (see below).

10.6.1 Velocity SD Impact on Vertical Dispersion

$$\sigma_y(R) \approx \left| \frac{\partial y}{\partial v_0} \right|_R \cdot \sigma_v \tag{10.1}$$

Chapter 11

Ballistic Reference Tables

11.1 Bullet Data for Common Competition Bullets

Table 11.1: Ballistic data for popular competition bullets [Litz, 2015b]

Bullet	Wt (gr)	Cal	BC G1	BC G7	SD	Twist
Berger 105 Hyb 6mm	105	.243	0.536	0.275	0.254	1:7.5
Berger 140 Hyb 6.5	140	.264	0.607	0.311	0.287	1:8
Hornady 147 ELD-M	147	.264	0.697	0.351	0.301	1:7.5
Berger 180 Hyb 7mm	180	.284	0.683	0.350	0.319	1:8.5
Sierra 175 MK .308	175	.308	0.505	0.243	0.264	1:10
Berger 185 Jugg .308	185	.308	0.552	0.283	0.279	1:10
Hornady 178 ELD-M	178	.308	0.535	0.274	0.268	1:10
Berger 300 Hyb .338	300	.338	0.818	0.419	0.375	1:9.4

11.2 Sample Trajectory Table

Table 11.2: Trajectory: 6.5 CM, 140 gr Berger Hybrid, $BC_{G7} = 0.311$, $v_0 = 2700$ fps, 100 yd zero, sea level standard atmosphere

Range (yd)	Drop (in)	Come-Up (MOA)	Velocity (fps)	Energy (ft-lb)	ToF (s)	10 mph Wind (in)	Spin Drift (in)
100	0.0	0.0	2553	2026	0.115	0.5	0.1
200	−3.9	1.8	2411	1806	0.236	2.3	0.3
300	−13.7	4.3	2273	1606	0.364	5.3	0.6
400	−30.2	7.2	2140	1424	0.500	9.6	1.1
500	−54.4	10.4	2012	1258	0.644	15.5	1.7
600	−87.2	13.9	1888	1108	0.798	23.1	2.5
700	−129.8	17.7	1767	971	0.962	32.5	3.5
800	−183.4	21.9	1651	847	1.138	43.8	4.8
900	−249.7	26.5	1538	735	1.326	57.4	6.3
1000	−331.1	31.6	1427	633	1.529	73.5	8.2

Chapter 12

Special Topics

12.1 Motivation: The Edges of the Envelope

Standard exterior ballistics hold true while the bullet is flying supersonic. However, new bizarre aerodynamic phenomena occur when the bullet slows down and breaks the sound barrier in reverse (the transonic zone). This chapter briefly introduces edge-case ballistics that ruin otherwise perfect shots at extreme long ranges.

12.2 Transonic Stability

The dynamic stability factor S_d must be considered alongside the gyroscopic stability factor S_g [McCoy, 2012]. For full stability: $S_g > 1.0$ and $0 < S_d < 2$.

As a bullet decelerates through the transonic zone ($0.9 \lesssim Ma \lesssim 1.2$), the centre of pressure shifts rapidly and the aerodynamic damping can change sign, potentially causing a well-stabilized supersonic bullet to become dynamically unstable. The practical consequence is increased dispersion—often dramatically so—once the bullet enters this regime. Long-range competitors should therefore know at what range their chosen load crosses into the transonic zone and treat that as the effective maximum range for precision fire.

Table 12.1: Transonic transition ranges for common competition cartridges at sea-level standard conditions, *computed with the solver of Chapter 7* rather than quoted. The transonic zone is defined as $0.9 \leq Ma \leq 1.1$ (≈ 310–$380\ \frac{\text{m}}{\text{s}}$). Ballistic coefficients from Table 11.1 where listed, otherwise from Litz [2015b].

Cartridge	**Bullet (gr)**	B_C **(G7)**	v_0 **(m/s)**	**Enters transonic (m)**	**Subsonic (m)**
.223 Rem	77 SMK	0.191	838	≈690	≈750
.308 Win	155 Lapua Scenar	0.237	860	≈890	≈970
.308 Win	175 SMK	0.243	775	≈780	≈860
6.5 Creedmoor	140 Berger Hybrid	0.311	823	≈1090	≈1200
.300 Win Mag	185 Berger Jugg	0.283	943	≈1210	≈1300
.338 Lapua Mag	300 Berger Hybrid	0.419	838	≈1510	≈1660

Bullets with higher BC values and higher muzzle velocities remain supersonic longer, but the relationship is not linear: the steep drag rise in the transonic zone means that once a bullet begins to slow through $Ma \approx 1.1$, it decelerates rapidly. The solver in Chapter 7 captures this behavior through the fine resolution of the G7 drag table in the transonic region.

12.3 Inclined Fire (Rifleman's Rule)

$$R_{\text{effective}} = R_{\text{slant}} \cdot \cos\alpha \tag{12.1}$$

The perpendicular gravity component $g_{\perp} = g\cos\alpha$ causes the bullet to drop away from the line of sight. Since $\cos\alpha < 1$ for any nonzero inclination (up or down), the drop is always less than flat fire.

Rather than applying the approximate range-scaling of Eq. (12.1) as a post-correction, the solver handles inclination exactly: it resolves gravity in the line-of-sight frame, applying $g_{\perp} = g\cos\alpha$ perpendicular to the sight line and $g_{\parallel} = g\sin\alpha$ along the flight path, then integrates normally. This captures the slight up/down asymmetry (the along-path component accelerates a descending shot and decelerates a climbing one) that the pure cosine rule omits. For the reference 6.5 mm load at $\pm 30^{\circ}$ and 1000 yd, the drop along the sight line falls from -331.1 inches (flat) to -285.2 inches (uphill) and -277.8 inches (downhill).

These figures have moved twice. They were -272, -233 and -228 until 2026-08-14, then -300.6, -258.4 and -252.2 once a $4/\pi$ factor was introduced on C_{D}. That factor was itself an error, compensating fabricated supersonic drag tables; both were removed on 2026-08-22, and the values above come from the corrected solver. The lesson is worth stating plainly: a global scale factor tuned to make one trajectory look right will hide a data error indefinitely, because it leaves the shape of the error untouched while moving its level.

12.4 Barrel Harmonics and Optimal Charge Weight

Barrel vibrations cause the muzzle to describe an elliptical pattern at the moment of bullet exit. The OCW method seeks charge weights where the muzzle vertical angle is at an extremum, creating a flat spot that compensates for velocity variation.

Chapter 13

Error Budget and Sensitivity Analysis

13.1 Motivation: Knowing Your Weakest Link

In competition shooting, you are constantly fighting physics. An "Error Budget" is a mathematical tool to figure out which physical variable is most likely to cause you to miss. It helps a shooter answer the question: *"Should I spend $500 on a better laser rangefinder, or $500 on a better scale to weigh my gun powder?"*

By running a sensitivity analysis, we systematically slightly tweak one variable at a time (like making the wind 1 mph faster, or the muzzle velocity 10 ft/s slower) and observe how much the bullet's impact point moves at a specific range.

13.2 Sensitivity Coefficients

For any given trajectory output Y (such as vertical drop or wind deflection) at a specific range R, we can define the sensitivity S_i to a specific parameter p_i:

Let's define the terms:

- Y: The output of the ballistic solver (e.g., vertical drop in inches).
- p_i: The input parameter being analyzed (e.g., Muzzle Velocity in fps).
- Δp_i: A small, realistic uncertainty or error in that parameter.

$$S_i = \frac{\partial Y}{\partial p_i} \approx \frac{Y(p_i + \Delta p_i) - Y(p_i - \Delta p_i)}{2\,\Delta p_i} \tag{13.1}$$

Table 13.1: Error budget: 6.5 Creedmoor, 140 gr, $\mathrm{BC_{G7}} = 0.311$, 2700 fps at 1000 yd

Parameter	**Uncertainty**	**Vertical (in)**	**Horizontal (in)**
Muzzle velocity	±10 fps	2.5	—
BC	±3%	3.2	1.8 (wind)
Wind speed (10 mph cross)	±2 mph	—	15.4
Wind direction	±10°	—	6.8
Temperature	±5.6 °C (±10 °F)	0.8	—
Range estimation	±5 yd	1.5	—
Spin drift (uncompensated)	—	—	5.1
Coriolis (45°N, uncomp.)	—	<1.0	2.8

Key insight: Wind reading dominates the error budget at long range. Wind-related errors are 3–5 times larger than all other sources combined.

Chapter 14

Dispersion, Hit Probability and Velocity Truing

14.1 Motivation: From Groups to Decisions

The sensitivity coefficients of Chapter 13 describe the weapon. This chapter adds the shooter and the conditions, and answers the two questions a competitor ultimately faces. First: given my measured dispersion and my uncertainty about the wind, what is my probability of hitting a target of a given size? Second: my chronograph and my impacts disagree about the muzzle velocity — which one should I believe, and by how much?

Both questions start from one assumption: the impact point is a bivariate normal random variable, independent on the horizontal and vertical axes. The classical models add a second one — the same standard deviation σ on each axis — which yields closed forms, derived below. It holds at short range, but not at long range, where the velocity spread stretches the group vertically and the wind uncertainty horizontally (Section 14.4).

Terminology. Following the International Vocabulary of Metrology [JCGM, 2012, § 2.13–2.15], *precision* is the closeness of agreement between repeated results — for a rifle, the tightness of the group, expressed by a standard deviation. *Trueness* is the closeness of the mean of infinitely many results to a reference value — the offset of the mean point of impact from the point of aim. *Accuracy* combines both, and is not a quantity. Shooters often say "accuracy" for group size, a usage Grubbs [1991] already called mistaken; this manual keeps *precision* for the group and reserves *accuracy* for the agreement of a prediction or a measurement with the truth. A sight adjustment corrects trueness; no adjustment tightens a group.

14.2 The Rayleigh Model of a Centered Group

Let the impact coordinates (x, y) be independent normal with mean zero and standard deviation σ on each axis. The radial distance of an impact from the group center,

$$R = \sqrt{x^2 + y^2},$$

then follows the **Rayleigh distribution**, whose cumulative form gives the probability of landing inside a circle of radius r:

$$P(R \le r) = 1 - \exp\left(-\frac{r^2}{2\sigma^2}\right). \tag{14.1}$$

Two closed-form summaries follow directly:

$$\mathrm{CEP}_{50} = \sigma\sqrt{2\ln 2} \approx 1.1774\,\sigma, \qquad \mathbb{E}[R] = \sigma\sqrt{\pi/2} \approx 1.2533\,\sigma,$$

where CEP_{50} (Circular Error Probable) is the radius containing half of all impacts, and $\mathbb{E}[R]$ is the mean radius of the group.

14.3 From Group Size to Sigma

Shooters measure the *extreme spread* (ES) of a group, not σ. For n shots from the same bivariate normal, the expected extreme spread is a known multiple of σ:

$$\mathbb{E}[\mathrm{ES}] = k_n\,\sigma, \qquad \sigma = \frac{\mathrm{ES}}{k_n}.$$

Table 14.1: Expected extreme spread of an n-shot group, in units of the per-axis σ (simulation of 2×10^6 and 4×10^6 groups per n, standard error 0.0004, cross-checked against the lookup table of the `shotGroups` package, Wollschläger, 2025, and Table 6 of Grubbs, 1991)

n	3	4	5	6	7	8	9	10
k_n	2.408	2.793	3.066	3.275	3.444	3.586	3.706	3.811

The extreme spread is the largest distance between two impacts *in the plane*. Its factors must not be confused with those of the range of a one-dimensional normal sample, $d_2 = 1.693$, 2.326 and 3.078 at 3, 5 and 10 shots, which apply to a single coordinate — the vertical extent of a group, used in Section 14.6. Only the case $n = 2$ has a closed form, $k_2 = \sqrt{\pi} \approx 1.772$.

Caution: the ES of a single small group is a poor estimator — its own variance is large. Average several groups before dividing. For a given total number of shots, groups of six or seven shots give the most precise average; five-shot groups cost 1 % more ammunition for the same precision, three-shot groups 14 % and two-shot groups 51 % (simulation of 4×10^6 groups per size, in agreement with Ballistipedia, b and Wollschläger, 2025).

14.4 Composing Independent Variance Sources, Axis by Axis

Independent sources compose in *quadrature*: variances add, standard deviations do not. But each source acts on its own axis, and the composition must be done axis by axis. Three sources matter:

- the **intrinsic dispersion** of rifle, ammunition and shooter, σ_a, on both axes. Measured on a group fired at short range, where velocity does not yet weigh, and scaled in proportion to range (angular dispersion);
- the **wind-reading uncertainty** σ_w (in speed units), through the solver's wind sensitivity S_w (lateral displacement per speed unit, by the finite differences of Eq. (13.1)): *horizontal only*;
- the **muzzle-velocity spread** s_v, through the drop sensitivity S_v at *constant launch angle* (shot-to-shot dispersion, not a re-zeroed rifle): *vertical only*;
- the **range-estimation uncertainty** σ_R: the elevation is dialled for $\hat{R}$ while the target stands at R, and the vertical miss is $R\,[a(R) - a(\hat{R})]$, with $a(R) = h(R)/R$ the drop expressed as an angle. Its sensitivity is $S_R = R\,|\mathrm{d}a/\mathrm{d}R|$: *vertical only.*

Hence

$$\sigma_x^2 = \sigma_a^2 + (S_w\,\sigma_w)^2\,, \qquad \sigma_y^2 = \sigma_a^2 + (S_v\,s_v)^2 + (S_R\,\sigma_R)^2\,. \tag{14.2}$$

For the .308 in 175 gr at 549 m, $S_R = 0.81$ cm per metre: dialling for 10 m too far puts the impact 8.2 cm high when the elevation is actually set in the solver, against 8.1 cm from the linear sensitivity.

These are the error sources of the Weapon Employment Zone (WEZ) analysis of Applied Ballistics (Litz, 2015a, ch. 16; Litz, 2021), which also treats rifle precision as the group size "at close range"; Litz [2012] is cited there for the extended treatment. That analysis, like the hit-probability tool of Zima Ballistics [Zima Ballistics], runs the point-mass solver repeatedly with each input drawn at random (Monte Carlo, 1000 shots, repeatable within 1 to 2 % according to Litz), so that each source lands on its own axis without any symmetry assumption. For independent Gaussian sources, the direct computation below is equivalent and free of sampling noise. One convention must be matched: in the Applied Ballistics analysis, a wind or range uncertainty stated as "±" is a 95 % bound, so that σ is half of it [Litz, 2021, footnote 1]. Entering such a bound as a standard deviation doubles its effect. Composing the wind into a single circular σ would spread it vertically as well, which it does not do.

At short range S_v is negligible and the group is circular. It grows quickly with time of flight. With an intrinsic dispersion of 0.5 MOA (5-shot extreme spread, so $\sigma_a \approx 0.047$ mrad) and $s_v = 3$ m/s, the ratio σ_y/σ_x at zero wind is 1.07 to 1.10 at 300 m, 1.4 to 1.5 at 600 m and 2.3 to 3.1 at 1000 m for the 6.5 mm Creedmoor 140 gr and the .308 in 175 gr. Other causes of anisotropy are not modelled: breathing and pulse (mostly vertical when prone), body sway (mostly horizontal when standing), and positive compensation, which reduces the velocity-induced vertical at a given range.

14.5 Hit Probability on a Circular Target

With $\sigma_x \neq \sigma_y$, the distance to the centre no longer follows a Rayleigh distribution but a **Hoyt** distribution [Ballistipedia, a], and the probability of hitting a disc of radius r has no elementary closed form. It is a one-dimensional integral,

$$P(r) = 2\int_0^r \frac{1}{\sigma_x\sqrt{2\pi}}\, e^{-x^2/(2\sigma_x^2)}\, \operatorname{erf}\!\left(\frac{\sqrt{r^2-x^2}}{\sigma_y\sqrt{2}}\right) \mathrm{d}x, \tag{14.3}$$

computed by Simpson's rule (400 intervals, error below 10^{-5}); the radii containing 50 % and 90 % of the hits are obtained by bisection. For $\sigma_x = \sigma_y$, Eq. (14.3) reduces to Eq. (14.1). Webb [2012] reviews the approximate CEP formulas used for non-circular impacts and shows by Monte Carlo that the circle given by the Grubbs–Patnaik formula receives at most 51.1 % of the hits instead of 50 % (2.17 % too many, in relative terms), which Eq. (14.3) reproduces, the maximum occurring at an axis ratio of about 4.5. Elder [1986] compares four such approximations, with and without an offset of the mean point of impact: their radius is usually within 1 % of the exact value, but the error reaches 1 to 5 % for very elongated groups and 2 to 10 % for some combinations of offset and elongation. The integral avoids the approximation altogether.

Eq. (14.3) rests on two assumptions. First, the dispersion ellipse is aligned with the axes ($\rho = 0$), which the axis-by-axis composition of Eq. (14.2) guarantees. For a measured group forming a tilted ellipse, the integral applies to the standard deviations σ_1, σ_2 of its principal axes,

$$\sigma_{1,2}^2 = \frac{\sigma_x^2+\sigma_y^2}{2} \pm \sqrt{\left(\frac{\sigma_x^2-\sigma_y^2}{2}\right)^2 + \rho^2\sigma_x^2\sigma_y^2}.$$

Second, the disc is centred on the mean point of impact. An imperfect zero offsets that point; the normal density must then be integrated over an offset disc, which the Rice distribution does in closed form when the dispersion is circular [Ballistipedia, a].

Worked example. A .308 in, 175 gr (G7 BC 0.243, 2600 fps) at 549 m (600 yd), calculator defaults otherwise. The load groups 3.0 cm extreme spread on 5 shots at 100 m: $\sigma_a = 3.0/3.066 \times 5.49 = 5.37$ cm at the target. The wind-reading uncertainty is $\sigma_w = 3$ km/h (a standard deviation, i.e. ±6 km/h in the 95 % convention); the solver's wind sensitivity is 5.23 cm per km/h, so $S_w\sigma_w = 15.70$ cm. The chronograph SD is 3 m/s; the drop sensitivity at constant launch angle is 0.89 cm per m/s, so $S_v s_v = 2.68$ cm. Eq. (14.2) gives $\sigma_x = 16.6$ cm and $\sigma_y = 6.0$ cm. On a 30 cm steel plate ($r = 15$ cm), Eq. (14.3) gives $P = 58\,\%$ — against 97 % with a perfectly known wind. The wind carries 79 % of the total variance $\sigma_x^2 + \sigma_y^2$: at this range, progress comes from reading the wind. A single circular σ combining all three sources (16.8 cm) would have given $P = 33\,\%$. The three probabilities agree with the `pHoyt` and `pRayleigh` functions of `shotGroups` [Wollschläger, 2025]: 58.2, 96.8 and 32.8 %.

14.6 Bayesian Truing of the Muzzle Velocity

The chronograph and the target give two independent estimates of the *same* quantity, the mean muzzle velocity of the load. Each must carry the uncertainty of that mean, not the dispersion of individual shots.

Prior: the chronograph mean. A string of n shots with mean $\bar{v}_0$ and standard deviation s estimates the mean velocity with standard error $s/\sqrt{n}$. The device's stated accuracy ϵ (a scale error, e.g. ±0.1 % for ballistic radars; in the terms of the VIM, a bound on its systematic error, hence on its trueness) adds almost nothing to s, but it shifts the whole mean, so it enters here. Treating the stated bound as a standard deviation, which overstates it,

$$\sigma_{\text{prior}}^2 = \frac{s^2}{n} + (\epsilon\,\bar{v}_0)^2 .$$

Using s itself as σ_{prior} confuses the dispersion of the shots with the uncertainty of their mean, and under-weights the chronograph by a factor of up to n.

Observation: the centre of a group. A group of k shots is fired at range R; its centre lies Δh (signed) above the predicted point. The forward sensitivity $\partial h/\partial v_0$ is measured by central finite differences on the solver, Eq. (13.1). The vertical standard deviation of the impacts is estimated from the group's vertical extent H with the one-dimensional range factor, $\sigma_y = H/d_2(k)$, so that the centre is known to $\sigma_y/\sqrt{k}$. The velocity implied by the observation and its uncertainty are

$$\hat{v}_0 = \bar{v}_0 + \frac{\Delta h}{\partial h/\partial v_0}, \qquad \sigma_{\text{obs}} = \frac{\sigma_y}{\sqrt{k}\;|\partial h/\partial v_0|}.$$

σ_y already contains the vertical dispersion caused by the shot-to-shot velocity spread; it must not be added a second time.

Update and compatibility. The conjugate Gaussian update combines prior and observation by adding their precisions, in the statistician's sense of inverse variances:

$$v_0^{\text{post}} = \frac{\bar{v}_0/\sigma_{\text{prior}}^2 + \hat{v}_0/\sigma_{\text{obs}}^2}{1/\sigma_{\text{prior}}^2 + 1/\sigma_{\text{obs}}^2}, \qquad \sigma^{\text{post}} = \left(\frac{1}{\sigma_{\text{prior}}^2} + \frac{1}{\sigma_{\text{obs}}^2}\right)^{-1/2}.$$

σ^{post} is always smaller than both σ_{prior} and σ_{obs}. The weighted mean is only meaningful if the two estimates agree; their difference has standard deviation $\sqrt{\sigma_{\text{prior}}^2 + \sigma_{\text{obs}}^2}$, and

$$z = \frac{|\hat{v}_0 - \bar{v}_0|}{\sqrt{\sigma_{\text{prior}}^2 + \sigma_{\text{obs}}^2}}$$

measures their disagreement. Below 1 there is no signal; above 2, something other than the velocity is suspect.

Worked example. A 6.5 mm Creedmoor, 140 gr (G7 BC 0.311), at 800 m without wind, other conditions at the calculator's defaults. The radar chronograph gives 823.0 m/s over 10 shots, $s = 3$ m/s, stated accuracy ±0.1 %: $\sigma_{\text{prior}} = \sqrt{0.95^2 + 0.82^2} = 1.26$ m/s. A 5-shot group 6 cm high has its centre 14.7 cm above the predicted point: $\sigma_y = 6/2.326 = 2.58$ cm, centre known to 1.15 cm. The solver's sensitivity is 1.66 cm of drop less per m/s, so $\hat{v}_0 = 831.9 \pm 0.70$ m/s. The posterior is 829.8 ± 0.61 m/s, the observation carrying 77 % of the weight — but $z = 8.9/1.44 = 6.2$. A radar does not read 1.1 % low when its stated accuracy is 0.1 %: the BC, the zero or the conditions must be checked before the velocity is corrected. Had $s = 3$ m/s been used as the prior uncertainty, the observation would have carried 95 % of the weight and z would have fallen to 2.9.

Assumptions and cautions. The truing absorbs any BC error into the muzzle velocity — a BC error mimics a velocity error, but *differently at each distance*, which is why truing at two distances separates them only approximately. The range must be velocity-sensitive (never near the zero). The update does not account for the uncertainty of σ_y itself, which is large for small groups: the range of 5 shots estimates σ to ±37 % (one standard deviation).

14.7 Implementation

The online calculator applies these three analyses to the active load: the sensitivity of Eq. (13.1) is measured by finite differences on the validated solver, and the constants of this chapter (the k_n table for the hit probability, the d_2 factors for the truing) are the ones the tools use. The hit probability is integrated with Eq. (14.3), never with the circular closed form.

Chapter 15

Ballistic Implications for Reloading

15.1 Motivation: Crafting the Perfect Formula

This chapter bridges the complex mathematical formulas of the preceding chapters with the tangible, practical decisions a competition handloader must make at their physical reloading bench. It demonstrates how to apply ballistic theories (like interior pressure curves and exterior sensitivity) to actual brass, powder, and projectiles to achieve peak performance.

15.2 The Reloader's Equation: What You Control

From the 3-DOF equation of motion (5.4), the trajectory depends on three groups of quantities:

1. **Bullet parameters** (m, d, B_{C}, L): fixed once the bullet is selected.
2. **Launch parameters** (v_0, σ_v, α_0): directly controlled by propellant charge, seating depth, neck tension, primer choice, and case preparation.
3. **Environmental parameters** (ρ, T, P, H, wind): not controllable, but the reloader can minimize their *impact* through component choices that reduce trajectory sensitivity.

15.3 Muzzle Velocity: The Central Reloading Output

15.3.1 Charge Weight and Velocity

The relationship between propellant charge weight C and muzzle velocity v_0 is approximately linear over the useful loading range:

$$v_0 \approx v_{\mathrm{base}} + k_C \, (C - C_{\mathrm{base}})$$

where k_C is the velocity gain per grain. It falls as case capacity rises, and the start and maximum loads of published tables give its order of magnitude: for the 6.5 Creedmoor with 140 to 147 gr bullets, the 13 Reload Swiss loads give 54 to 70 fps/gr (median 62) [Reload Swiss, 2025]; for the .308 Winchester, the 606 Vihtavuori loads have a median of 60 fps/gr [Vihtavuori, 2026]. Small cases exceed 100 fps/gr.

15.3.2 Velocity Consistency and Vertical Dispersion

From Eq. (10.1), the vertical group size at range R due to velocity variation:

$$\sigma_y(R) = \left| \frac{\partial y}{\partial v_0} \right|_R \cdot \sigma_v$$

Table 15.1: Velocity sensitivity: vertical shift per 1 fps change, 6.5 CM 140 gr

Range (yd)	$\lvert\partial y/\partial v_0\rvert$ **(in/fps)**	**Vertical for SD=10 fps (in)**
300	0.02	0.2
600	0.08	0.8
800	0.15	1.5
1000	0.25	2.5
1200	0.40	4.0
1500	0.72	7.2

15.3.3 Achieving Low SD: Quantitative Checklist

Assuming independent error sources, the combined SD is:

$$\sigma_{v,\text{total}} = \sqrt{\sigma^2_{\text{charge}} + \sigma^2_{\text{brass}} + \sigma^2_{\text{primer}} + \sigma^2_{\text{seat}} + \sigma^2_{\text{neck}} + \sigma^2_{\text{lot}}}$$

Table 15.2: Estimated velocity SD contributions by reloading variable

Variable	**Typical σ (fps)**	**Careful prep (fps)**
Charge weight (±0.1 gr thrown)	6–12	2–4 (weighed ±0.02 gr)
Brass volume variation (unsorted)	4–8	1–2 (sorted)
Primer seating depth variation	2–5	1–2 (uniformed pockets)
Seating depth variation	2–4	<1 (consistent BTO)
Neck tension variation	2–6	1–2 (turned, annealed)
Propellant lot variation	0–3	0 (single lot)
RSS total (typical)	**9–17**	
RSS total (prepared)		**3–5**

- **Annealing:** Heating the case neck and shoulder to ≈ 750°F (incipient red) is essential for maintaining consistent neck tension. Without annealing, brass work-hardens, resulting in inconsistent bullet release force and increased SD.
- **Tempilaq:** For torch-based annealing, temperature-indicating liquids are recommended to calibrate heating times accurately and avoid overheating the case body.

15.4 BC Sensitivity and Bullet Selection

A 10% higher BC reduces wind deflection by approximately 8–12%. **Choosing the highest-BC bullet your twist rate can stabilize is the single most impactful choice for reducing wind sensitivity**, which is the dominant error source (Table 13.1).

15.5 Temperature Effects: Propellant and Atmosphere

15.5.1 Combined Temperature Effect

$$\boxed{\Delta y_{\text{total}}(R, \Delta T) = \underbrace{\frac{\partial y}{\partial v_0}\,\sigma_T\,\Delta T}_{\text{velocity effect}} + \underbrace{\frac{\partial y}{\partial \rho}\,\frac{\partial \rho}{\partial T}\,\Delta T}_{\text{density effect}}} \tag{15.1}$$

where Δy_{total} is the total vertical shift at range R, ΔT is the temperature deviation from a reference point, σ_T is the propellant's temperature sensitivity, and ρ is the air density. The terms $\partial y/\partial v_0$ and $\partial y/\partial \rho$ represent the trajectory's sensitivity to muzzle velocity and air density changes, respectively.

When the velocity rises with temperature, as it usually does, the two effects act in the same direction: warmer ammunition leaves faster, and warmer air drags less. They oppose each other for the loads that shoot faster when cold (Table 10.2).

Table 15.3 gathers published coefficients, from the military ammunition of the 1920s to the loads made with powders sold as temperature stable. Hatcher's figures for the .30-06, between 1.55 and 1.83 fps/°F, are of the same order as the Navy's 2009 measurement with IMR 4895 in the 7.62×54R; the commercial and military loads measured since then mostly fall between 0.6 and 1.3 fps/°F. With powders sold as temperature stable, the published figures run from 0.03 to about 0.9 depending on the test (Table 10.2).

Table 15.3: Published velocity coefficients σ_T of rifle ammunition

Ammunition (powder)	**Range**	σ_T **(fps/°F)**	**Source**
.30-06 military, 1920s–1940s	−50 to 140 °F	1.55–1.83	Hatcher [1962, p. 399]
7.62×54R, reduced load (IMR 4895)	32 to 100 °F	1.86	Tyson [2009]
5.56 mm, spherical double base, EPVAT barrel	21 to 71 °C	2.57	Boulkadid et al. [2016]
same, cold side	−54 to 21 °C	1.09	Boulkadid et al. [2016]
7.62 mm M118LR, Lake City production	−65 to 160 °F	≈0.94 (graph)	St. Marks Powder (General Dynamics OTS) [2010]
same, SMP 768 propellant	−65 to 160 °F	0.09	St. Marks Powder (General Dynamics OTS) [2010]
.308 Win factory, Highland SX 168 gr	−15 to 53 °C	0.95	Jackson [2013]
.223 Rem factory, Winchester Supreme 55 gr	−15 to 53 °C	0.97	Jackson [2013]
.308 Win factory, ADI Outback ("BTI" powder)	−15 to 53 °C	0.15	Jackson [2013]
.308 Win handloads, 11 powders	1 to 36 °C	−0.25 to 1.89	Castleman [2022a]
median of the 11		0.79	

Three cautions apply to any single figure. Several responses are not linear: the 5.56 mm velocity falls faster between 71 and 21 °C than between 21 and −54 °C [Boulkadid et al., 2016], and AR-Comp in the .308 is slower at 19 °C than at both 1 and 36 °C [Castleman, 2022a]. Some loads reverse: four of the 29 loads tested by Barsness [2017] were faster at 0 °F than at 70 °F. And the cold is not always the safe side: Vihtavuori does not recommend N570 in heavy loads below −20 °C, for risk of high pressure [Vihtavuori, 2026, p. 14]. The value to use in Eq. (15.1) is the one measured with one's own load over the temperatures expected.

15.6 Seating Depth and Internal Ballistic Coupling

Seating depth affects freebore volume (pressure curve), engraving resistance (pressure peak timing), and initial alignment (reducing α_0). The empirical relationship:

$$\frac{\partial v_0}{\partial(\text{jump})} \approx -3 \text{ to } -8 \text{ fps per } 0.001 \text{ in. increase}$$

The group size model:

$$G(j) = \sqrt{G_{\text{base}}^2 + G_\alpha^2(j) + G_v^2(j)}$$

No jump is best in general. For its hybrid bullets, Berger tests 0.015, 0.030, 0.045 and 0.060 in. off the lands, where "your bullet seating depth accuracy node is usually found" [Hoham, 2021]; for its VLDs, Berger's earlier test went from 0.010 in. into the lands to 0.120 in. off, the good band being 0.030 to 0.040 in. wide and located anywhere between jam and 0.150 in. of jump [Stecker, 2009]. Secant ogives are the most sensitive to seating depth, and a common remedy is to seat them into the lands [Litz, 2015a, p. 341].

15.7 Pressure Estimation and Safety Margins

Table 15.4: SAAMI maximum average pressure (transducer) for competition cartridges [Sporting Arms and Ammunition Manufacturers' Institute, 2025]

Cartridge	MAP (psi)	MAP (MPa)
.223 Remington	55,000	379
6.5 Creedmoor	62,000	427
.308 Winchester	62,000	427
.300 Winchester Magnum	64,000	441
.338 Lapua Magnum	65,000	448

The C.I.P. maximum for the .338 Lapua Magnum, 4200 bar (420 MPa, 60,916 psi), is a different figure from a different organisation and measuring protocol; the two are not interchangeable.

From the Le Duc model peak pressure (3.2):

$$P_{\text{peak}} \approx 1.6 \times P_{\text{avg}} = 1.6 \times \frac{m_e \, v_0^2}{2 \, A_{\text{bore}} \, L_{\text{travel}}}$$

15.8 Barrel Life

There is no standard of barrel life. The published figures are estimates by barrel makers, reports from shooters and, for a few service rifles, military tests, and each counts to a different end point: loss of match accuracy, a throat-erosion gauge reading, a round count fixed by regulation, or a rejection limit on group size (Table 15.5). For the .284 Winchester, the only figure found is one F-Class shooter's projection: a barrel still shooting well at 1,036 rounds and expected to last to 3,000 or more, against 900 rounds for his 6.5-284 [Ballard, 2008].

Table 15.5: Published barrel lives and the end point each one counts to

Cartridge	Rounds	End point	Source
6mm BR	2200–3000	“accurate life”	AccurateShooter [2008b]
6mm BRX, one barrel	2900	competitive 10-shot groups at 100 yd	AccurateShooter [2008a]
6.5 Creedmoor	2000–3000	replacement, untreated barrel	Criterion Barrels [2017]
6.5×284 Norma	1500–1800	replacement, F-Class	Criterion Barrels [2017]
.308 Win and similar	2000–3000	“accurate life”, stainless barrel	Lilja Precision Rifle Barrels
.308 Win	$\geq$ 4000	“remain competitive”	AccurateShooter [2008b]
.308 Win, AR-10, M118LR	5000–8000	“serviceable”, untreated bore	Criterion Barrels [2017]
7.62 mm, M24 sniper rifle	5000	replacement by round count	Headquarters, Department of the Army [1994]
.30-06 National Match, 1923	4700, 5200	barrels worn out (two powders)	Hatcher [1962, p. 331]
Magnum hunting cartridges	1500–3000	“accurate rounds”	Lilja Precision Rifle Barrels
Magnums	1000–2000	throat “burnt out”	Vaughn [1998, p. 83]
5.56 mm M16, 12 rifles	25,000 (mean)	mean extreme spread of five 10-shot groups at 100 yd above 9 in.	Landry and Nilsson [1966]

Wear does not follow a smooth law from the first round. In the Springfield Armory test of twelve M16 rifles, the rejection limit was reached after 25,000 rounds on average; the velocity at the end of the test was 40 fps lower on average, from 6 fps faster to 111 fps slower depending on the rifle, and neither the bullet seat advance nor the change in velocity correlated reliably with accuracy [Landry and Nilsson, 1966]. The 6BRX barrel followed over its whole life kept competitive groups to 2900 rounds, then opened up as the throat roughened [AccurateShooter, 2008a]. Where the throat erosion was measured, it progressed at a roughly steady rate: about 0.001 in. per 1000 rounds in the M16A1 bore [Yalamanchili, 1977], and a lands advance of 0.004 to 0.006 in. per 100 rounds in 6 and 6.5 mm match cartridges [Zant, 2020]. Following the seating depth to the lands and the velocity on the chronograph tells a shooter how the throat is wearing; the group size is what retires the barrel.

15.9 Load Development Workflow

Based on the mathematical models above:

Step 1: Bullet selection. Maximize B_C. Verify $S_g > 1.4$ using Eq. (6.1).

Step 2: Propellant selection. Temperature-stable. Calculate Δv_0 over competition temperature range using Eq. (3.4).

Step 3: Brass preparation. Sort by weight/capacity. Uniform necks and primer pockets.

Step 4: Charge weight exploration. Satterlee ladder or OCW test. Identify velocity nodes.

Step 5: Seating depth optimization. Test at 0.010 in. increments from lands.

Step 6: Validation. 20+ rounds over chronograph. SD $<$ 8 fps (target $<$ 5). Run the solver (Chapter 7) to verify vertical dispersion at max range.

Step 7: Temperature verification. Compute come-up shift using Eq. (15.1).

Appendix A

Detailed Mathematical Derivations

A.1 Motivation: Showing the Work

The models and formulas used throughout this manual are not mere rules of thumb—they are robust physical laws rooted in classical mechanics and aerospace engineering. This appendix provides the rigorous mathematical derivations for these core equations.

A.2 Derivation of the Point-Mass Equations of Motion

Starting from Newton's second law, neglecting lift (valid for small yaw):

$$m\,\ddot{\boldsymbol{r}} = -m\,g\,\hat{\boldsymbol{e}}_y - \frac{1}{2}\,\rho\,C_{\mathrm{D}}\,A\,\|\boldsymbol{v}_{\mathrm{rel}}\|\,\boldsymbol{v}_{\mathrm{rel}}$$

Expressing in component form with $\boldsymbol{v}_{\mathrm{rel}} = \boldsymbol{v} - \boldsymbol{v}_w$ and dividing by m, introducing $C_{\mathrm{D}}\,A/(2m) = \pi\,C_{\mathrm{D}}^{\mathrm{std}}/(8\,B_{\mathrm{C}})$, recovers Eqs. (5.5)–(5.6).

A.3 Derivation of the Coriolis Terms

In a rotating reference frame:

$$m\,\boldsymbol{a}_{\mathrm{rot}} = \boldsymbol{F} - 2m\,(\boldsymbol{\omega} \times \boldsymbol{v}_{\mathrm{rot}}) - m\,\boldsymbol{\omega} \times (\boldsymbol{\omega} \times \boldsymbol{r})$$

The centrifugal term is absorbed into local g. In local coordinates at latitude ϕ:

$$\boldsymbol{\omega} = \omega_E\,(0, \cos\phi, \sin\phi)^T$$

Computing the cross product, the dominant terms for $v_x \gg v_y, v_z$ (where x is downrange, y is vertical, and z is cross-range):

$$a_z^{\mathrm{Cor}} \approx 2\omega_E\,v_x \sin\phi$$
$$a_y^{\mathrm{Cor}} \approx 2\omega_E\,v_x \cos\phi \sin\psi$$

where ψ is the firing azimuth. Integrating these twice with respect to time yields the deflection approximations used in Chapter 6.

A.4 Derivation of Spin Drift via Yaw of Repose

The equilibrium yaw angle from gyroscopic precession:

$$\alpha_{\mathrm{repose}} = \frac{g}{v^2} \cdot \frac{I_x\,\omega_s}{C_{M_\alpha}\,\frac{1}{2}\rho\,v^2\,A\,d}$$

This produces $F_{\mathrm{side}} = C_{L_\alpha}\,\frac{1}{2}\rho\,v^2\,A\,\alpha_{\mathrm{repose}}$, causing the spin drift deflection.

Appendix B

Companion Julia Package

The complete Julia implementation of all mathematical models in this manual is provided as a standalone file: `CompetitionBallistics.jl`. This file contains six sub-modules:

1. `BallisticUtils` — Unit conversions, sectional density, form factor, Miller stability, Greenhill twist.
2. `Atmosphere` — ICAO standard atmosphere, humidity correction, density altitude.
3. `InteriorBallistics` — Le Duc model, burn fraction, barrel length correction, temperature sensitivity, closed-bomb pressure.
4. `DragModels` — G1 and G7 BRL tabular data with both linear and cubic spline interpolation.
5. `ExteriorBallistics` — Full 3-DOF RK4 solver with wind, Coriolis, spin drift, zero-finding, and trajectory table output.
6. `ReloadingAnalysis` — Chronograph statistics, velocity-induced vertical dispersion, ladder test analysis, seating depth sensitivity, temperature shift tables, BC estimation from two chronographs, load quality scoring.

```
include("CompetitionBallistics.jl")
using .CompetitionBallistics
using .CompetitionBallistics.ExteriorBallistics
using .CompetitionBallistics.ReloadingAnalysis

params = ShotParameters(
    mass_grains=140.0, caliber_in=0.264,
    bc=0.311, drag_model=:G7,
    muzzle_vel_fps=2700.0, zero_range_yd=100.0,
    wind_speed_mph=10.0, wind_angle_deg=90.0,
    target_range_yd=1000.0,
    twist_in=8.0, bullet_length_in=1.34,
)
trajectory_table(params, step_yd=100)

# Chronograph analysis
v = [2695, 2702, 2688, 2710, 2699, 2693, 2701, 2707]
stats = chronograph_stats(v)
vert = velocity_vertical_dispersion(params, stats.sd,
                                    range_yd=1000.0)
```

Listing B.1: Quick-start usage of CompetitionBallistics.jl

The file requires only the Julia standard library (`Statistics`, `Printf`).

Appendix C

Greenhill's Formula and Twist Rate Selection

C.1 Motivation: Keeping the Bullet Pointy-End Forward

A rifle barrel contains spiral grooving called "rifling" to impart intense spin to the bullet. Without this spin, the bullet would tumble end-over-end as soon as it hit the air. The "twist rate" characterizes how aggressive this spiral is (e.g., 1 turn in 8 inches, or 1:8).

Alfred George Greenhill, professor of mathematics to the artillery officers at Woolwich, derived his rule in 1879 [Greenhill, 1879]. It is not empirical: unable to compute the aerodynamic moments of a real bullet, he modelled it as a prolate spheroid in slow, frictionless flow, the only shape whose flow was then known, and his stability criterion is equivalent to a gyroscopic stability factor of 1.0 [Miller, 2006].

Let's define the variables:

- t: the twist, in calibers per turn; $T = t\,d$ the twist in inches per turn.
- d: the diameter of the bullet (inches).
- L: the overall length of the bullet (inches); $l = L/d$ its length in calibers.
- ρ_b: the density of the bullet (g/cm^3).

The form used by shooters is a later simplification — its earliest known appearance is in 1929 [Miller, 2006]:

$$\boxed{t\,l = 150 \qquad \Longleftrightarrow \qquad T = \frac{150\,d^2}{L}}$$

The constant 150 holds for a lead-alloy bullet ($\rho_b = 10.9$) 3.27 calibers long; in Greenhill's original rule the product $t\,l$ decreases slowly with length, from 158 at 2.5 calibers to 142 at 5 and 137 at 8. For other densities and conditions, the constant is multiplied by

$$f = \sqrt{\frac{\rho_b}{10.9} \cdot \frac{273.15 + \theta}{288.15} \cdot \frac{1\ \text{atm}}{P}},$$

with θ the temperature in °C and P the pressure.

The rule contains no velocity. The variant found in some sources, which raises the constant to 180 above 2800 fps, is not Greenhill's, and such arbitrary velocity factors do not follow the real variation of the overturning moment [Miller, 2006]. Applied to modern bullets 3.3 to 4.3 calibers long, Greenhill's original rule corresponds to $S_g \approx 1.6$–2.0 at Mach 2.5; for a 105 gr 6 mm bullet 5.17 calibers long at 2950 fps, the simplified rule gives 1:7.05 ($S_g = 1.85$ by Miller's rule) while the 180 variant gives 1:8.5 ($S_g = 1.29$), below the full-BC threshold.

Modern Gyroscopic Stability Guidance (S_g): While Greenhill's is an excellent historical rule of thumb, modern shooters use Miller's gyroscopic stability factor (S_g).

- $S_g < 1.0$: Unstable (tumbling).

- $S_g \in [1.0, 1.5]$: Marginally stable. The bullet flies straight but with residual yaw that costs BC — up to 9% at $S_g = 1.2$.
- $S_g \gtrsim 1.5$: Full BC realised. This is the threshold Litz recommends [Litz, 2015a, p. 161].
- $S_g > 2.0$: Amply stable. Spin drift grows with S_g, but Doppler radar data contradicts the older claim that "over-stabilisation" costs precision: at flat-fire ranges a higher S_g *reduces* drag, especially transonic. Over-spinning matters mainly for jacket integrity on thin-jacketed bullets.

Bibliography

AccurateShooter. 6brx: Long-term accuracy and barrel life report. AccurateShooter Daily Bulletin, 2008a. URL https://bulletin.accurateshooter.com/2008/09/6brx-long-term-accuracy-and-barrel-life-report/. 28 September 2008; one barrel. Consulted 2026-10-20.

AccurateShooter. Barrel life and the cost of shooting. 6mmBR.com, 2008b. URL https://www.6mmbr.com/barrelcost.html. Consulted 2026-10-20.

AccurateShooter.com. Barrel length and velocity — barrel cut-down tests. Daily Bulletin, 2011. URL https://bulletin.accurateshooter.com/2011/12/barrel-length-and-velocity-barrel-cut-down-tests/. 20 December 2011; J. Schmidt's 6 mm BR barrel cut from 33 to 28 in.

ADI (Thales Australia). Load data. adi-powders.com.au, 2026. Online load data, pages read 2026-10-15.

Philip R. Alger. The Le Duc velocity formula. *Proceedings of the United States Naval Institute*, 37(2):535–540, 1911. URL https://www.tireur.org/articles/Alger1911_Le_Duc_velocity_formula.pdf.

Alliant Powder. Reloder 16. alliantpowder.com, product page. URL https://www.alliantpowder.com/products/powder/reloder16.aspx. Undated. Consulted 2026-10-20.

American Rifleman. American rifleman guide: Precision rifle series. americanrifleman.org, 2018. URL https://www.americanrifleman.org/articles/2018/2/27/american-rifleman-guide-precision-rifle-series/. 27 February 2018. Secondary source: the PRS rulebook itself could not be retrieved (2026-10-20).

Ronald D. Anderson and Kurt D. Fickie. IBHVG2 – a user's guide. Technical Report BRL-TR-2829, U.S. Army Ballistic Research Laboratory, Aberdeen Proving Ground, MD, July 1987. DTIC AD-B117104.

Charles Ballard. Caliber choice: The case for the .284 win. 6mmBR.com, 2008. URL https://www.6mmbr.com/7mm284.html. Undated page, copyright 2008. Consulted 2026-10-20.

Ballistipedia. Circular Error Probable. Wiki article, a. URL https://ballistipedia.com/wiki/Circular_Error_Probable/. Consulted 2026-09-30. Rayleigh for equal, uncorrelated axis variances centred on the aim point; Hoyt for unequal or correlated variances; Rice for an offset centre.

Ballistipedia. Range Statistics. Wiki article, b. URL https://ballistipedia.com/wiki/Range_Statistics/. Consulted 2026-09-30. Most economical group size for averaged extreme spread.

John Barsness. Rifle powder temperature sensitivity: Testing modern powders in hot and cold conditions. *Handloader*, 2017. URL https://handloadermagazine.com/rifle-powder-temperature-sensitivity. December 2017–January 2018 issue, table p. 43 (29 loads, 70 °F against 0 °F or 115 °F). Consulted 2026-10-20.

Francis Bashforth. *A Mathematical Treatise on the Motion of Projectiles, Founded Chiefly on the Results of Experiments Made with the Author's Chronograph*. Asher & Co., London, 1873.

Berger Bullets. Bullet reference charts. bergerbullets.com. URL https://bergerbullets.com/information/lines-and-designs/bullet-reference-charts/. Published overall lengths and G1 and G7 ballistic coefficients. Retrieved 2026-08-13.

M. K. Boulkadid, M. H. Lefebvre, L. Jeunieau, and A. Dejeaifve. Temperature sensitivity of propellant combustion and temperature coefficients of gun performance. *Central European Journal of Energetic Materials*, 13(4):1005–1022, 2016. doi: 10.22211/cejem/67229. Royal Military Academy (Brussels) and PB Clermont; Table 3, TC(v) in %/°C, velocity 795 m/s at 21 °C.

Walter F. Braun. The free flight aerodynamics range. Technical Report Report No. 1048, Ballistic Research Laboratories, Aberdeen Proving Ground, MD, July 1958. DTIC AD0202249.

Donald E. Carlucci and Sidney S. Jacobson. *Ballistics: Theory and Design of Guns and Ammunition*. CRC Press, Boca Raton, FL, 2008. ISBN 978-1-4200-6618-0.

W. L. Castleman. Temperature sensitivity of 11 powders for .308 winchester. wlcastleman.com, 2022a. URL https://wlcastleman.com/equip/shoot/t308/index.htm. 6 July 2022; 24-in. barrel, Hornady 168 gr, 5 shots per temperature at 1, 19 and 36 °C. Table read on the image, 2026-10-20.

W. L. Castleman. 6br powder temperature-velocity responses. wlcastleman.com, 2022b. URL https://wlcastleman.com/equip/shoot/tv6BR/index.htm. 30 March 2022; 28-in. barrel, Berger 105 gr VLD, 5 shots per temperature at 3, 22 and 36 °C. Consulted 2026-10-20.

J. Challéat. Théorie des affûts à déformation, à lien élastique et bêche de crosse. *Revue d'artillerie*, 65:161–199, 1904. URL https://gallica.bnf.fr/ark:/12148/bpt6k64398706/f190.item. Leduc's formulas, pp. 184–185 and note p. 194.

Gordons Reloading Channel. *Gordons Reloading Tool – Documentation & User Manual (Version 2021)*, 2021. https://grtools.de.

John Corner. *Theory of the Interior Ballistics of Guns*. John Wiley & Sons, New York, 1950.

Criterion Barrels. What sort of barrel life can i expect from a criterion barrel? criterionbarrels.com, 2017. URL https://web.archive.org/web/20200922163057/https://criterionbarrels.com/media/what-sort-of-barrel-life-can-i-expect-from-a-criterion-barrel/. 2 November 2017, updated 7 November 2018; read in the Internet Archive copy of 22 September 2020, 2026-10-20; page removed by the publisher (HTTP 410, 2026-11-04).

Eagleman Long Range. 6.5 prc / 300 prc / 7 prc barrel test. Long Range Hunting forum, 2023. URL https://www.longrangehunting.com/threads/6-5-prc-300-prc-7-prc-barrel-test.341137/#post-2918453. 6 October 2023; barrels cut from 26 to 18 in.

Richard L. Elder. An Examination of Circular Error Probable Approximation Techniques. Master's thesis afit/gst/ens/86m-6 (dtic ada172498), U.S. Air Force Institute of Technology, Wright-Patterson AFB, OH, 1986. URL https://archive.org/details/DTIC_ADA172498. Consulted 2026-09-30: abstract and Chapter V.

Explosia a.s. *LOVEX Reloading Guide*, 2019.

Gavin Gear. Extreme powder temperature testing: Varget vs tac. UltimateReloader.com, 2022. URL https://ultimatereloader.com/2022/04/01/extreme-powder-temperature-testing-varget-vs-tac/. 1 April 2022; .308 Win, −65, 70 and 140 °F. Consulted 2026-10-20.

A. G. Greenhill. On the rotation required for the stability of an elongated projectile. *Minutes of Proceedings of the Royal Artillery Institution*, 10:577–593, 1879.

Frank E. Grubbs. *Statistical Measures of Accuracy for Riflemen and Missile Engineers*. The author, Havre de Grace, MD, 2nd edition, 1991. URL https://ballistipedia.com/images/3/33/Statistical_Measures_for_Riflemen_and_Missile_Engineers_-_Grubbs_1964.pdf. First printing 1964; second edition March 1991, third printing December 1991. Consulted 2026-09-30 (Tables 5, 6 and 9 read as images).

Julian S. Hatcher. *Hatcher's Notebook*. Stackpole, Harrisburg, PA, 3rd edition, 1962. Temperature and velocity, p. 398–399; barrel life of the 1923 National Match ammunition, p. 331.

Joseph Haviland. Loading bench: Hit the mark, weather or not. *American Rifleman*, 2022. URL https://americanrifleman.org/content/loading-bench-hit-the-mark-weather-or-not/. 4 April 2022; summer 94 °F against winter 8 °F. Consulted 2026-10-20.

Headquarters, Department of the Army. *FM 23-10: Sniper Training*, 1994. 17 August 1994, paragraph 2-8 (round-count book of the M24).

Hodgdon Powder Company. Extreme rifle powders: Actual data comparing extreme spreads. hodgdon.com, page printed 13 July 2012, 2012. URL https://hodgdonpowderco.com/wp-content/uploads/2023/04/hodgdon-extreme-series-powders-test-results-for-temperature-sensitivity-1.pdf. Velocities at 0, 70 and 125 °F in four cartridges; number of shots and barrels not published. Tables read on the page image, 2026-10-20.

Hodgdon Powder Company. *Hodgdon 2024 Annual Manual*. New York, 2024.

Hodgdon Powder Company. Barrel length versus velocity. hodgdonpowderco.com, 2026. URL https://hodgdonpowderco.com/articles/barrel-length-versus-velocity/. 12 March 2026; one 6.5 Creedmoor and two .223 Wylde barrels cut from 24 to 16 in.

Phil Hoham. How to load a hybrid bullet. Berger Bullets, 2021. URL https://bergerbullets.com/shoot-better/shooting-knowledge/how-to-load-a-hybrid-bullet/. Consulted 2026-10-02.

James M. Ingalls. *Exterior Ballistics in the Plane of Fire*. D. Van Nostrand, New York, 1886.

International Civil Aviation Organization. *Manual of the ICAO Standard Atmosphere: Extended to 80 Kilometres (262 500 Feet)*, 1993. ICAO Doc 7488/3, 3rd edition.

International Confederation of Fullbore Rifle Associations. *Rules & Regulations for F-Class Rifle Shooting*, 2023 (text of 1 june 2024) edition, 2024a. URL https://icfra.com/wp-content/uploads/2024/11/FC_Rules_2023-Rev-2.pdf. Rules F2.1–F2.3. Consulted 2026-10-20.

International Confederation of Fullbore Rifle Associations. *Technical Rules & Regulations for Fullbore Target Rifle Shooting*, 2024 edition, 2024b. URL https://icfra.com/wp-content/uploads/2025/03/TR_Technical_rules-2024.pdf. Rules T2.1 and T2.19. Consulted 2026-10-20.

International Shooting Sport Federation. *Rifle Rules*, 2025 (in force 1 january 2026) edition, 2026. Rule 7.4.6.

Breil Jackson. Australian outback ammunition review. In *ADI Powders Handloaders' Guide*, pages 15–19. Thales Australia, 6th edition, 2013. Factory ammunition conditioned at −15, ambient and 53 °C, one rifle per cartridge.

JCGM. International Vocabulary of Metrology – Basic and General Concepts and Associated Terms (VIM). JCGM 200:2012, 3rd edition, BIPM, 2012. URL https://www.bipm.org/documents/20126/2071204/JCGM_200_2012.pdf. Bilingual edition consulted 2026-09-30; § 2.13–2.15: accuracy, trueness, precision.

Beat P. Kneubühl. *Ballistik – Theorie und Praxis*. Springer, Berlin, Heidelberg, 2018. ISBN 978-3-662-58299-2. doi: 10.1007/978-3-662-58300-5.

Wilhelm Kutta. Beitrag zur näherungsweisen Integration totaler Differentialgleichungen. *Zeitschrift für Mathematik und Physik*, 46:435–453, 1901. URL https://archive.org/details/zeitschriftfrma12runggoog.

kwk.us. Powley computer for handloaders (online calculator) and notes on the powley computer. URL http://kwk.us/powley.html. JavaScript source read 2026-10-03; after Davis, Handloading, NRA, 1981.

P. R. Landry and C. E. Nilsson. Barrel erosion study of rifles, 5.56mm, m16 and xm16e1: A joint army-air force test. Technical Report SA-TR11-5000, Springfield Armory, 1966. January 1966; DTIC AD0483309. Velocity summary (Table III) read on the image.

Lilja Precision Rifle Barrels. Faq: What barrel "life" in number of rounds fired can i expect from my new barrel? riflebarrels.com. URL https://riflebarrels.com/support/faq/. Undated, page modified 4 January 2021. Consulted 2026-10-20.

Bryan Litz. *Accuracy and Precision for Long Range Shooting: A Practical Guide for Riflemen*. Applied Ballistics, LLC, 2012. ISBN 978-0-615-67255-7. Cited by Litz [2015a] for the extended treatment of WEZ analysis; not consulted for this manual.

Bryan Litz. Twist rate stability calculator updated. Berger Bullets, 2014. URL https://bergerbullets.com/twist-rate-stability-calculator-updated/. Consulted 2026-10-02.

Bryan Litz. *Applied Ballistics for Long Range Shooting*. Applied Ballistics, LLC, Cedar Springs, MI, 3rd edition, 2015a. ISBN 978-0-9909206-1-8.

Bryan Litz. *Ballistic Performance of Rifle Bullets*. Applied Ballistics, LLC, 2nd edition, 2015b.

Bryan Litz. Weapon Employment Zone (WEZ) Analysis: A Conceptual Overview. Applied Ballistics, 2021. URL https://appliedballisticsllc.com/wp-content/uploads/2021/06/Weapon-Employment-Zone-Analysis.pdf. Consulted 2026-09-30; ABDOC115 appears only in the file metadata. Footnote 1: a "±" uncertainty is a 95 % bound, σ = half.

Lyman Products Corporation. *Lyman Reloading Handbook*. Lyman Products Corporation, 48th edition, 2002.

Bill Marr. Barrel length and velocity: cut-down tests (.223 rem., .224 valkyrie, 7.62x39, 6mm and 6.5 creedmoor, .243 win., .308 win., .300 win. mag.). Rifleshooter.com, 2013–2018. URL https://rifleshooter.com/category/barrel-length/. Data tables published as images, read on screen 2026-10-02.

Bill Marr. 308 winchester / 7.62x51mm nato: Barrel length versus velocity (28 to 16.5 inches). Rifleshooter.com, 2014. URL https://rifleshooter.com/2014/12/308-winch

ester-7-62x51mm-nato-barrel-length-versus-velocity-28-to-16-5/. Consulted 2026-10-02.

Robert L. McCoy. *Modern Exterior Ballistics: The Launch and Flight Dynamics of Symmetric Projectiles*. Schiffer Publishing Ltd., Atglen, PA, 2nd edition, 2012. ISBN 978-0-7643-3825-0. 1st edition 1999; 2nd edition 2012, ISBN 978-0-7643-3825-0.

Don Miller. A new rule for estimating rifling twist: An aid to choosing bullets and rifles. *Precision Shooting*, pages 43–48, March 2005.

Donald G. Miller. Where did Greenhill's twist rule come from? *International Journal of Impact Engineering*, 32(11):1786–1799, 2006. doi: 10.1016/j.ijimpeng.2005.06.001.

Norma Precision. *Reloading Data*, 2023. Edition of November 2023.

Norma Precision. Norma diamond line 6 mm norma br 6.8g. norma-ammunition.com, 2026. URL https://www.norma-ammunition.com/products/shooting/norma-diamond-line/norma-diamond-line-6-mm-norma-br-105gr---10160162. 105 gr, 850 m/s (2789 fps) from a 660 mm barrel. Consulted 2026-10-20.

G. W. Patterson. The Le Duc ballistic formulae. *Proceedings of the United States Naval Institute*, 38(3):885–892, 1912. URL https://www.tireur.org/articles/Patterson1912_Le_Duc_ballistic_formulae.pdf.

Reload Swiss. Temperature coefficient. reload-swiss.com, Hints from the experts, 2019. URL https://www.reload-swiss.com/en/about-us/tips-tricks/temperature-coefficient. 28 January 2019. Coefficients in m/s per K, one cartridge per powder, means of several lots; temperatures, bullets and barrels not given. Consulted 2026-10-20.

Reload Swiss. *Ladedaten / Reloading Data, Ausgabe 2025 / Issue 2025*, 2025.

Francesco Siacci. *Balistica*. F. Casanova, Libraio-Editore, 2nd edition, 1888. "2a edizione, interamente rifusa"; first form: Corso di balistica teorico-pratica, 1870–1875.

Sierra Bullets. *Rifle Reloading Data, 6th edition: 6.5 x 47 Lapua*, 2020a. 24-in. test barrel, 1:8 twist. Consulted 2026-10-20.

Sierra Bullets. *Rifle Reloading Data, 6th edition: 6mm BR Norma*, 2020b. URL https://sierrabullets.com/content/load-data/rifle/243-6mm/6mm-br-norma.pdf. 24-in. test barrel, 1:8 twist. Consulted 2026-10-20.

Sporting Arms and Ammunition Manufacturers' Institute. *ANSI/SAAMI Z299.4-2025: Voluntary Industry Performance Standards for Pressure and Velocity of Centerfire Rifle Sporting Ammunition*. Newtown, CT, 2025.

St. Marks Powder (General Dynamics OTS). Small caliber propellant solutions for the u.s. military. NDIA Armaments conference, 19 May 2010, 2010. URL https://ndia.dtic.mil/wp-content/uploads/2010/armament/WednesdayCumberlandSteveFaintich.pdf. Slide 11, M118LR velocity from −65 to 160 °F; production value read on the graph. Consulted 2026-10-20.

Eric Stecker. Berger tips for loading vld bullets. AccurateShooter Daily Bulletin, 2009. URL https://bulletin.accurateshooter.com/2009/03/berger-tips-for-loading-vld-bullets/. Berger's seating-depth test for VLD bullets, as reproduced by AccurateShooter; consulted 2026-10-02.

J. H. Tyson. Temperature compensated loading curves for the 7.62 x 54r armor piercing incendiary (api) round. Technical Report NAWCWD TM 8598, Naval Air Warfare Center

Weapons Division, China Lake, CA, 2009. DTIC ADA510537, read in the Internet Archive copy (DTIC under maintenance on 2026-10-20).

U.S. Committee on Extension to the Standard Atmosphere. U.s. standard atmosphere, 1976. Technical Report NOAA-S/T 76-1562, NOAA, NASA, USAF, Washington, D.C., October 1976.

Harold R. Vaughn. *Rifle Accuracy Facts*. Precision Shooting, Inc., 1998.

Vihtavuori. *Vihtavuori Reloading Guide*, 2026.

David W. Webb. Circular Probable Error for Circular and Noncircular Gaussian Impacts. Technical Report ARL-MR-830 (DTIC AD1043284), U.S. Army Research Laboratory, Aberdeen Proving Ground, MD, September 2012. URL https://www.tireur.org/books/libres/arl_mr_830_webb_circular_probable_error_2012.pdf. Approved for public release, distribution unlimited. Full report read 2026-09-30.

Western Powders. *Handloading Guide*. Miles City, MT, 8.0 edition, 2020.

Daniel Wollschläger. shotGroups: Analyze Shot Group Data. R package version 0.8.4, 2025. URL https://CRAN.R-project.org/package=shotGroups. Used 2026-09-30 to cross-check the extreme-spread factors and the Hoyt hit probabilities.

R. Yalamanchili. Bore erosion and accuracy of m16a1 rifle. Technical Report R-TR-77-055, Rock Island Arsenal, 1977. February 1977; DTIC ADA037533.

Hyun Dal Yoon, Sung Hoon Choi, and Sang Kil Lee. An experimental study for the projectile velocity versus travel distance in the gun barrel. *Korean Journal of Military Art and Science*, 66(2):55–69, 2010. doi: 10.31066/kjmas.2010.66.2.003.

Cal Zant. How fast does a barrel wear? PrecisionRifleBlog.com, 2020. URL https://precisionrifleblog.com/2020/03/24/how-fast-does-a-barrel-wear/. 24 March 2020. Consulted 2026-10-20.

Cal Zant. Powder temperature sensitivity: The hidden factor affecting your long-range accuracy. PrecisionRifleBlog.com, 2025. URL https://precisionrifleblog.com/2025/03/08/powder-temperature-sensitivity/. 8 March 2025; 10 shots per temperature. Consulted 2026-10-20.

Cal Zant and Patrick Middlebrook. Powder temp stability: Hodgdon extreme vs. imr enduron. PrecisionRifleBlog.com, 2016. URL https://precisionrifleblog.com/2016/06/19/powder-temp-stability-hodgdon-extreme-vs-imr-enduron/. Consulted 2026-10-02.

Zima Ballistics. Operator's guide. Online documentation. URL https://zimaballistics.com/guide/. Section 7.2, "Hit Probability (WEZ)".

Glossary

BC	Ballistic Coefficient — ratio of sectional density to form factor.
BRL	Ballistic Research Laboratory (US Army, Aberdeen Proving Ground).
COAL	Cartridge Overall Length.
BTO	Base To Ogive length.
DA	Density Altitude.
ELR	Extreme Long Range ($>$ 1500 yd).
ES	Extreme Spread (max velocity $-$ min velocity).
MOA	Minute of Angle ($\approx$ 1.047 in. at 100 yd).
Mil	Milliradian ($\approx$ 3.6 in. at 100 yd).
OCW	Optimal Charge Weight.
PRS	Precision Rifle Series.
NRL	National Rifle League.
SD	Sectional Density or Standard Deviation (context-dependent).
VLD	Very Low Drag (bullet design).
S_g	Gyroscopic Stability Factor.
G1/G7	Standard drag model designations.